CALIFORNIA'S FIFTH
CLIMATE CHANGE
ASSESSMENT

The Impacts of Climate Change on Atmospheric River Storms and California's Water Resource Infrastructure

An Original Research Report for:

California's Fifth Climate Change Assessment

CALIFORNIA NATURAL RESOURCES AGENCY

ciee California Institute for Energy and Environment

CITRIS and the BANATAO INSTITUTE

CA Governor's Office of Land Use and Climate Innovation

Gavin Newsom, Governor

Authors and Contributors

Alan Rhoades[1]
Emily Bercos-Hickey[1]
Julia Szinai[1]
Michael Wehner[1]
David Yates[2]
Yang Zhou[1]

Acknowledgements

We thank the U.S. Department of Energy's National Energy Research Scientific Computing Center at Lawrence Berkeley National Laboratory and the U.S. National Science Foundation's National Center for Atmospheric Research Wyoming Supercomputing Center. Without these computational resources, we could not have effectively conducted our analyses. We greatly appreciate the feedback and guidance provided by our technical committee members, including Michael Anderson, Darren Bonfantine, Scott Ligare, and Jake Sahl. We would also like to thank Dr. Christina Patricola for making several of the WRF storyline simulations available to us. We sincerely appreciate the constructive comments provided by our three anonymous reviewers that enhanced the clarity and rigor of our report.

1 Lawrence Berkeley National Laboratory (LBNL)
2 National Center for Atmospheric Research (NCAR)

About California's Fifth Climate Change Assessment

California's Climate Change Assessments are the state's scientific foundation for understanding future climate-related vulnerability across California's regions and systems. Senate Bill 1320 (Stern, 2020) requires the State to report the impacts and risks of climate change across California at least every five years, beginning with California's Fifth Climate Change Assessment (Fifth Assessment). Building on decades of climate research and previous Assessments, the Fifth Assessment presents new findings about California's climate future, with a dedicated focus on Tribal partnerships, public engagement, and communities most vulnerable to climate impacts.

The Fifth Assessment's research and tools are designed to fill knowledge gaps about California's climate future, inspire strategic climate actions, and shape planning, investments, and policies at the state, regional, and local scales. Guided by research priorities identified by state, Tribal, and local leaders, community representatives, and subject matter experts, its findings are designed to help illuminate potential climate futures, the challenges they may present, and the opportunities to build resilience through adaptation pathways.

For the full suite of Fifth Assessment research products, please visit: www.ClimateAssessment.ca.gov.

DISCLAIMER:
This report was prepared as the result of work sponsored by the California Natural Resources Agency. It does not necessarily represent the views of the Natural Resources Agency, its employees, or the State of California. The Natural Resources Agency, the State of California, its employees, contractors, and subcontractors make no warrant, express or implied, and assume no legal liability for the information in this report; nor does any party represent that the uses of this information will not infringe upon privately owned rights. This report has not been approved or disapproved by the Natural Resources Agency nor has the Natural Resources Agency assessed the accuracy or adequacy of the information in this report.

Suggested Citation:
Rhoades, A., Bercos-Hickey, E., Szinai, J., Wehner, M., Yates, D., & Zhou, Y. (2026). *The Impacts of Climate Change on Atmospheric River Storms and California's Water Resource Infrastructure* (California's Fifth Climate Change Assessment). Lawrence Berkeley National Laboratory. https://www.climateassessment.ca.gov/2708/

Use of Artificial Intelligence (AI):
We acknowledge the use of AI tools in the preparation of this report. More specifically, ChatGPT was used to develop and debug code to post-process and visualize some of the downscaled climate data (e.g., LOCA-2 and WRF-Hydro-based results).

Abstract

Atmospheric rivers (ARs) and extratropical cyclones (ETCs) largely drive the amount of precipitation that California receives each year. These storm events could respond to climate change in unique ways that alter the state's historical water year characteristics. In this report, we investigate how the flood potentials of these storm events, particularly when they occur in isolation (AR-only) or co-occur (AR-ETC), could change in a future, warmer world. We leverage multiple modeling methodologies to decipher how climate change could alter AR-only and AR-ETC flood drivers (e.g., precipitation, snowpack, and soil moisture) and how the interactions between changes in those flood drivers influence managed hydrologic systems of Northern California. We show that California's water year total precipitation could increase or decrease (based upon the model used, region assessed, and if evaluated at mid- or end-century), with a greater share of the precipitation coming from more extreme and clustered AR-only and AR-ETC events that produce more rainfall. AR-ETC events are projected to have higher extreme precipitation rates, whereas AR-only events are projected to have higher rain-on-snow potential. In both AR-only and AR-ETC events, rain-on-snow potential is projected to shift from the northern to central and southern portions of the Sierra Nevada under future warming. Despite enhanced rainfall, more ripened snowpacks, and saturated soils that result in markedly higher peak inflows, major Northern California reservoirs (e.g., Folsom, New Bullards Bar, and Oroville) show resilience to certain warming-enhanced AR-only and AR-ETC flood events (e.g., January 1982, December 1995, and December 2022 through January 2023), although these events are not representative of all possible future flood events.

Keywords: Atmospheric Rivers, Extratropical Cyclones, Extreme Precipitation, Rain-on-Snow, Reservoir Inflows

Highlights

- California's annual total precipitation may not appreciably change in the future, but could become even more reliant on atmospheric rivers that are more extreme, rainier and more clustered.
- Future atmospheric river events associated with an extratropical cyclone produce higher extreme precipitation rates but have less rain-on-snow potential than atmospheric river events not associated with an extratropical cyclone.
- Rain-on-snow risk during all atmospheric river events in the future is elevated and expected to shift southward in the Sierra Nevada.
- In Northern California, future warming is expected to produce higher peak reservoir inflows at an earlier time within storm events, with antecedent snowpack and soil moisture conditions critically shaping inflow dynamics.
- Results suggest that Northern California reservoirs (e.g., Oroville, Folsom and New Bullards Bar) are resilient and responsive to warming-induced changes to certain flood events (e.g., January 1982, December 1995, and January-December 2022–2023), although these events are not representative of all possible future flood events.

WEB LINKS

The catalogs for AR-only, ETC-only, and AR-ETC events are available on a National Energy Research Scientific Computing Center (NERSC) Science Gateway - https://portal.nersc.gov/archive/home/y/yangzhou/www/CMIP6. These catalogs are provided as CSV files and were produced for eight historical simulations and six future simulations from the Community Model Intercomparison Project 6, which were then statistically downscaled using Localized Constructed Analogs version 2 (LOCA2) to produce California-wide precipitation estimates. Additionally, we analyzed another LOCA2-based dataset, LOCA2-Hybrid, that leverages the LOCA2 methodology, but learns from a set of Weather Research and Forecasting (WRF) model simulations. These results are made available on a NERSC Science Gateway - https://portal.nersc.gov/cfs/m3318/5thCCA/ - and include changes in annual mean and extreme precipitation and temperature. Finally, the WRF storyline simulations data for 1982, 1995, and 2022–2023 are staged on another NERSC Science Gateway - https://portal.nersc.gov/archive/home/projects/cascade/www/SFPUC

Table of Contents

1: Introduction 1
2: Methods 3
2.1 Climatological projections of California precipitation 3
2.2 Feature tracking of AR-only and AR-ETC events 3
2.3 Storyline recreations of flood-producing AR-only and AR-ETC events 4
2.4 Hydrologic and hydraulic recreations of flood-producing AR events 7
3: Results 10
3.1 21st century responses of AR-only and AR-ETC precipitation over California 10
3.1.1 AR-contributed precipitation is projected to increase in the future 10
3.1.2 Future AR-contributed precipitation is driven by extreme events 15
3.1.3 Competing mechanisms in future precipitation projections 19
3.2 Deciphering the physical mechanisms for AR characteristic changes using storyline simulations 24
3.2.1 AR flood potential is enhanced in the future 24
3.2.2 AR-contributed precipitation is enhanced in the future, although less efficiently over mountains 26
3.2.3 AR-ETC events produce more extreme precipitation rates and AR-only events have more rain-on-snow potential 32
3.3 Northern California infrastructural resilience to future AR-ETC characteristic changes 35
3.3.1 Antecedent land surface conditions shape AR flood potential 36
3.3.2 Northern California infrastructure is resilient to future AR events tested . 37
4: Conclusions and Future Directions 50
5: References 52
Appendix A: Additional WRF and WRF-Hydro Storyline Event Results 58
A.1 Storyline Event Land Surface Conditions 61
A.2 2022-2023 Storyline 64
A.3 1995 Storyline 69
A.4 1982 Storyline 76

1: Introduction

California precipitation totals are dominated by two main storm types, atmospheric rivers (ARs) and extratropical cyclones (ETCs) (Bao et al., 2006; Dettinger et al., 2011). ARs are warmer storms that transport vast and narrow plumes of water vapor to coastal regions, including California. ETCs are cyclonic low-pressure systems that often originate near the Aleutian Gulf and typically convey cooler storms toward coastal regions. 82% of all ARs are associated with an ETC, as the ETC warm-conveyor belt focuses poleward moisture transport, and pre-existing ARs can in turn intensify moisture inflow during ETC genesis (Dacre et al., 2025; Peng et al., 2025; Zhang, Ralph, and Zheng, 2019; Zhang & Ralph, 2021). Landfalling AR events produce half of California's annual total precipitation amounts in under 120 hours each year (Lamjiri et al., 2018), often at temperatures that are above or near freezing (Bales et al., 2006; Gonzales et al., 2022). ARs are also responsible for nearly all flood hazards in California (Corringham et al., 2019; Gershunov et al., 2025; Ralph et al., 2019).

How ARs and ETCs interact with one another, and how their isolated occurrence or co-occurrence influences California flood drivers (e.g., precipitation, snowpack, and soil moisture) remains an outstanding and important research topic. Future AR and ETC events will be shaped by warmer conditions that enhance their potential to produce extreme rainfall over saturated soils and/or a more ripened snowpack that, in turn, elevates flood potentials (Ombadi et al., 2023; Rhoades et al., 2021; Siirila-Woodburn et al., 2021). Importantly, the nature of precipitation produced by future AR-only and AR-ETC events (e.g., intensity, duration, frequency, and phasing) could respond differently to climate change. AR frequency and intensity are projected to increase (Shields et al., 2023), and several studies suggest more frequent co-occurring explosive AR-ETC events (Lopez-Marti et al., 2025). However, as discussed in Patricola et al. (2022), projected precipitation responses differ markedly between ARs that co-occur with ETCs and those that do not. The warming sensitivity of these precipitation characteristics changes and the antecedent land surface conditions (e.g., soil moisture and snowpack conditions) will have important implications for California's future water supply and flood planning resiliency.

To help California water managers and flood planners proactively respond to future changes in AR-ETC characteristics, we present a series of experiments and analyses spanning a multitude of methodological approaches (e.g., dynamical and statistical downscaling). These approaches utilize both traditional climatological and storyline-based analyses to identify where, when, how, and why landfalling AR-only and AR-ETC events in California could respond to warming. The goal of using these different approaches is to build confidence about the sign and magnitude of change in AR-only and AR-ETC event characteristics and build multiple lines of evidence for

those changes. If those lines of evidence are in agreement, water managers and flood planners can be more confident in making decisions that are shaped by future changes in their event characteristics.

This report is set up as follows: Section 2 provides more details on the datasets and methodological approaches employed. In Section 3.1, we highlight climatological analyses of storm event characteristics (e.g., AR-only versus AR-ETC frequency and differences in water year total precipitation contributions) across a myriad of global climate models that were statistically downscaled using the Localized Constructed Analogs version 2 (LOCA2; Pierce et al., 2023). LOCA2 is chosen as it is the featured dataset used in California's Fifth Climate Change Assessment (Fifth Assessment). In Section 3.2, we utilize a widely used and trusted dynamical downscaling approach (the Weather Research and Forecasting (WRF) model; Skamarock & Klemp, 2008) within a storyline-based approach (Shepherd, 2019) to better understand why AR event characteristics are changing with warming. Storyline recreations of major flood events include one AR-ETC and five AR-only events spanning December 2022–January 2023, an AR-only event in January 1982, and an AR-ETC event in December 1995. We then intercompare these storyline-based analyses with LOCA2-based results to identify where the methodologies are in agreement or disagreement. Section 3.3 focuses on how well Northern California's built infrastructure and historical management strategies resiliently respond to future hydrometeorological changes in AR-only and AR-ETC event characteristics.

2: Methods

We utilize multiple methodologies that span different spatiotemporal scales to assess how California landfalling AR-only and AR-ETC event characteristics differ in past and future climates. These methodologies are outlined in greater detail in the next few subsections.

2.1 Climatological projections of California precipitation

The Fifth Assessment guidance recommends that the LOCA2, LOCA2-Hybrid, and WRF-based data products be used for future projections of precipitation. Notably, these recommended datasets exhibit substantial model-to-model variability and spatial uncertainty in their California precipitation estimates that could differ from other methodological approaches in the peer-reviewed literature (this is discussed in greater detail in the Results and Discussion sections). The LOCA2 data product was constructed by statistically downscaling 14 selected Coupled Model Intercomparison Project version 6 (CMIP6; Eyring et al., 2016) global climate models (GCMs) chosen for their ability to simulate California's climate (Krantz et al., 2021). The LOCA2-Hybrid data product utilizes the LOCA2 statistical downscaling methodology, but updates estimates based upon what is learned from a set of WRF model simulations. Fifth Assessment guidance also recommends that a set of five dynamically downscaled simulations performed with the WRF model can supplement LOCA2-based analyses. All of these data products were constructed from single ensemble members of the coarser CMIP6 GCMs at similar fine horizontal resolutions (~3 km grid spacing). One historical and three future emissions scenarios (O'Neill et al., 2016) are utilized, including SSP245 (middle of the road scenario), SSP370 (regional rivalry scenario), and SSP585 (fossil-fueled development scenario). All three of these scenarios are used to generate the LOCA2 and LOCA2-Hybrid products, but only the historical and SSP370 futures are used to generate the WRF data product.

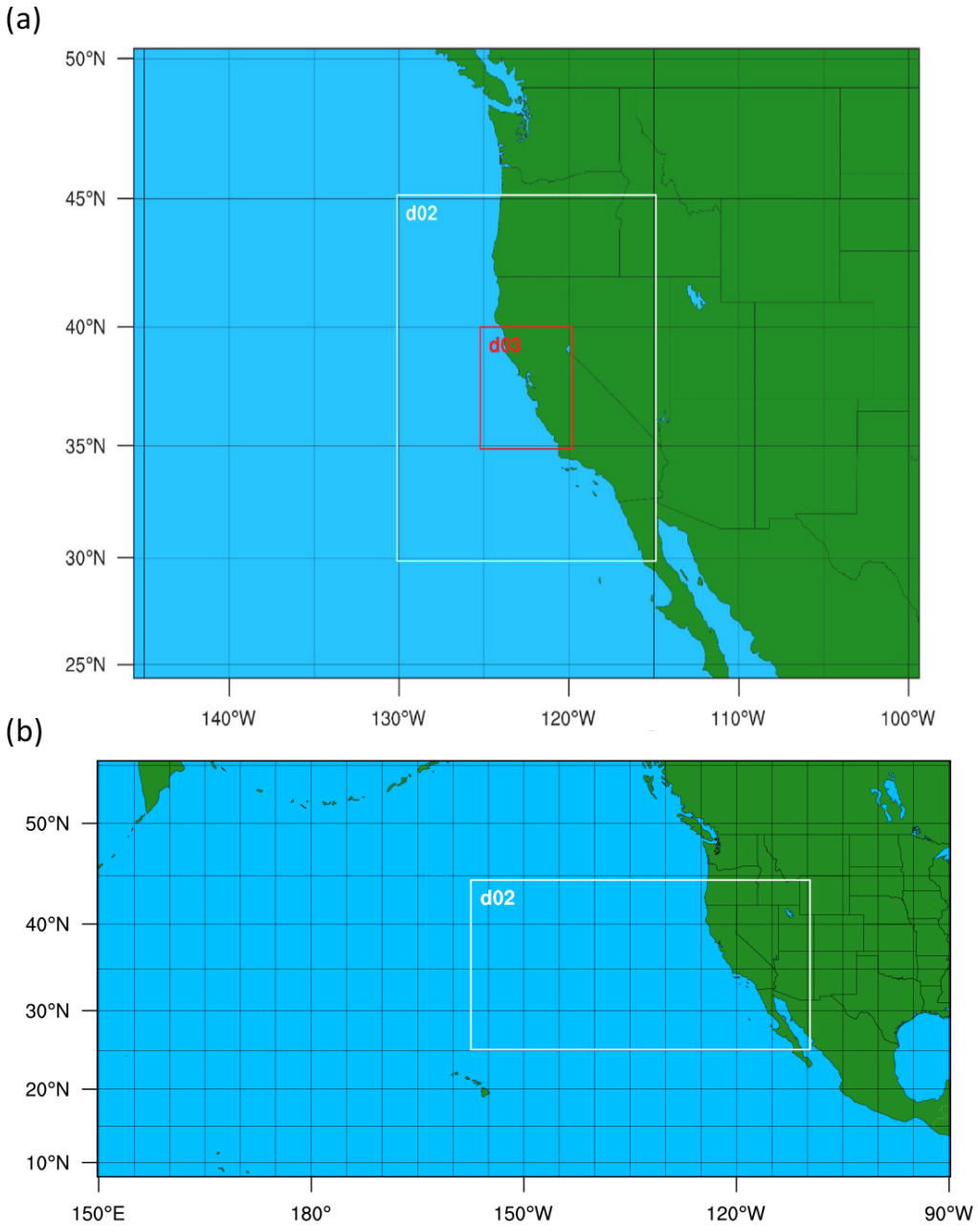
2.2 Feature tracking of AR-only and AR-ETC events

TempestExtremes version 2 (TEv2) is used to track AR-only, ETC-only, and AR-ETC events (Ullrich et al., 2021). Specific details on how the storm events are identified in the LOCA2 and WRF-based experiments are outlined in the Appendix. AR-only, ETC-only, and AR-ETC event catalogs are provided (see Figure A.0.2 for an example event catalog CSV file) for six CMIP6 models and only one SSP scenario (SSP585), as these were the only CMIP6 simulations that provided the necessary sub-daily atmospheric fields needed for storm tracking. These event catalogs (e.g., landfall flags) are used to isolate non-AR, AR-only, and AR-ETC related precipitation in LOCA2 across California.

2.3 Storyline recreations of flood-producing AR-only and AR-ETC events

A storyline-based approach is used with the WRF model version 3.8.1 to dynamically downscale several major AR-only and AR-ETC flood events over California. The flood events simulated include the January 3–5, 1982, and December 10–13, 1995 events (Patricola et al., 2022) with 10 different realizations (or ensemble members) of each storyline event. These 10-member storyline ensembles were then recreated in a warmer world representative of an end-century SSP585 scenario by adjusting the initial and lateral boundary conditions to include the thermodynamic component of anthropogenic climate change (Schar et al., 1996; Patricola & Cook, 2010, 2013). Specifically, temperature, relative humidity, geopotential height, sea level and surface pressure, sea surface temperature, surface temperature, soil moisture and temperature, and snow water equivalent (SWE) were modified using future climate change differences, or deltas, from global climate model data to account for future climate change (see Patricola et al. [2021] for additional details). Unique to this project, another 10-member set of WRF-storyline simulations was also produced for the period spanning December 24, 2022 through January 24, 2023, in both a historical and future climate (similar to the storyline events of 1982 and 1995). For the 1982 and 1995 simulations, the WRF domain spanned 30–45 N and 115–130 W at ~9 km grid spacing. For the 2022–2023 simulations, the WRF domain spanned 25–45 N and 110–157 W at ~12 km grid spacing (Figure 2.3.1).

Figure 2.3.1 The WRF domains for the (a) 1982 and 1995 and (b) 2022–2023 simulations.



Domain d01 represents the entire region of the map shown in (a) and (b). Boxes labeled d02 and d03 show the nested grid domains. For (a), domains d01, d02, and d03 had horizontal grid spacings of ~27, ~9, and ~3 km, respectively, and for (b), domains d01 and d02 had horizontal grid spacings of ~36 and ~12 km, respectively. Domain d02 was used for all analyses for the 1982, 1995, and 2022–2023 simulations.

As discussed in more detail in the Appendix, TEv2 is used to isolate AR-only and AR-ETC events within the WRF storyline simulations. TEv2 helps to identify when AR-only and AR-ETC event landfalls start and end within California. We then use this information to compute their Ralph et al. (2019) AR Category Scale (across each grid cell within California) as described in more detail in Rhoades et al., 2020). 1982 had an AR-only event, and 1995 had an AR-ETC event. These two storyline events were chosen for the following reasons: the AR-ETC event of December 10-13, 1995, delivered up to 8–10 inches (~203–254 mm) of precipitation in the Bay Area and the AR-only event from January 3–5, 1982, delivered 8 inches (~203 mm) of precipitation in the Bay Area. Additionally, as described in the Center for Western Weather and Water Extremes (CW3E) AR Catalog - https://cw3e.ucsd.edu/Projects/ARCatalog/catalog.html, the 1995 AR-ETC event had the highest maximum integrated vapor transport (IVT) reached of any AR-ETC event since the 1960s. According to the CW3E AR Catalog, the 1982 AR-only event reached a Category 2 and the 1995 AR-ETC event reached a Category 5 which were lower and higher, respectively, than our storyline event recreations (Table 2.3.1). This is partly due to the fact that we compute our AR Category estimates across all of California, whereas CW3E computes them only along the California coastline (see Appendix).

The back-to-back AR-only and AR-ETC events from December 24, 2022 to January 25, 2023 were highlighted by our Fifth Assessment Technical Advisory Committee (i.e., California Department of Water Resources and the State Water Board representatives) as a high-impact event, producing considerable flood damages throughout the SF Bay Area and other portions of California (e.g., Pajaro Valley and Tulare Basin). Notably, the 2022–2023 storyline event simulated 5±1 AR only and 1±1 AR-ETC events according to TEv2 (plus minuses represent the 95% mean confidence intervals across the 10-member ensemble; Table 2.3.1). We note that this count of AR events was fewer than was identified in DeFlorio et al. (2024), who identified nine AR events. This difference in AR landfall count could be due to several sources of uncertainty including: model structural uncertainty, atmospheric river detection algorithm uncertainty, the length of the WRF storyline simulation (which can lead to forecast divergence from the observations), and/or reanalysis dataset used. Notably, the CW3E AR Catalog agrees with our storyline event recreations showing that AR Categories spanned levels 2–3 across the AR-only and AR-ETC events that occurred (Table 2.3.1 and Appendix). Additionally, California-wide observed rainfall rates are well estimated across the WRF 10-member ensemble (Figure A.0.1).

Table 2.3.1 Average AR-only and AR-ETC landfall characteristics (e.g., maximum integrated vapor transport, max IVT, California-wide mean storm total precipitation) over California for the three WRF storyline events.

Storyline Event	AR-only Counts	AR-ETC Counts	AR Category	Max IVT (kg/m/s)	AR Landfall Duration (days)	Storm Total Precip (mm)
Historical 1982	1 ± 0	–	2.8 ± 0.3	1000 ± 6.7	0.8 ± 0.0	47 ± 0.6
Future 1982	1 ± 0	–	4.0 ± 0.0	1300 ± 13	0.9 ± 0.0	50 ± 0.7
Historical 1995	–	1 ± 0	3.5 ± 0.0	1400 ± 14	0.6 ± 0.0	52 ± 0.7
Future 1995	–	1 ± 0	4.0 ± 0.0	2000 ± 14	0.7 ± 0.0	61 ± 1.1
Historical 2022–2023	5 ± 1	1 ± 1	3.3 ± 0.5	920 ± 69	2.3 ± 0.4	34 ± 0.8
Future 2022–2023	4 ± 1	2 ± 1	3.8 ± 0.4	1200 ± 75	2.9 ± 0.6	41 ± 1.0

The 10-member mean estimates are provided with 95% mean confidence intervals for both historical (blue) and future (yellow) storyline events.

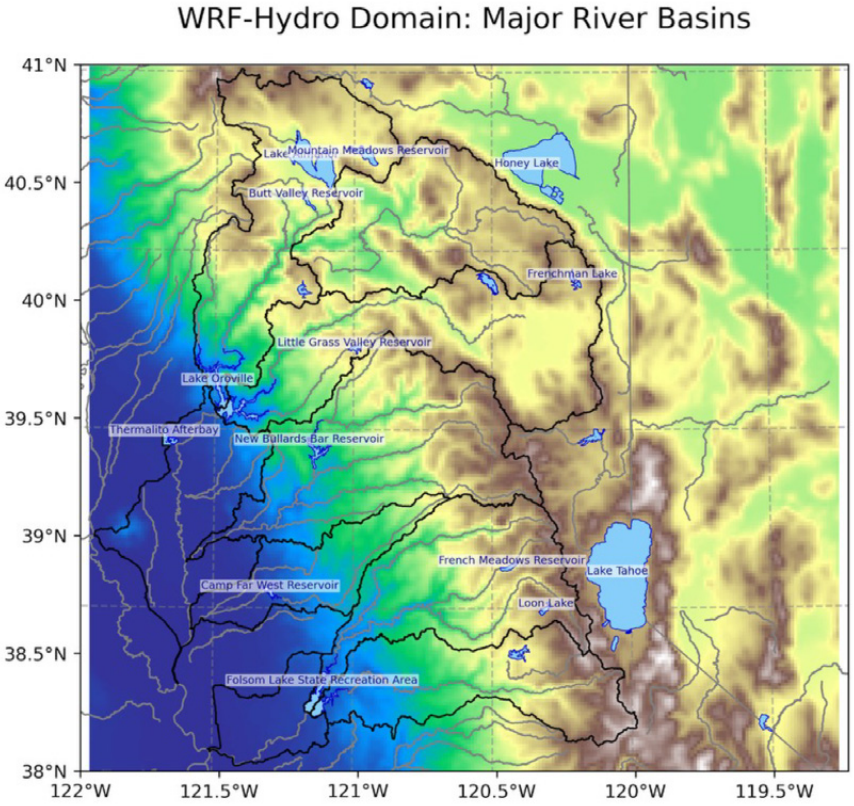
2.4 Hydrologic and hydraulic recreations of flood-producing AR events

The Weather Research and Forecasting hydrological modeling system (WRF-Hydro; Gochis et al., 2018) is used to assess the surface-through-subsurface hydrologic interactions and hydraulic responses during AR-only and AR-ETC events. The WRF-Hydro simulations are one-way coupled, with the meteorological forcing provided by the Analysis of Record for Calibration (AORC; Fall et al., 2023) and outputs from the WRF storyline simulations at three hourly intervals.

To spin up the antecedent land surface conditions in WRF-Hydro prior to each storyline event, we use the AORC which is an observationally-constrained gridded (~800 m) reconstruction of hourly, near-surface meteorological conditions covering

the continental United States and Alaska. The WRF-Hydro initialization occurs on 1 October prior to each WRF-simulated flood event and is run up to the start time of the flood event. The model is then run from that time forward, using the forcing from the WRF storyline event simulations. The meteorological forcing fields required to run WRF-Hydro from both AORC (prior to the flood event) and WRF (during the flood event) include precipitation, 2-meter air temperature, surface pressure, 10-meter windspeed, 2-meter specific humidity, and long and shortwave radiation. We note that the antecedent conditions for the future WRF-Hydro simulations also use the historical AORC dataset for the spin-up period, and therefore may not capture the full effect of warming on the atmosphere (e.g., rain-snow partitioning of the storms) and land surface conditions prior to the event (e.g., ripened snowpack and drier soils). The WRF-Hydro domain is a spatial subset of the WRF storyline simulation domain (Figure 2.4.2). Within this domain, we include 18 reservoirs in Northern California, including Folsom, New Bullards Bar, Oroville, and others. The WRF-Hydro domain also includes the contributing streams and tributaries to these reservoirs, such as the Feather, Yuba, and American Rivers.

Figure 2.4.2



The Northern California WRF-Hydro domain, including river networks, natural lakes, and reservoirs. Watersheds are delineated with black borders.

In the WRF-Hydro model, reservoirs are integrated into the terrestrial water cycle, serving as storage features that influence downstream hydrology. Their implementation is primarily based on a level-pool routing scheme, where the water surface within the lake is assumed to be horizontal. This simplification allows for an efficient representation of storage and release dynamics. An innovation of this work was the development of an orifice parameterization to more realistically control storage and release dynamics. Water release is controlled through simulated physical structures, where an orifice represents the low-level outlet in the dam structure, typically used for controlled releases. The flow through an orifice is calculated using the standard orifice equation, which relates the discharge to the hydraulic head (the height of the water surface above the center of the orifice). The general form of the equation is:

$$Q_o = C_d\,(c_o A)\,\sqrt{(2gH)}$$

where, Q_o is the discharge from the orifice (cms); C_d is the coefficient of discharge (a dimensionless value that accounts for energy losses); A is the cross-sectional area of the orifice (m^2), which can be adjusted on a daily basis to control reservoir releases, where co = 0 assumes fully closed and c_o = 1.0 is fully open; g is gravity acceleration; and H is the hydraulic head above the centerline of the orifice.

The other control structure in WRF-Hydro is a weir that serves as a release control for high water elevations, and serves as either a controlled or uncontrolled spillway. Spillways are designed to release excess water when reservoir levels exceed a certain elevation, preventing the overtopping of a dam. The flow over a spillway is modeled using a weir equation

$$Q_s = C_w(c_w L H^{3/2})$$

where, Q_s is the discharge through the spillway (cms), C_w is the weir coefficient (an empirical coefficient), L is the length of the spillway crest, and H is the height of the water surface above the spillway crest. L*H gives the effective area and its relative opening is controlled by c_w, where a value of 1.0 implies an uncontrolled spillway, and a value of 0.0 implies a fully closed spillway, that will result in the reservoir reaching a full reservoir height and where an uncontrolled spill could result, which is assumed to occur across the length of the dam width. In WRF-Hydro, control of the orifice and weir outlets are made by simply prescribing co and wo on a daily basis for each reservoir in the LAKEPARMS.nc parameter file.

3: Results

3.1 21st century responses of AR-only and AR-ETC precipitation over California

In this section, we quantify how AR-related precipitation could change through the 21st century using LOCA2 daily precipitation and TEv2-based landfall classifications that separate AR-only events from AR-ETC events. Analyses are performed on a water-year (Oct–Sep) basis for a historical climatology (1980–2010) and two future climatologies under SSP585: mid-century (2040–2070) and end-century (2070–2100). We address two questions in this section:

1. How will California's water year precipitation contributions of AR-only and AR-ETC events change in a future climate?
2. How will the frequency and severity of AR-driven extremes in a future climate differ across California?

3.1.1 AR-contributed precipitation is projected to increase in the future

Table 3.1.1

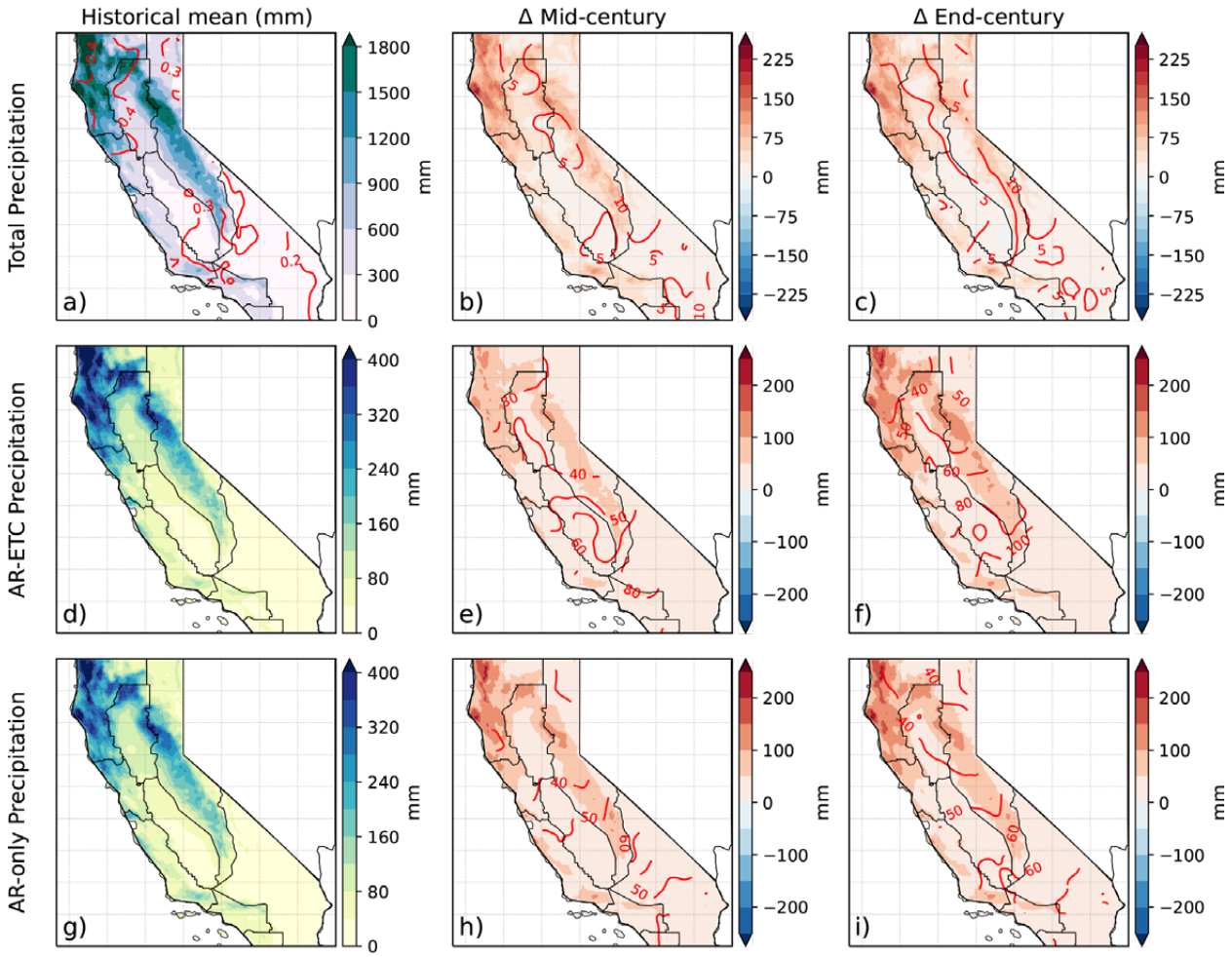
Storm Type	Historical (1980–2010)	Mid-century (2040–2070)	End-century (2070–2100)
	Number of events per year	Number of events per year	Number of events per year
AR-ETC	11±3	13±4	15±4
AR-only	12±2	17±2	19±3
	Event duration (days)	Event duration (days)	Event duration (days)
AR-ETC	1.8±0.1	2.0±0.2	2.4±0.3
AR-only	1.6±0.1	1.7±0.1	1.8±0.1
	Event interval (days)	Event interval (days)	Event interval (days)
All ARs	15.3±1.8	11.9±1.0	10.5±0.8

LOCA2 multi-model mean AR-only and AR-ETC California landfall event frequency, duration, and event interval spacing per water year and their landfall durations for historical, mid-century, and end-century climatological periods. 95% mean confidence intervals are provided as plus minuses. The event interval spacings are calculated with both AR types considered.

A projected increase in the number of AR-only and AR-ETC events that make landfall in California is found at mid- and end-century (Table 3.1.1). The number of AR-only events increases from 12 per water year historically to 17 and 19 per water year by mid- and end-century, respectively. AR-ETC events also increase from 11 per water year historically to 13 and 15 per water year by the mid- and end-century, respectively. Additionally, landfalling AR-only and AR-ETC events last longer. AR-only event durations increase from 1.6 days per event historically to 1.7 and 1.8 days per event at mid- and end-century, respectively. AR-ETC durations increase from 1.8 days per event in the historical period to 2.1 and 2.4 days per event at mid- and end-century, respectively. In summary, there are roughly 35–55% more AR-only events and 20–36% more AR-ETC events by end-century, with landfall durations lengthening by ~13% (AR-only) and ~30% (AR-ETC). In addition to increases in event frequency and duration, the temporal spacing between consecutive AR events decreases across all LOCA2 models. Overall, there is a 30–35% reduction in inter-event spacing, indicating that ARs occur in closer succession with warming. In particular, we find AR clustering occurs most during midwinter from November to January, with about 9.2 interval days between events historically, and decreases to 7.7 days by mid-century, and further decreases to 7.3 days by end-century. Together with the increases in event counts and event duration, these results provide multi-model evidence that AR activity could become more temporally clustered in California with warming.

Future changes in the number of AR-only and AR-ETC event landfalls and the duration of their landfalls likely reshapes the spatial pattern of precipitation over California. Figure 3.1.1 shows maps of California's historical water year precipitation. California precipitation is defined by north–south and windward–leeward gradients. A precipitation maximum is found along the North Coast and the windward portions of the California Sierra Nevada. A precipitation minimum is found in Southern California, namely in the desert regions. The AR-contributed precipitation (both AR-only and AR-ETC) is a dominant component of the historical water-year accumulation, particularly in the coastal and mountainous regions, underscoring the central role of ARs in delivering California's wet-season precipitation. More specifically, ARs contribute ~40–50% of total precipitation over Northern California and ~20–40% over Southern California. This LOCA2-based result is consistent with observations (Dettinger et al., 2011). Contributions from AR-only and AR-ETC events are comparable over Northern California: ~20% to ~25% of precipitation is attributed to AR-only and AR-ETC events, respectively. Panel (a) of Figure 3.1.1 shows the spatial pattern of this AR-contributed fraction.

Figure 3.1.1
LOCA2 Ensemble: Annual-accumulated Precipitation

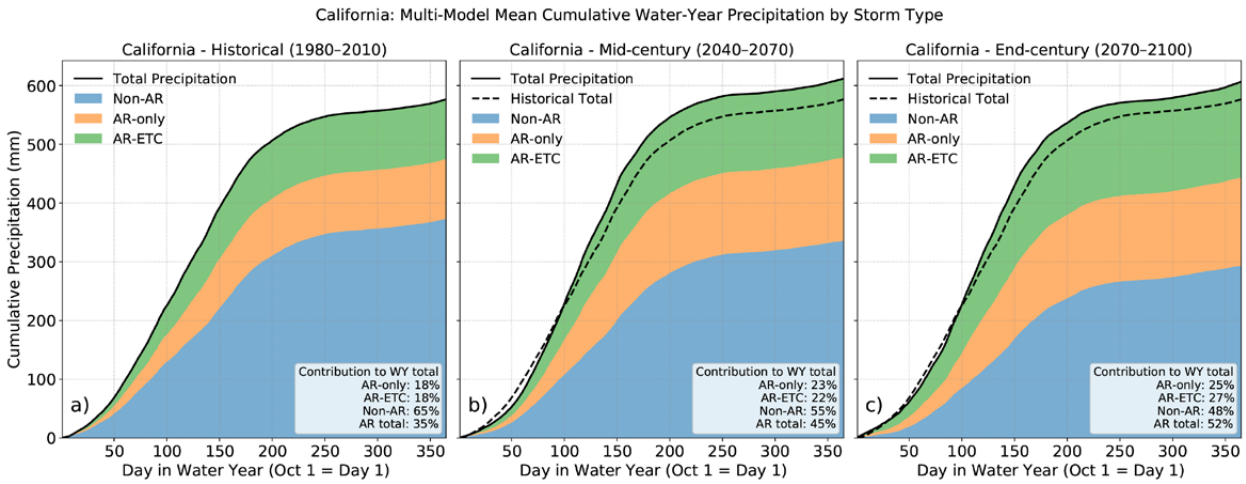


LOCA2 multi-model climatological water year mean precipitation for the historical period (1980–2010; first column) and percentage changes from historical to mid-century (2040–2070; second column), and end-century (2070–2100; third column) for total precipitation (first row), AR-ETC contributed precipitation (second row), and AR-only contributed precipitation (third row). Shading shows absolute changes (mm), while red contours show percentage changes. In panel (a), red contours instead show the historical AR-contributed fraction of total water-year precipitation. Percentage contours are masked in regions where historical annual-accumulated precipitation is less than 10 mm.

Future changes in precipitation indicate broad increases in AR-related precipitation by mid-century and further amplification by end-century (Figure 3.1.1). This is consistent with the projected increase in the number of AR events per year in the future (Table

3.1.1). In absolute terms (shading in Figure 3.1.1), the largest increases occur along the North Coast and the windward Sierra Nevada, where historical precipitation is highest. Across the LOCA2 models, the combined absolute increase from AR-only and AR-ETC precipitation exceeds the absolute increase in total precipitation, implying a modest decline in non-AR precipitation contributions with warming (see also Figure 3.1.2). In contrast, the largest percentage increases (contours in Figure 3.1.1) occur in hydroclimatologically dry regions, including Southern California, the Inland South, and desert regions, where small historical totals cause even modest absolute increases to translate into large relative changes. Notably, the LOCA2 multi-model mean estimates indicate that increases in AR-related precipitation typically outpace the change in total precipitation across all storm events. This is consistent with observational evidence (Najibi & Steinschneider, 2023). In Northern California, AR-only and AR-ETC precipitation increase by ~30–40% by end-century, whereas Southern California shows much larger relative changes (often exceeding 100% for AR-ETC events) due to its low historical precipitation baseline.

Figure 3.1.2

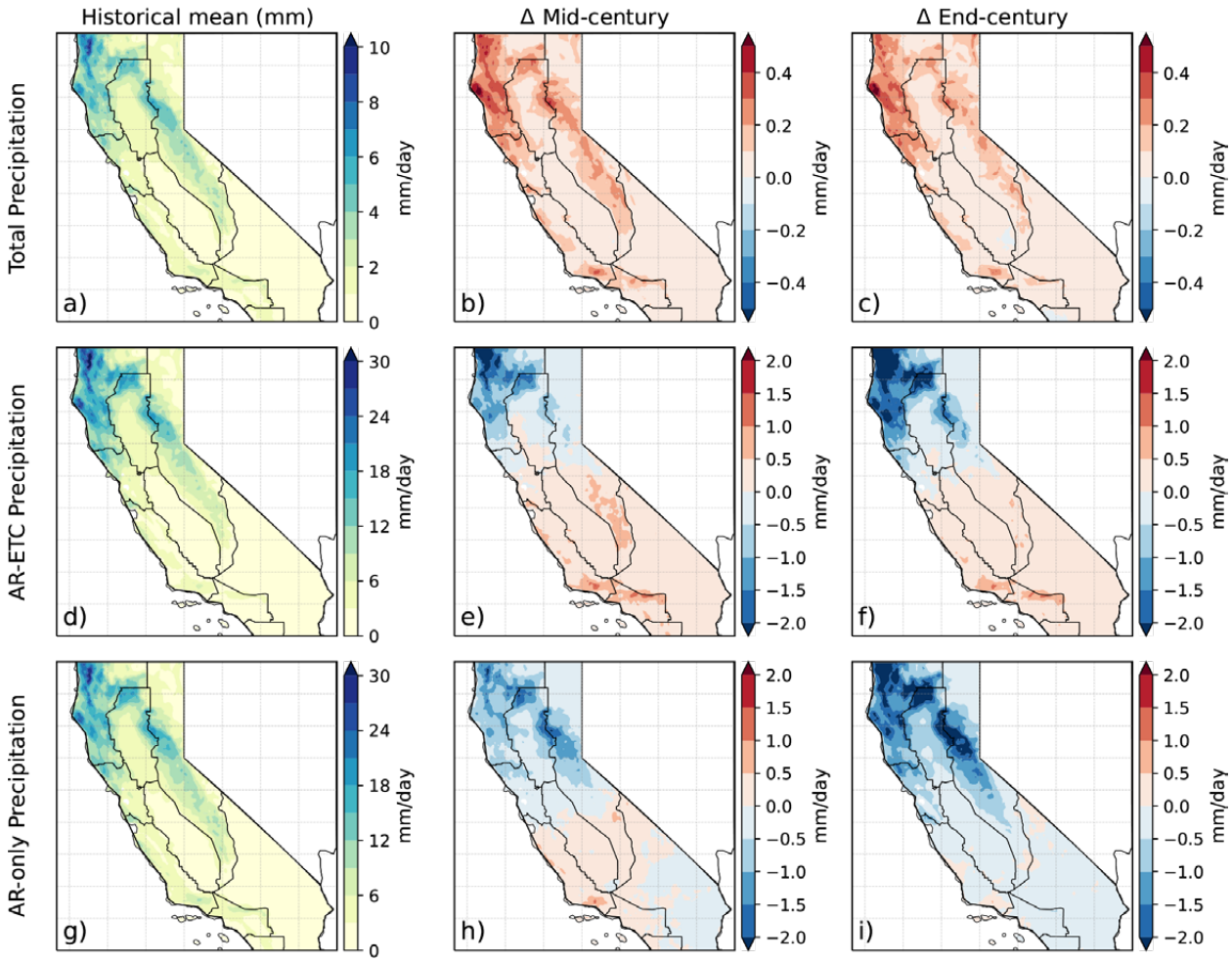


California-wide mean cumulative water year precipitation delineated by contributions from non-AR, AR-only, and AR-ETC events for the historical (left), mid-century (middle), and end-century (right) time periods. The box located in the lower right of each subpanel plot shows the percentage contribution from each storm event type to the total precipitation.

Figure 3.1.2 shows California mean water year cumulative precipitation and is split by storm type contributions. Between December-March (the time of year when AR activity is often highest) precipitation accumulation occurs more quickly at mid- and end-century compared to the historical period, indicating that more of the annual total precipitation could come clustered in these midwinter months. This December–March amplification of the rate of precipitation is consistent with more

AR days and higher conditional intensity on AR days (Figure 3.1.3). Second, despite the slight increase in the water year total precipitation by end-century, the fraction of precipitation delivered by ARs grows steadily, from ~35% historically to ~45% by mid-century and ~52% by end-century. This highlights that ARs will play a larger role in shaping California's future water budgets. The increased contribution of precipitation from ARs at a faster rate could be important for both water-supply and flood-management operations, particularly if that precipitation comes more in the form of rainfall rather than snowfall.

Figure 3.1.3
LOCA2 Ensemble: Precipitation Intensity (mm per day)



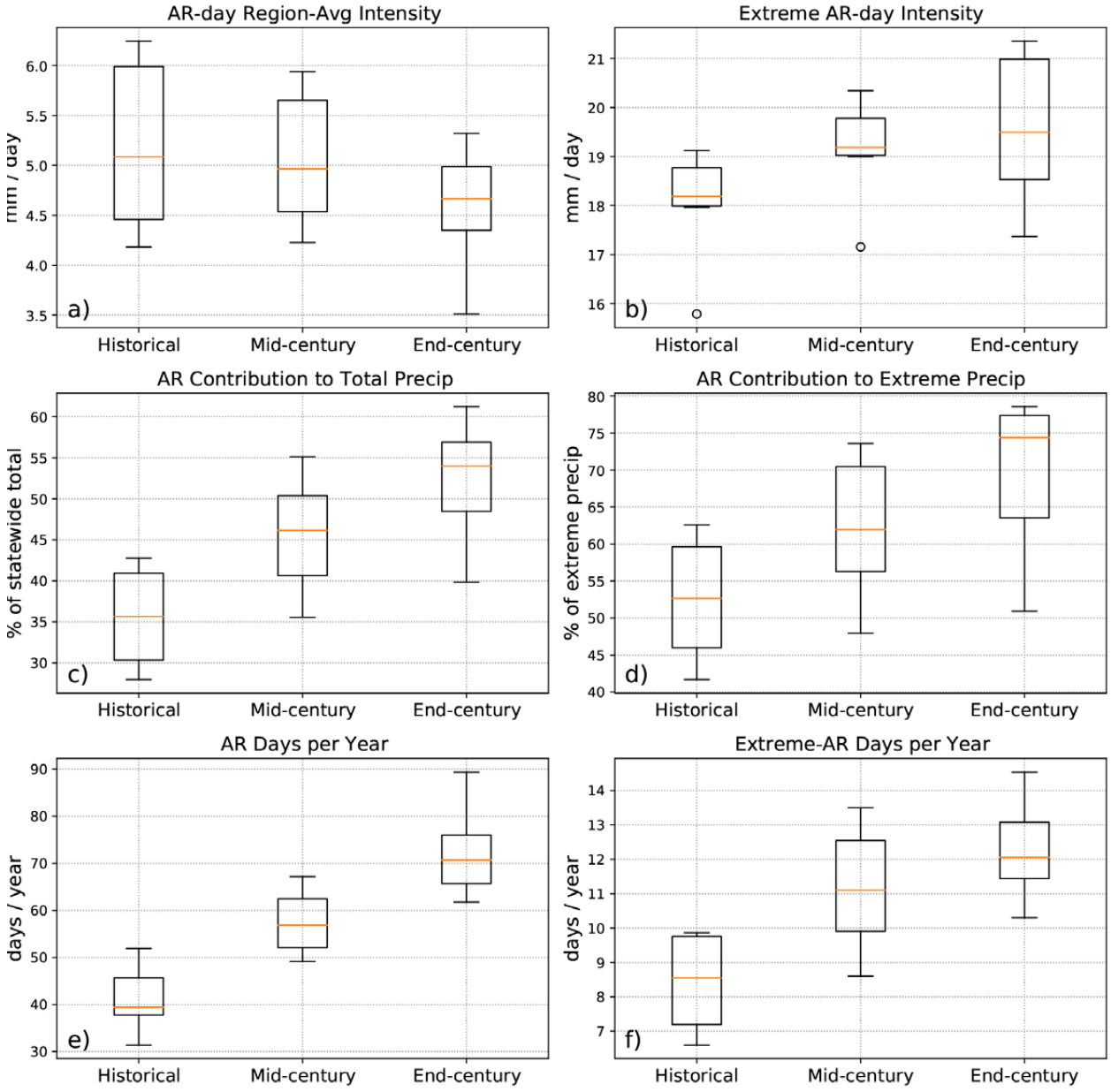
Multi-model mean of LOCA2 historical (1980–2010) precipitation intensity (first column) and absolute changes from mid-century (2040–2070; second column), and end-century (2070–2100; third column) for annual total precipitation (first row), AR-ETC contributed precipitation (second row), and AR-only contributed precipitation (third row).

We now shift from a water year total perspective to a more granular perspective with particular focus on the intensity of precipitation on storm days. Figure 3.1.3 shows the historical mean daily precipitation intensity and the absolute change in intensity under SSP585 at mid- and end-century. The historical pattern in daily precipitation rates mirrors the water year total precipitation changes described earlier. A clear maximum in precipitation rates is seen along the North Coast and windward portions of the Sierra Nevada and a minimum in Southern California, specifically in the Desert regions. In absolute terms, precipitation intensification is modest statewide, with typical increases of a few millimeters per day in regions with historically frequent heavy precipitation. Over Northern California, AR-related precipitation intensity tends to decrease by end-century for both AR-only and AR-ETC events, consistent with a shift toward a larger number of weaker AR events. In contrast, Southern California shows small but positive absolute increases in intensity, with AR-ETC events strengthening more than AR-only events. Notably, changes in precipitation intensity can reflect a shift in the frequency of weaker vs. stronger events, or overall intensification of individual events, both of which can contribute to future AR-only and AR-ETC hydrometeorological impacts. As shown in the next section (Figure 3.1.4), extreme ARs strengthen across all regions, including Northern California, even as the mean AR-day intensity weakens in some regions due to an increased frequency of weaker AR occurrences. Together, these distributional changes offer a more complete view of how AR-related precipitation characteristics evolve in a warming climate.

3.1.2 Future AR-contributed precipitation is driven by extreme events

We now isolate precipitation characteristics in the most extreme AR-only and AR-ETC events, since these events play a key role in flood planning. Extreme AR days are defined as AR-related extreme precipitation days that exceed the 95th percentile of the historical region-wide mean daily precipitation days (days without precipitation were excluded from this calculation). We apply this same 95th percentile historical threshold at mid- and end-century. Figure 3.1.4 summarizes how extreme AR events contribute to California-wide annual precipitation totals relative to all AR events. We describe three key findings. First, ARs become more dominant in shaping California's total and extreme precipitation. The AR contribution to the statewide total rises from ~30–40% historically to ~40–50% by mid-century and ~50–55% by end-century. This contributional increase to precipitation is even more pronounced for extremes, where ARs contribute ~45–60% of the precipitation historically and steadily increase to ~55–70% by mid-century and ~65–80% by end-century. Second, a larger fraction of the water year is influenced by AR conditions. The number of AR days increases by ~75% by end-century, coinciding with an increase in AR event counts and longer AR durations (Table 3.1.1). Specifically, the number of extreme-AR days also increases by ~40% at end-century. Third, consistent with Figure 3.1.3, AR-day mean precipitation intensity (averaged over all AR days) changes slightly and negatively, whereas precipitation intensity on extreme-AR days strengthens.

Figure 3.1.4

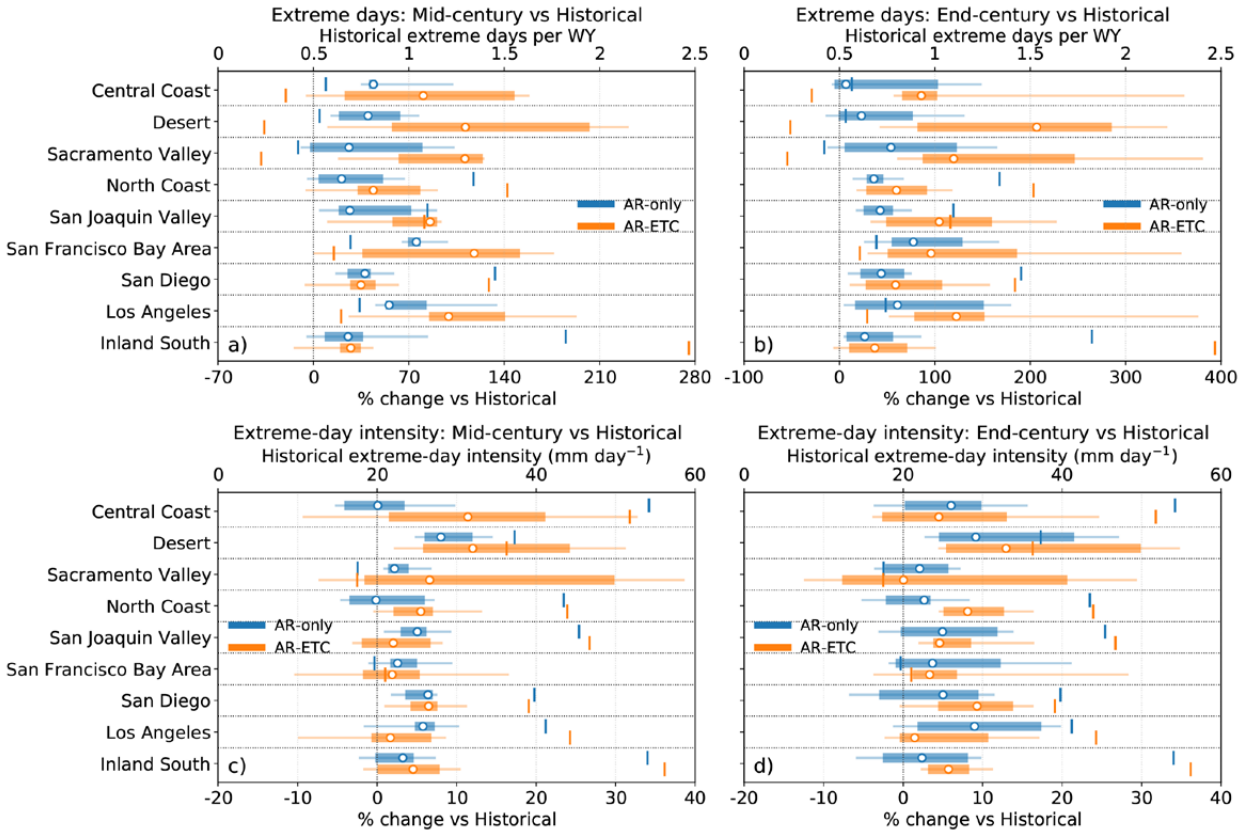


Region-averaged AR-related precipitation intensity (first row), AR contribution to precipitation (second row), and AR days per year (third row) for all AR events (left column) and only the most extreme AR events (right column). Boxes show the 25th–75th percentile range across models, the horizontal red line is the median, and whiskers indicate the 5th–95th percentile.

In summary, statewide AR statistics show that AR days increase and the most extreme ARs intensify across the multi-model ensemble, indicating that ARs will continue to play an increasingly dominant role in California's precipitation trends. Regional

patterns (i.e., Northern California versus Southern California), and differences between AR-only and AR-ETC extremes, are shown in Figure 3.1.5 and highlight important spatial heterogeneity in the magnitude of these changes. Our results underscore a few key messages for AR impacts: California-wide water year total precipitation changes have less certainty in the sign and magnitude of change (as these depend on the model used, region of California assessed, and if mid-century or end-century changes are evaluated). Yet, across models used, regions assessed, and at mid- and end-century, projections of California-wide water year total precipitation show more consistency in the fact that extreme ARs will account for more of the AR-related precipitation (because they both intensify and occur more frequently), increasing exposure to AR-related flood risk (particularly when saturated soils and ripened snowpacks are present). These enhanced flood risks could also challenge historical assumptions in reservoir operations and flood planning (e.g., necessary flood pool spaces) and engineering design standards (e.g., intensity-duration-frequency curves). Notably, there are important inter-model variances in projected change to extreme precipitation over the western United States, including spatial and magnitude differences across models and regions of California (i.e., Northern California versus Southern California), as discussed in previous studies (Pierce et al., 2023; Choi et al., 2025).

Figure 3.1.5



Boxplots of percentage changes in the number of extreme AR days and extreme AR precipitation intensity across Fifth Assessment regions per water year (WY). The white dots denote the median of LOCA2 multi-model estimates. The dark bars show the quartiles (25th and 75th percentile) and the whiskers represent the deciles (10th to 90th percentile) across models. The vertical lines represent the historical baseline precipitation rates (upper x-axis) associated with AR-ETC and AR-only events.

We now examine future changes in the frequency and intensity of precipitation within extreme AR-only and AR-ETC events and if those changes differ across Fifth Assessment regions. The number of extreme-AR days increases in most regions, with AR-ETC events generally showing larger median increases than AR-only events. The relative percentage increases are strongest over the Central Coast, San Francisco Bay Area, Sacramento Valley, and Desert regions. Note that regions with small historical baselines (e.g., Southern California regions) can result in larger percentage changes in the future. Smaller relative changes occur over the North Coast and Southern California regions, except for Los Angeles. A consensus is found across Fifth Assessment regions that extreme AR-only and AR-ETC precipitation intensity increases in the future. However, differences in the magnitude and sign of relative precipitation change between AR-only and AR-ETC extreme events is mixed across

the Fifth Assessment regions. LOCA2 projections show that AR-ETC precipitation strengthens from mid- to end-century at a faster rate than AR-only precipitation (e.g., North Coast and Desert) and other regions show the opposite trend (e.g., Los Angeles). Overall, Figure 3.1.5 emphasizes that future projections indicate that both more extreme-AR days and higher precipitation intensity on those days could occur, expanding the role that AR events play in California's precipitation trends. Figure 3.1.5 also highlights important precipitation-related uncertainty that could arise at the regional scale across model projections. The widest spread in the percentage change of extreme-AR days occurs in Southern California, including the Los Angeles, San Diego, Inland South, and Desert regions. In these regions the model spread is broad, especially for AR-ETC events, indicating strong inter-model disagreement on how frequently extreme AR events occur in the future. Notably, Patricola et al. (2022) showed that dynamically downscaled storyline simulations over the Bay Area indicated that AR-ETC precipitation displays consistent positive increases in precipitation rates with warming, while AR-only storms show both positive and negative precipitation changes in the future. Our results indicate that the Central Coast and, to a lesser extent, San Francisco Bay Area exhibit notable model spread, and, in line with those findings of Patricola et al. (2022), AR-only events show a wider spread by end-century. By contrast, the North Coast and Sacramento Valley display tighter spreads and more inter-model consistency.

3.1.3 Competing mechanisms in future precipitation projections

We posit that there are two main competing mechanisms controlling California's future precipitation changes. First, a fully saturated and warmer atmosphere is moister because of the Clausius-Clapeyron (C-C) relationship (Allen & Ingram, 2002). This 19th-century empirical thermodynamic rule (C-C scaling) states that saturation-specific humidity increases at about 6–7% per degree centigrade warming. Second, despite increases in AR-only and AR-ETC events, there could be fewer total storms reaching California (e.g., ETC events; Lopez-Marti et al., 2025), a possible consequence of large-scale dynamical changes (Gershunov et al., 2025) coming from the CMIP6 global models that were downscaled in the LOCA2 and LOCA2-Hybrid datasets.

Table 3.1.2

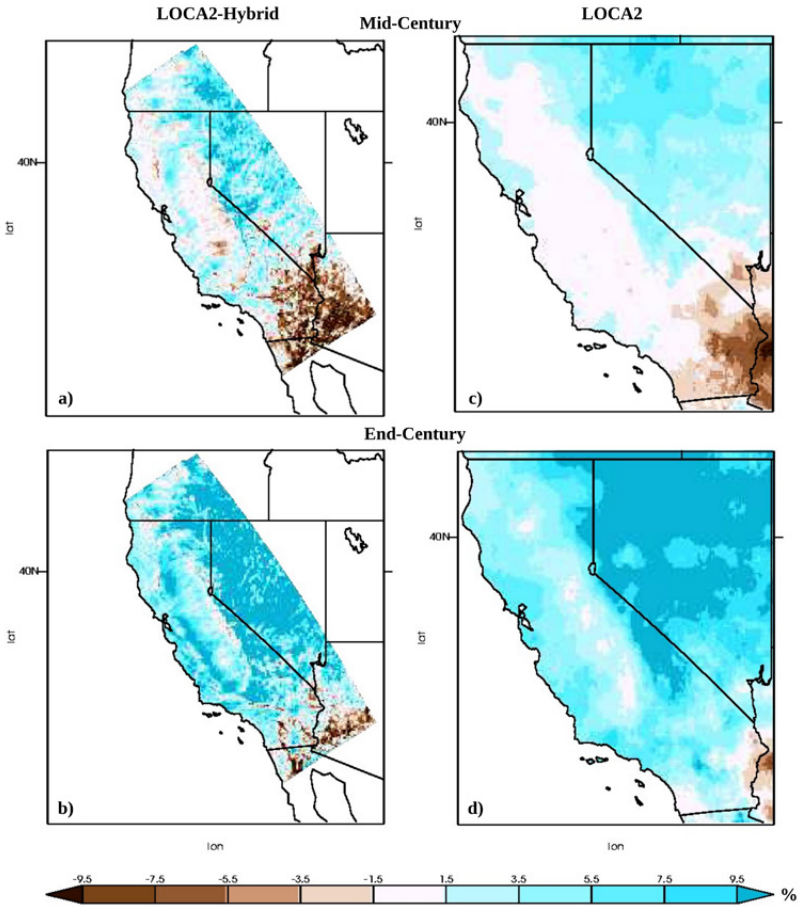
Storm Type	Historical (1980-2010)	Mid-century (2040-2070)	End-century (2070-2100)
	Precipitation days per water year	Precipitation days per water year	Precipitation days per water year
AR-ETC	8.7±2.3	10.8±3.1	12.9±2.5
AR-only	8.5±0.7	11.8±1.8	12.4±1.8
non-AR	43.9±3.7	38.0±4.8	32.4±4.8
	Region-averaged precipitation intensity (mm per day)	Region-averaged precipitation intensity (mm per day)	Region-averaged precipitation intensity (mm per day)
AR-ETC	11.6±0.8	12.5±0.6	12.6±1.0
AR-only	12.0±0.9	12.1±0.4	12.1±1.1
non-AR	7.2±0.3	7.5±0.5	7.4±0.8

LOCA2 multi-model mean, regional-averaged AR-only, AR-ETC, and non-AR precipitation days and daily intensity over California for historical, mid-century, and end-century climatological periods. Only days with precipitation larger than 2.5 mm are selected. 95% mean confidence intervals are provided as plus minuses.

The combined effect of decreasing non-AR precipitation days, increasing AR-associated precipitation, and shorter intervals between AR landfalls results in less future storm events overall, that are wetter on average, and more clustered in time. Table 3.1.2 shows that non-AR precipitation days decline substantially from historical to end-century, while AR-only and AR-ETC precipitation days increase and become a larger fraction of the wet season. Despite this compositional shift, total precipitation days decrease modestly, and AR-day intensities change only slightly. Notably, not all AR landfall days have precipitation. Therefore, the number of AR-precipitation days shown in Table 3.1.2 is a subset of AR landfall days from Table 3.1.1 (calculated by multiplying event numbers and event durations). As shown in Figure 3.1.6, fewer storms in mid-century lead to drying in Southern California and weak changes (sub C-C scaling) elsewhere. However, by end-century, although there are fewer storms, they become wet enough to counteract the decrease in storm frequency, resulting in a nearly statewide increase in annual precipitation totals. The sign and magnitude of precipitation change is spatially consistent between LOCA2 and LOCA2-Hybrid simulations at mid- and end-century. Some differences arise in California's coastal

regions (more precipitation enhancement in LOCA2-Hybrid), southern regions (more drying in LOCA2-Hybrid), and the leeside of mountains (more enhancement in LOCA2-Hybrid). Additionally, comparisons of the Fifth Assessment-provided WRF simulations to their LOCA2-Hybrid counterparts (not shown) reveal a general consistency in the spatial pattern, magnitude, and sign of the percent change in annual mean precipitation. This is not unexpected as the LOCA2-Hybrid algorithm is partially informed by these WRF simulations. Notably, three of the five WRF models show decreases in annual mean precipitation when downscaled either statistically or dynamically. This finding highlights a clear uncertainty in how California mean precipitation will respond to future warming. However, despite this uncertainty in mean precipitation change, there is high confidence (based on multiple lines of evidence in this manuscript and the broader literature) that extreme precipitation from AR events, and specifically AR-ETC events, will increase with warming.

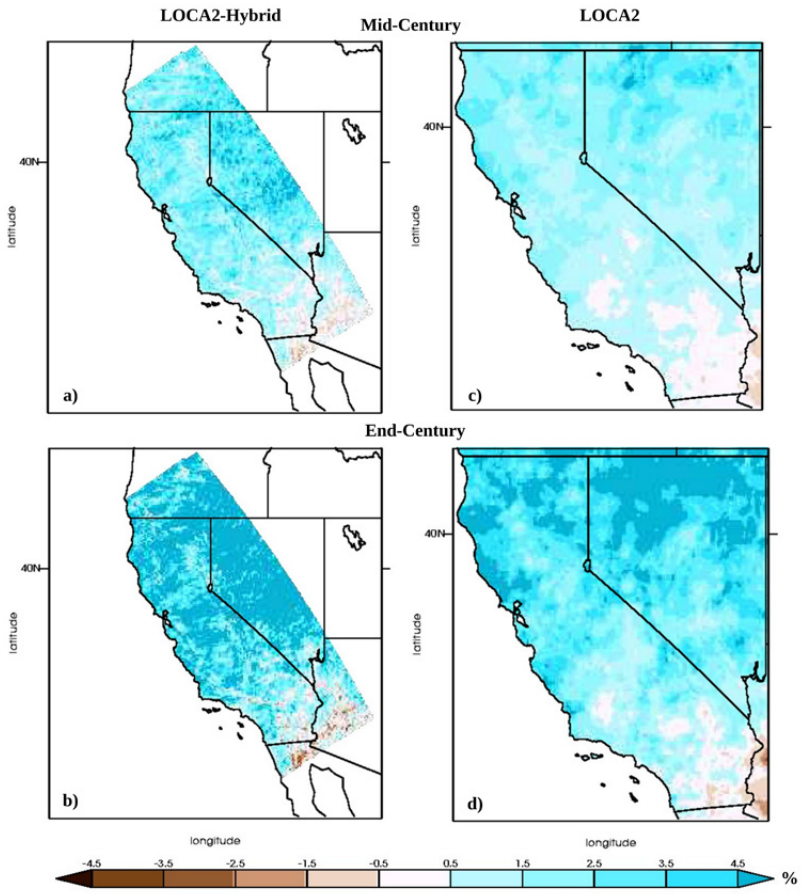
Figure 3.1.6



Unweighted multi-model annual mean precipitation percentage changes of LOCA2-Hybrid (a-b) and LOCA2 projections (c-d) at mid- and end-century (first and second row, respectively) relative to the historical reference period (1981–2010) under the SSP370 scenario.

Percent changes in the twenty-year return value of the annual maximum daily precipitation at mid- and end-century from the LOCA2-Hybrid and LOCA2 simulations are shown in Figure 3.1.7. The twenty-year return value is the precipitation amount that is expected to occur once every 20 years over a long period in a stationary climate and is a useful metric for extreme precipitation (e.g., infrastructure design). In a transient climate, one may consider this metric as the time-varying value that has a 5% chance of occurrence in any given year. We note that most extreme precipitation is associated with ARs (as shown in more detail in Section 3.1.2). As with mean precipitation changes at mid- and end-century, the 14 statistically downscaled CMIP6 models vary greatly from one to the next. Part of this variation is from the above-mentioned natural variability in storm count, and part is due to model structural uncertainty (Lafferty & Sriver, 2024). However, with only a single realization (or ensemble member) from each model, a separation of these two sources of uncertainty cannot be performed. Because of the data limitations of LOCA2 and LOCA2-Hybrid, confidence in the magnitude of future precipitation change is low. However, our confidence in the general message of fewer but more intense storms is high.

Figure 3.1.7



Unweighted LOCA2-Hybrid (a-b) and LOCA2 (c-d) multi-model mean projections of percentage changes in extreme precipitation (20-year return value) at mid- and end-century (first and second rows, respectively) relative to the historical reference period (1981–2010) under the SSP370 scenario.

The larger CMIP6 global model ensemble robustly exhibits scaling in extreme precipitation according to the C-C relationship (Li et al., 2021). As the atmosphere is fully saturated in extreme storms, one would expect that extreme precipitation would also increase at this scaling rate in the absence of either local or large-scale dynamical changes (e.g., changes in the Jet stream location and spatiotemporal variability). However, fine-scale global and regional model results reveal that extreme precipitation often increases at super C-C rates because of complex local storm dynamical changes (Patricola et al., 2022) and/or thermodynamic feedbacks (Rhoades et al., 2024) that cannot always be simulated in the coarse CMIP6 global models because of their coarse horizontal resolutions (>100 km grid spacing).

We also note that high-resolution simulations reveal a complex pattern of sub- and super-C-C scaling of extreme AR precipitation in California, dictated in part by its complex topography that can act to enhance (leeside) and suppress (windward) precipitation efficiencies in a warmer world (discussed later and in Rhoades et al., 2024). Comparison of Figure 3.1.7 with warming rates (not shown) reveals that for all three future emission scenarios, the multi-model LOCA2 and LOCA2-Hybrid precipitation projection estimates scale, almost everywhere, at sub-C-C rates. Also unusual is that the percent changes in extreme precipitation are less than the mean precipitation changes, contrary to most other projections (Easterling et al., 2017). The reasons for these differences between the parent CMIP6 models and the downscaled LOCA2 estimates are unclear. With only 14 realizations, one cannot rule out the chance that the choice of downscaled simulations has fewer California storms than the entire CMIP6 ensemble. However, it is also possibly a result of the treatment of the tails of the precipitation distribution by the statistical downscaling algorithm. Siler et al. (2026) provides some guidance on this (e.g., LOCA2 algorithms use of quantile mapping). In general, extreme precipitation percent changes are larger in the hybrid and dynamically downscaled simulations than in the statistically downscaled products.

3.2 Deciphering the physical mechanisms for AR characteristic changes using storyline simulations

The WRF storyline approach enables us to better understand how warming influences AR-only versus AR-ETC characteristic changes, particularly for decision-relevant impacts (e.g., flood potential). This is because dynamical downscaling of storyline events can lead to better insights on the physical feedbacks that give rise to changes in precipitation totals—scaling, phasing, and efficiency and land surface feedbacks—with warming that can't necessarily be pinpointed in statistical downscaling based approaches. In this section, we outline how AR-only and AR-ETC-related characteristics were influenced by warming for the three storyline flood events and answer the following questions:

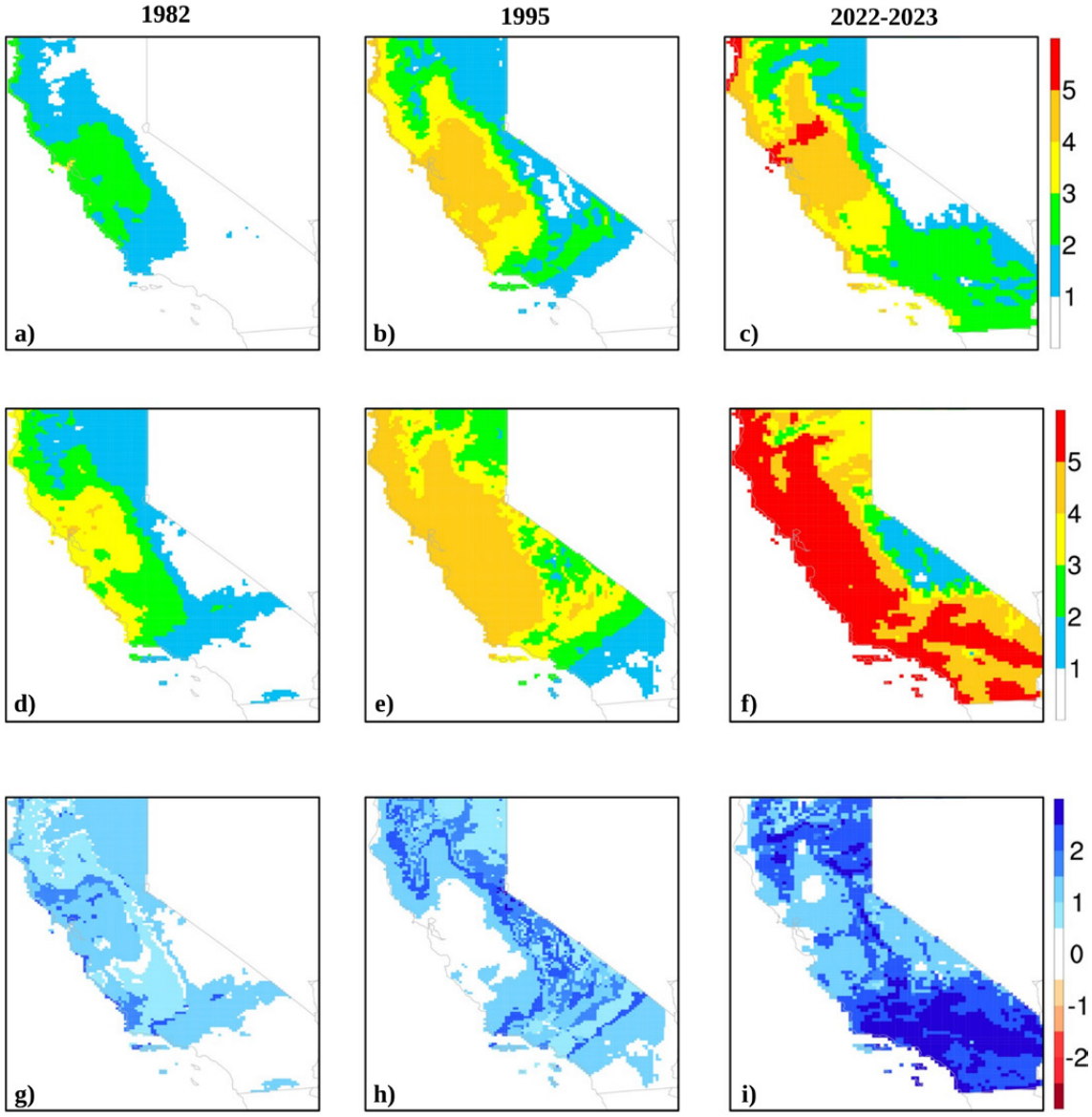
1. Will precipitation from historically impactful AR-only and AR-ETC events respond differently to future warming?
2. How do extreme precipitation rates from AR-only and AR-ETC events change in response to future warming?
3. How will future warming affect the frequency of rain-on-snow days in AR-only and AR-ETC events?

3.2.1 AR flood potential is enhanced in the future

Figure 3.2.1 shows the three AR events that reached the highest Ralph et al. (2019) AR Category over their landfall durations in a historical and future, end-century-like warming level (SSP585 scenario), across the three storyline flood events. Notably,

regions with AR Category levels between 3 and 5 are those that indicate the most potential to produce flooding across the 10-member ensemble. Across each of the storyline flood events, in a future, warmer world, the regions where a value of Category 3–5 exists increases across California. The 1982 flood event expands from only reaching Category 3 in the Bay Area to most of the North and Central Coast by end-century. Similarly, although with higher AR Categories reached, the 1995 event also shows an expansion of the Category 3–4 area to most of California, save for Southern California. Most notably, the 2022–2023 storyline event shows marked increases in the area of highest flood potential. In the historical simulations, the Category 3–5 potential is primarily constrained to the Bay Area and North Coast; however in the end-century simulation that area expands to nearly every portion of California (when flood potential is estimated from the entire 10-member ensemble). This underscores that in a warmer world, if another 2022–2023-like storyline event were to happen, the AR associated-benefits during this event (e.g., "drought busting" and reservoir replenishment) could be undermined by an increase in the potential hazards (e.g., flooding, high winds, and debris flows). This is important as the series of AR events in 2022–2023 already produced $5–7 billion dollars in damages, with particular impacts on communities in the Central Coast (e.g., Pajaro Valley and Santa Cruz), Central Valley (e.g., Tulare Basin), and Sierra Nevada (DeFlorio et al., 2024). In later analyses we will analyze if the flood potentials identified by the AR Category scale are realized, as the atmospheric drivers of flood events (e.g., integrated vapor transport and precipitation) do not solely determine if flooding occurs.

Figure 3.2.1



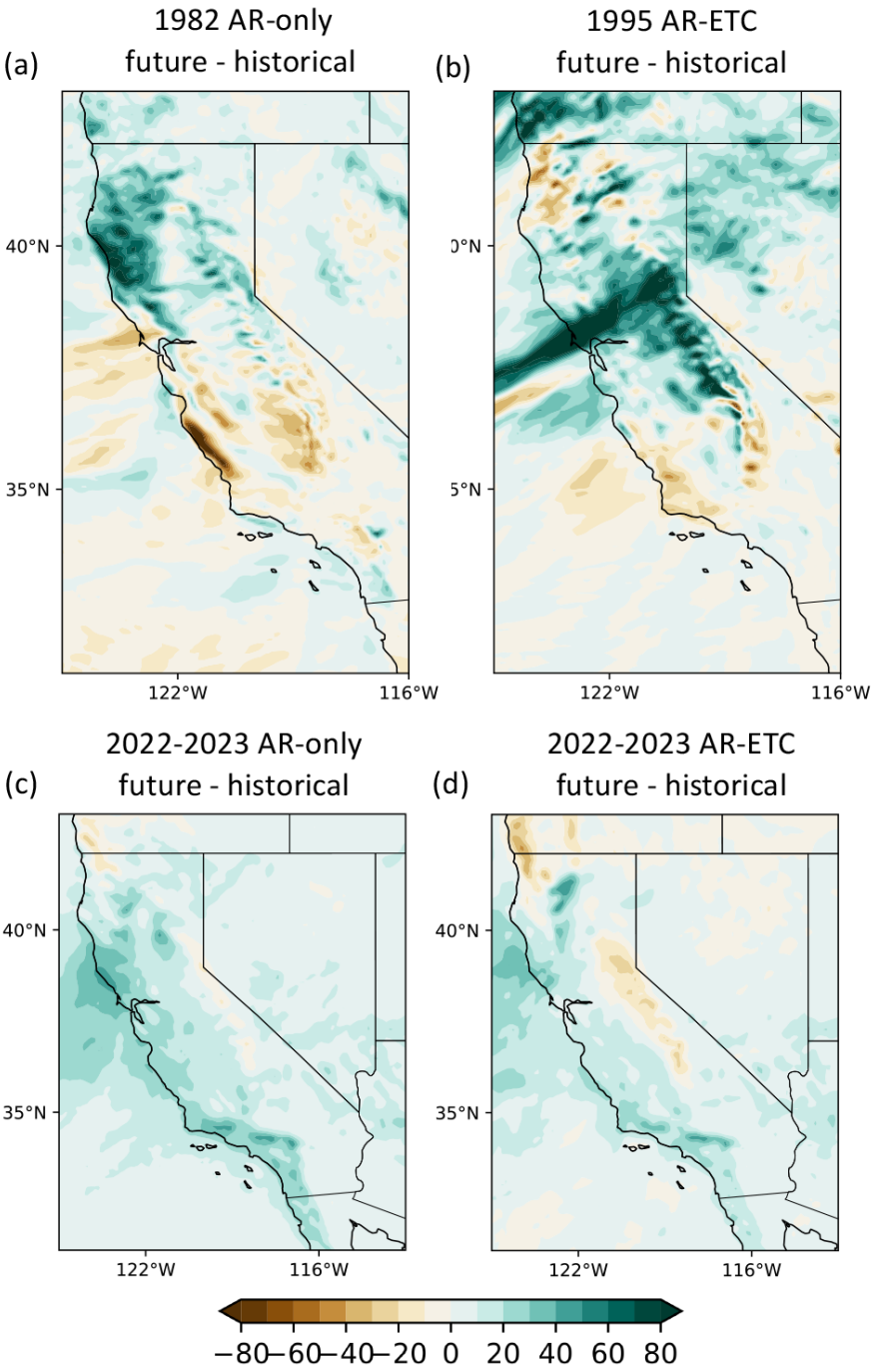
The highest Ralph et al. (2019) AR Category Scale reaching ARs within each of the three storyline flood scenarios. Each gridcell represents the maximum AR Category reached over the duration of the AR landfall across the 10-member ensemble for the historical (a-c) and future (d-f) periods. The differences (future - historical) are shown in g-i).

3.2.2 AR-contributed precipitation is enhanced in the future, although less efficiently over mountains

We next quantify the future changes in event-total accumulated precipitation for the AR-only and AR-ETC events across the three storyline simulations. From Table 2.3.1, the storm total precipitation is larger in the future compared to the historical

for the 1982, 1995, and 2022–2023 simulations, indicating a robust future increase in statewide precipitation across all storyline events. To examine changes in the spatial distribution of historical and future precipitation, Figure 3.2.2 shows the difference between the ensemble-averaged future minus historical accumulated precipitation for the (a) AR-only 1982 simulation, (b) AR-ETC 1995 simulation, (c) AR-only events from the 2022–2023 simulation, and (d) AR-ETC events from the 2022–2023 simulation. More information about the storm structure (e.g., precipitable water, pressure and wind fields) and response to warming can be found in Patricola et al. (2022). The event-total accumulated precipitation was averaged across all AR-only and AR-ETC events for the 2022–2023 simulation (spanning several weeks), which is why the differences shown in panels (c) and (d) are more muted compared with the shorter duration (spanning multiple days) event differences shown in panels (a) and (b).

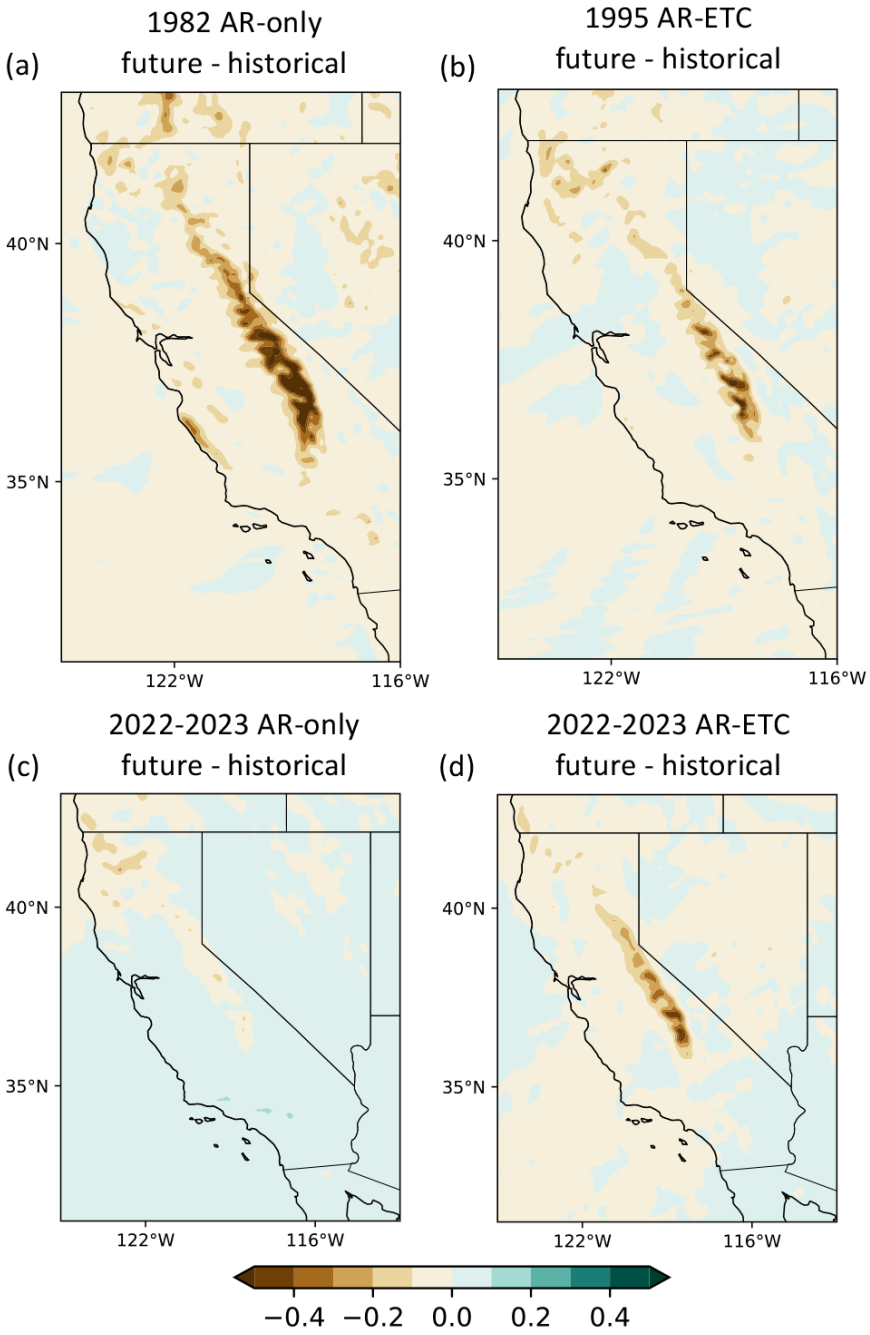
Figure 3.2.2



Event-total accumulated precipitation differences (unit: mm) from the future minus historical WRF simulations for the (a) 1982 AR-only event, (b) 1995 AR-ETC event, (c) 2022–2023 AR-only events, and (d) 2022–2023 AR-ETC events.

Overall, a future increase in California-wide event-total accumulated precipitation is projected for both AR-only and AR-ETC events (Figure 3.2.2), although decreases are found in regions of California (e.g., mountainous regions). The event-total accumulated precipitation from the 1982 AR-only and 1995 AR-ETC had a stronger precipitation response to future warming than the 2022–2023 results, which demonstrates that individual events will likely have localized responses to a warmer climate that may not be indicative of the average response of AR-only and AR-ETCs to climate change. With future warming, the event-total accumulated precipitation from the 1982 AR increased in Northern California and decreased along the Central Coast, whereas the 1995 AR-ETC produced a strong increase over the Bay Area, Central Valley, and Sierra Nevada. In contrast, the average precipitation response of the AR-only and AR-ETC events to future warming in the 2022–2023 simulation shows that event-total accumulated precipitation increased along the entire California coastline and decreased in the Sierra Nevada. Despite some disagreement among the different storyline simulations, there is good agreement that both AR-only and AR-ETC events will produce a future increase in event-total accumulated precipitation California-wide, most notably in the North Coast which shows a future increase in all panels in Figure 3.2.2. This is, at least qualitatively, in agreement with the LOCA2-based analyses in Section 3.1.

Figure 3.2.3



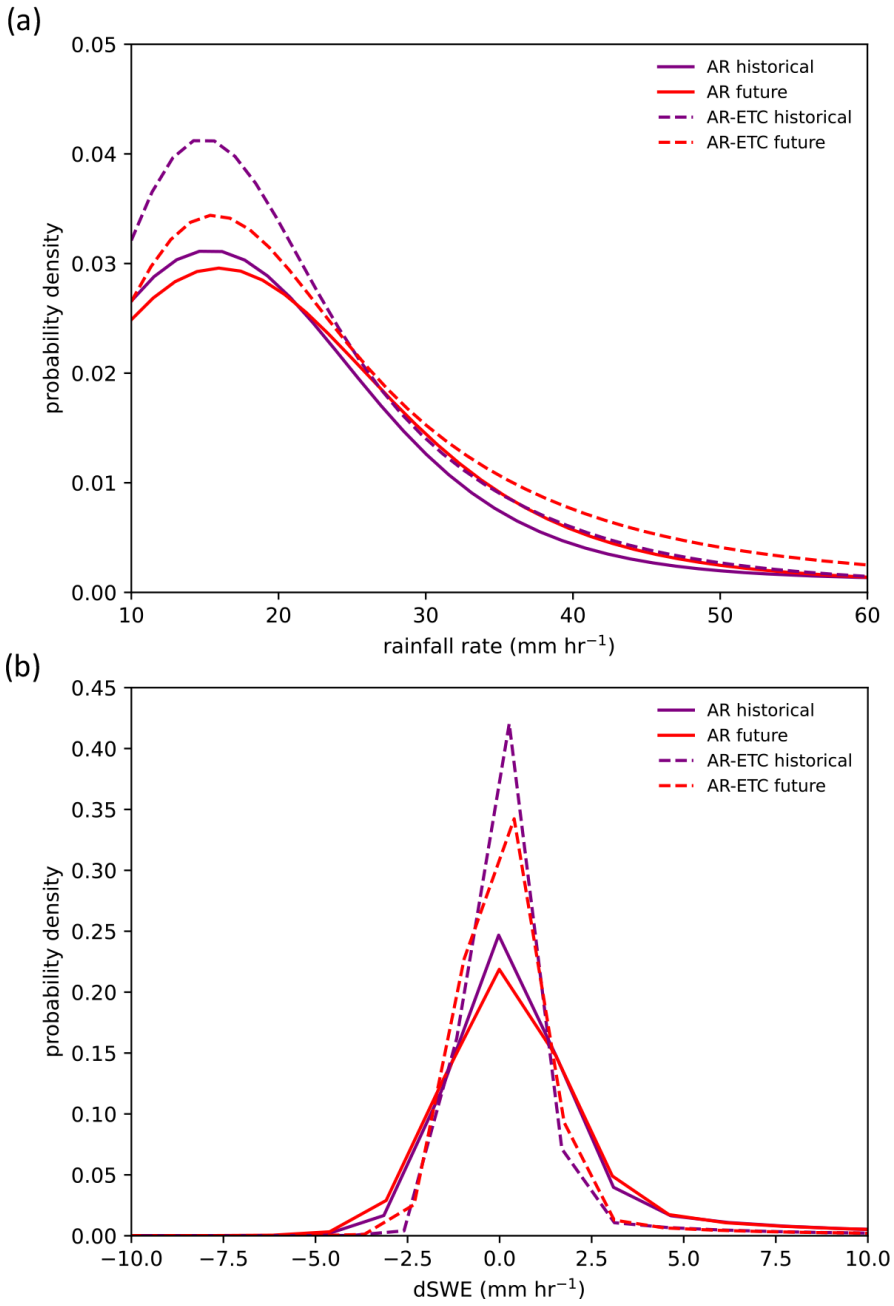
Precipitation efficiency differences from the future minus historical WRF simulations of the (a) 1982 AR-only event, (b) 1995 AR-ETC event, (c) 2022–2023 AR-only events, and (d) 2022–2023 AR-ETC events.

To further examine changes in precipitation, we next consider precipitation efficiency. Precipitation efficiency is the ratio of the water that is lost from the atmosphere through precipitation to the available moisture in the atmosphere, or event-total precipitation divided by the event-total integrated water vapor (Dacre et al., 2023). From an area mean perspective, precipitation efficiency associated with California ARs has been found to span from close to zero to 0.3(Zhou et al., 2025), although higher values can be found in localized regions of mountains (Rhoades et al., 2024). Values of precipitation efficiency that are greater than one indicate that during the simulation a hydrometeor formed in one grid cell, but was then advected and fell out as precipitation in another grid cell. Precipitation efficiency greater than one has been found in the Sierra Nevada (Rhoades et al., 2024), and is likely due to the slower hydrometeor fall rate of snowfall when compared to rainfall, which leads to a more frequent advection of snowfall to neighboring grid cells. Values of precipitation efficiency less than one indicate that a portion of the atmospheric moisture did not fall out as precipitation. Figure 3.2.3 shows the difference between the ensemble-averaged future minus historical precipitation efficiency for the (a) AR-only 1982 simulation, (b) AR-ETC 1995 simulation, (c) AR-only events from the 2022–2023 simulation, and (d) AR-ETC events from the 2022–2023 simulation. As in Figure 3.2.2, the precipitation efficiency was averaged across all AR-only and AR-ETC events for the 2022–2023 simulation. All panels of Figure 3.2.3 indicate a future decrease in precipitation efficiency in the Sierra Nevada, particularly in the windward portion, which is consistent with previous research on future changes in precipitation efficiency in mountainous regions (Eidhammer et al., 2018; Rhoades et al., 2024). This result suggests that for future AR-only and AR-ETC events, a smaller fraction of the available precipitable water would reach the ground as precipitation in the Sierra Nevada. Decreases in mountainous precipitation efficiency in a warmer world could be due to increases in static stability (which inhibits orographic uplift), increases in the lifting condensation level, and alterations to in-cloud processes that shape the form and fate of precipitation (Siler & Roe, 2014; Rhoades et al., 2024). The large future decreases in precipitation efficiency in the high elevation portions of the Sierra Nevada in Figure 3.2.3 are also likely a function of more precipitation falling as rainfall in a warmer world, which is less likely to be advected to a downstream or neighboring grid cell due to a faster hydrometeor fall rate than snowfall (Rhoades et al., 2024). Additionally, the future decrease in precipitation efficiency in the high elevations of the Sierra Nevada is likely a driving factor for the future decrease in accumulated precipitation seen in the same region in Figure 3.2.2. Such changes in precipitation efficiency could have important implications for future water resources in mountainous regions and downstream communities, particularly if there is less water stored as snowpack (due to shifts from snowfall to rainfall with warming) and drier soils over which that rainfall occurs. This will be explored in more detail in the next section.

3.2.3 AR-ETC events produce more extreme precipitation rates and AR-only events have more rain-on-snow potential

In addition to examining the event-total accumulated precipitation across AR-only and AR-ETC events, we also evaluate changes to extreme precipitation rates, which are important for local-scale flooding and debris flows. We calculated probability density functions (PDFs) using the precipitation data from all model grid points over California and over the lifetime of each storm event, across all 10 ensemble members. The calculation is intentionally different from the accumulated precipitation shown in Figure 3.2.2, so that we can retain information regarding extreme rainfall rates, rather than smoothing them out by using ensemble-averaging. Figure 3.2.4 shows PDF curves of (a) the precipitation rate and (b) the change in snow water equivalent (dSWE) for all historical and future AR-only and AR-ETC events from the 1982, 1995, and 2022–2023 simulations. The PDF curves shown in Figure 3.2.4a demonstrate two important results from the WRF simulations. First, there is a future increase in extreme precipitation rates in both AR-only and AR-ETC events, as seen by comparing the righthand tails of the solid (AR-only) and dashed (AR-ETC) purple and red curves in Figure 3.2.4a, which is in agreement with Patricola et al. (2022) and the LOCA2-based analyses presented in Section 3.1. Second, AR-ETC events produce more extreme precipitation rates in the historical and future climate than AR-only events, as seen by comparing the righthand tails of the solid (AR-only) and dashed (AR-ETC) curves. These results suggest that the potential for AR-related extreme precipitation rates, especially from AR-ETC events, will increase with future warming.

Figure 3.2.4



Probability density function curves of (a) the hourly precipitation rates (greater than 10 mm hr-1), and (b) the hourly change in snow water equivalent (dSWE) for the historical (blue) and future (red) WRF simulations across the 1982, 1995, and 2022–2023 AR-only and AR-ETC events.

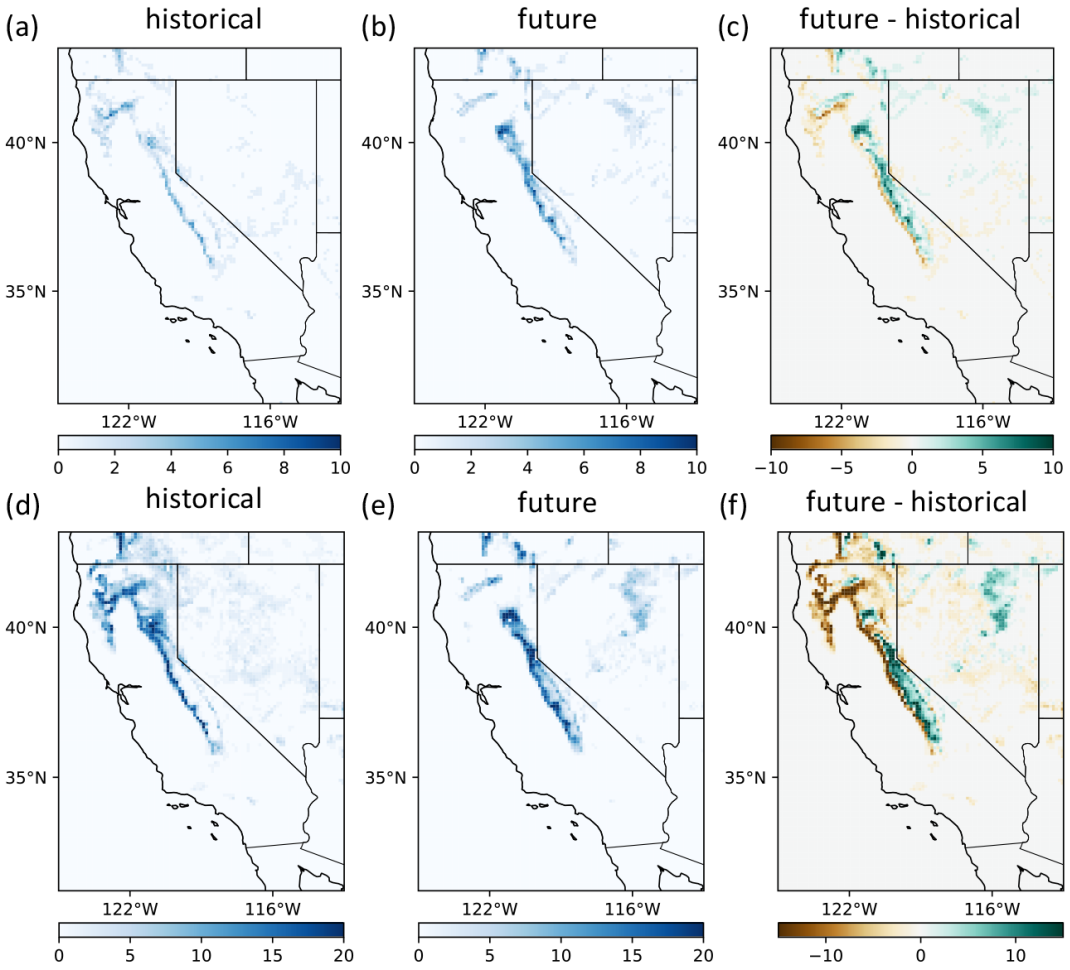
Historically, a large fraction of California's precipitation already occurs at or near freezing (Bales et al., 2006), largely due to AR events (Gonzales et al., 2022).

Therefore, warming will undoubtedly shift more of that precipitation to rainfall and elevate the Sierra Nevada's rain-on-snow potential. Figure 3.2.4b allows us to better understand the differences in precipitation phasing between rainfall and snowfall and changes in the snowpack between the historical and future AR-only and AR-ETC events across the 1982, 1995, and 2022–2023 simulations. A comparison of the AR-only and AR-ETC events in Figure 3.2.4b reveals that the PDF curves for the historical and future AR-ETCs are narrower and skewed to the right toward positive dSWE. This result indicates that AR-ETC events more consistently produce more snowfall than AR-only events. In contrast, the PDF curves for the historical and future AR-only events are wider and centered closer to zero. This result indicates that compared to AR-ETCs, AR-only events produce a wider range of rainfall and snowfall outcomes, which could lead to more rain-on-snow potential.

Rain-on-snow events are particularly hazardous as they can produce rapid snow melt that can lead to dangerous flooding (Henn et al., 2020). To better understand potential differences in rain-on-snow occurrences between AR-only and AR-ETC events, we focus specifically on the 2022–2023 simulation which has a larger sample of storms. Figure 3.2.5 shows the total number of rain-on-snow days for each grid cell across all 10 ensemble members and all AR-ETC and AR-only events for the historical and future simulations. Note that the scales between AR-ETC and AR-only events are different in Figure 3.2.5 as there were more AR-only events (Table 2.3.1). We calculated rain-on-snow days based on Musselman et al. (2018), where a rain-on-snow day occurred when there was 10 mm day-1 of rain falling on snowpack of at least 10 mm SWE, dSWE from the current day to the next day was less than zero, and the fraction of dSWE contributed, at least, 20% to runoff (i.e., dSWE / (dSWE + rainfall rate) ≥ 0.2). It is important to note that although this metric is widely used, it does not account for all possible types of feedback, such as active versus passive snowpacks during rain-on-snow events (Brandt et al., 2022). From Figure 3.2.5, the number of rain-on-snow days increases at higher elevations and decreases at lower elevations in the Sierra Nevada across AR-only and AR-ETC events in the end-century compared to the historical simulation. These changes are likely due to less antecedent snowpack at lower elevations, less snowfall at lower elevations, and more rainfall at higher elevations in a future, warmer climate. The changes are consistent with a dramatic reduction in the area of the freezing level elevation (Figure A.1.1), a key indicator used by water managers to identify rain-on-snow potential (Lynn et al., 2020). AR-only events, and to some extent AR-ETCs, show a future decrease in rain-on-snow days in Northern California, but a future increase in the southern portion of the Sierra Nevada. This result indicates a future latitudinal shift in rain-on-snow risk to the southern Sierra Nevada, most notably for AR-only events. This is particularly important as southern Sierra Nevada has less hardened infrastructure, smaller reservoirs, and fewer monitoring networks than northern Sierra Nevada (Rhoades et al., 2024) and already faced near-record precipitation, flood-stage breaching river

flows, and unusual inundation (e.g., Tulare Basin) at current levels of global warming during the 2022–2023 flood event (CNRFC NOAA Storm Summary of 2022–2023 - https://www.cnrfc.noaa.gov/storm_summaries/dec2022Jan2023storms.php).

Figure 3.2.5



Total number of rain on snow days for each grid cell across all ensemble members for all (a)-(c) AR-ETC and (d)-(f) AR-only events of the 2022–2023 simulation for the (a) (d) historical, (b)(e) future, and (c)(f) future minus historical. Note the different scales between panels (a)-(c) and (d)-(f).

3.3 Northern California infrastructural resilience to future AR-ETC characteristic changes

To this point in the report, we have only assessed AR-only and AR-ETC meteorological changes (e.g., precipitation) and associated impacts on the natural stores of water (e.g., snowpack), without accounting for the influences of infrastructure and

management decisions. Water infrastructure and their operating rules play a central role in the mitigation of flood potential. We now analyze how future changes in hydrometeorological conditions during AR-only and AR-ETC events could influence both natural and managed hydrological systems in Northern California. More specifically, we answer the following questions:

1. How do Northern California streamflow dynamics change during AR-only and AR-ETC events?
2. What land surface conditions most affect streamflow dynamics both prior-to and amidst AR-only and AR-ETC events?
3. Can Northern California reservoirs resiliently respond to future changes in hydrometeorological conditions during AR-only and AR-ETC events?

To answer these questions, we first establish the antecedent land surface conditions for each storyline event. Next, we juxtapose the predicted (i.e., Ralph et al., 2019 AR Category Scale) and realized flood potential from the AR storyline events by examining how streamflow dynamics respond to changes in both the hydrometeorological conditions (e.g., rain-snow transition) and land surface conditions prior-to and amidst the storm events. Finally, we examine how reservoir inflows and outflows, reservoir elevation levels, and total volumetric inflows under historical and future conditions change. For example, we compare the magnitude of the peak inflows and the timing of the peak between historical and future conditions. Notably, the major reservoirs (i.e., Folsom, New Bullards Bar, and Oroville) in the WRF-Hydro simulations utilize historical management strategies (i.e., rule curves).

Because of computational limitations, for each storyline we select three of the 10 ensemble members to run with the WRF-Hydro model, based on the minimum, median, and maximum California-wide event-total accumulated precipitation. Those ensemble members include E7 (maximum), E0 (median), and E8 (minimum) for the 2022–2023 storyline; E0 (maximum), E5 (median), and E7 (minimum) for the 1995 storyline; and E0 (maximum), E3 (median), and E8 (minimum) for the 1982 storyline.

3.3.1 Antecedent land surface conditions shape AR flood potential

The antecedent land surface conditions (e.g., SWE and soil moisture) leading up to the storyline events play an important role in shaping their flood potentials. As such, we ran the WRF-Hydro simulations with observationally-constrained meteorological conditions using the AORC dataset starting on October 1st of each year up to the beginning of the storyline event start date. We then used the WRF-forecasted meteorological conditions during the storyline event.

We find that the antecedent conditions going into each storyline event are distinct (Figures A.1.2 and A.1.3). For example, the SWE conditions prior to the January 3-5, 1982 storm event are among the top five measured between 1980–2024, along with

elevated soil moisture conditions that are the highest soil moisture conditions across the three storyline events. In contrast, prior to the December 10-13, 1995 storm event, record low-to-no snow conditions are measured along with the driest soil moisture conditions across the three storyline events. Last, prior to the series of storm events from December 24, 2022 to January 24, 2023, analogous to 1995, low-to-no snow was observed on December 1, 2022, however, a considerable snowpack developed by January 1, 2023 along with moderate soil moisture conditions.

3.3.2 Northern California infrastructure is resilient to future AR events tested

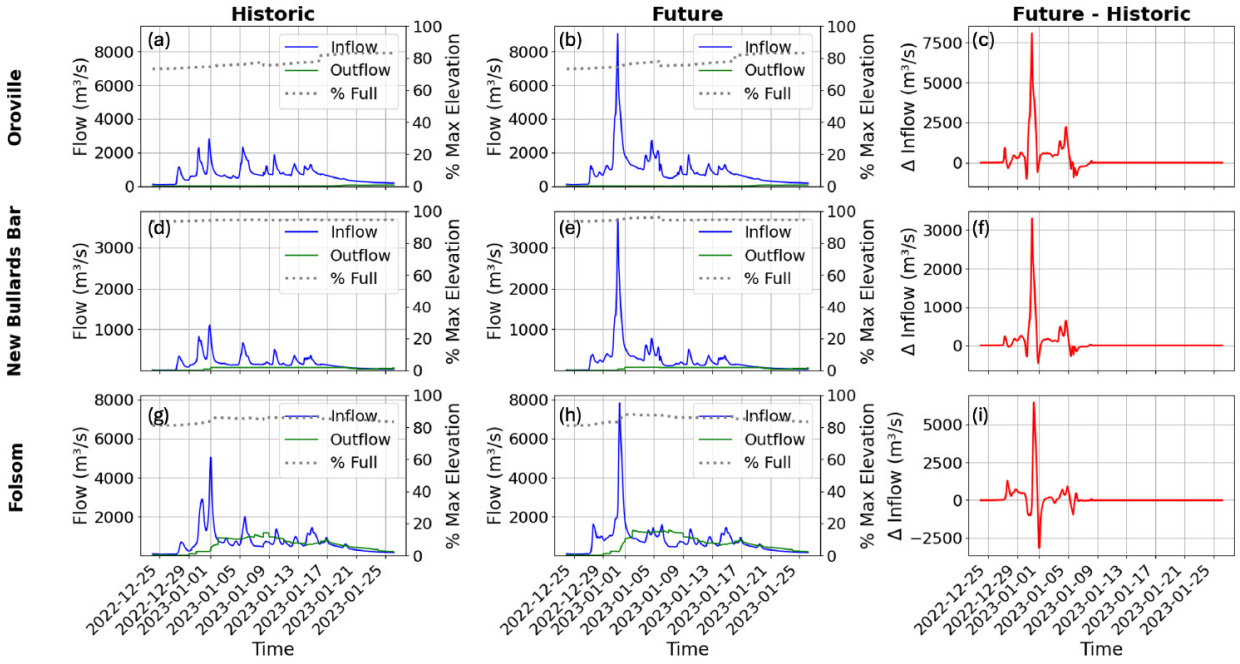
We primarily focus our discussion below on the results of the median ensemble member for each storyline, which are largely representative of the trends across the WRF-Hydro simulations. Results for the maximum and minimum ensemble member for each storyline are available in the Appendix.

3.3.2.1 2022-2023 Storyline

The AR-induced flood potential during the 2022–2023 storyline simulation is drastically increased in a future, warmer world (Figure A.2.1). Notably, a greater share of the state experiences AR Category 4–5 conditions in the future compared to historically, especially along the coastal, mountainous, and valley regions of Northern California. For the median ensemble (E0), these results suggest a potential for more severe flooding in Northern California in the future where a shift from Category 1–2 to Category 3–5 conditions is projected.

Figure 3.3.1

Reservoir Time Series for Ensemble E0



Reservoir inflows, outflows, and percent full for Lake Oroville, New Bullards Bar, and Lake Folsom under historical (a, d, g) and future (b, e, h) conditions from the median ensemble member (E0) WRF-Hydro 2022–2023 storyline simulation. Differences in future minus historical inflows (c,f,i) are also shown. The percent full in the first two columns is the ratio of modeled reservoir elevations to maximum elevations, including flood pool levels.

In line with these AR Category Scale predictions (Figure A.2.1), the future median ensemble member (E0) WRF-Hydro simulations have a significant increase in inflows to the major reservoirs (i.e., Lake Oroville, New Bullards Bar, Folsom) over the December 2022–January 2023 period compared to historically (Figure 3.3.1), especially during the most extreme AR event (December 30, 2022–January 3, 2023). However, our results suggest that the reservoir infrastructure can resiliently receive the higher future inflows with minimal spill needed. For both historical and future simulations, this storyline appears to be a beneficial "fill event", whereby 59% of Oroville's capacity (3.4 million acre-feet (MAF) total reservoir capacity) is filled under the future conditions, compared to 43% of its capacity under historical conditions (Table 3.3.1). For New Bullards Bar (0.97 MAF total reservoir capacity), the filled capacity is 48% in the future compared with 30% historically. Lake Folsom, a reservoir to the south (0.98 MAF total reservoir capacity) on the American River with flood control as its primary function, also fills during the event historically (33.5% of capacity) and in the future (38.9%) but to a smaller extent because of the need to make releases for flood control.

Several factors contribute to the higher future streamflow and subsequent reservoir inflows, particularly during the most extreme AR event during this storyline period (December 30, 2022 to January 3, 2023) (Figure 3.3.2). Adding to the moderate snowpack and volumetric soil moisture levels that had developed by January 1, 2023 (Section 3.3.1), there is an increase in event-total accumulated precipitation, especially in the headwaters of Oroville and New Bullards Bar reservoirs (Figure 3.3.3), consistent with increases seen statewide in the ensemble mean from the WRF forcing (Figure 3.2.2). There is also an increase in snowmelt and elevated volumetric soil moisture levels in the headwaters of the reservoirs over the duration of the extreme AR event (Figure 3.3.3).

In addition to the future set of storms filling a greater share of reservoir capacity over the course of the month, reservoir operators may need to plan for higher peak inflows that occur earlier during an AR event. Our results show that during the most extreme AR event during the storyline period (December 30, 2022 to January 3, 2023) the inflows under future warming have a higher and earlier peak in streamflow (~17 hours earlier), originating from the main stems of the rivers flowing into Oroville and New Bullards Bar (Figure 3.3.2). In summary, we find that under future warming, the 2022–2023 back-to-back series of AR events produce greater reservoir inflows at a higher peak flow rate and earlier timing than occurred historically, but that the reservoirs have sufficient storage space to benefit from filling a significant share of capacity without flooding.

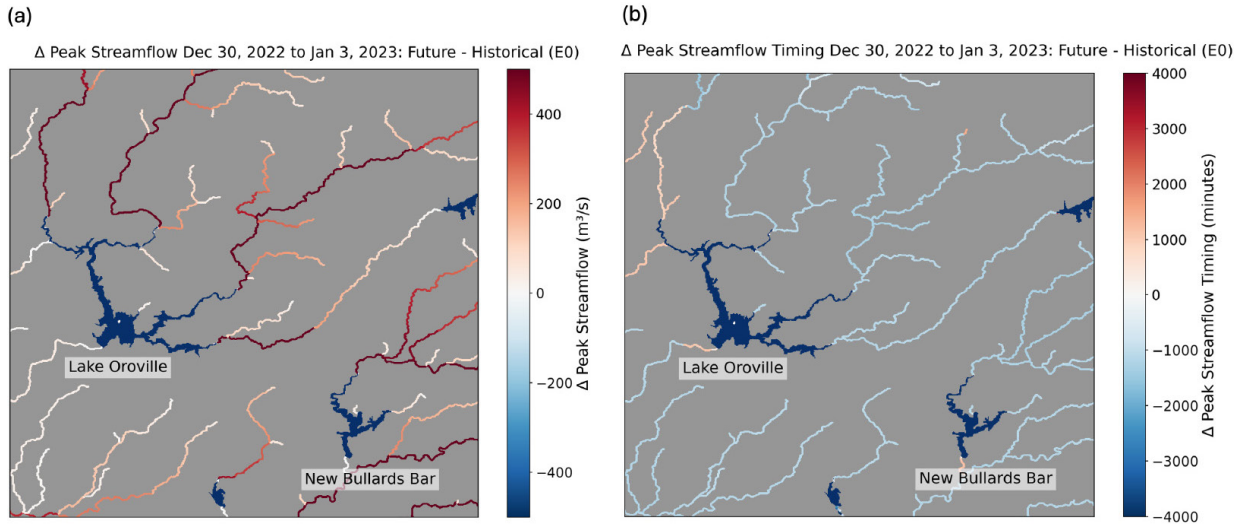
Table 3.3.1

	Total cumulative inflow (MAF)	**Total cumulative inflow (MAF)**	**Total cumulative outflow (MAF)**	**Total cumulative outflow (MAF)**	**Net change in storage from event (MAF)**	**Net change in storage from event (MAF)**	**% share of total capacity Δ from event**	**% share of total capacity Δ from event**
Reservoir (Storage capacity)	Historic	Future	Historic	Future	Historic	Future	Historic	Future
Oroville (3.43 MAF)	1.51	2.05	0.04	0.04	1.47	2.03	43.0%	58.9%
New Bullards Bar (0.97 MAF)	0.39	0.57	0.11	0.11	0.29	0.46	29.5%	48.0%

	Total cumulative inflow (MAF)	Total cumulative inflow (MAF)	Total cumulative outflow (MAF)	Total cumulative outflow (MAF)	Net change in storage from event (MAF)	Net change in storage from event (MAF)	% share of total capacity Δ from event	% share of total capacity Δ from event
Folsom (0.98 MAF)	1.53	1.76	1.21	1.39	0.32	0.38	33.5%	38.9%

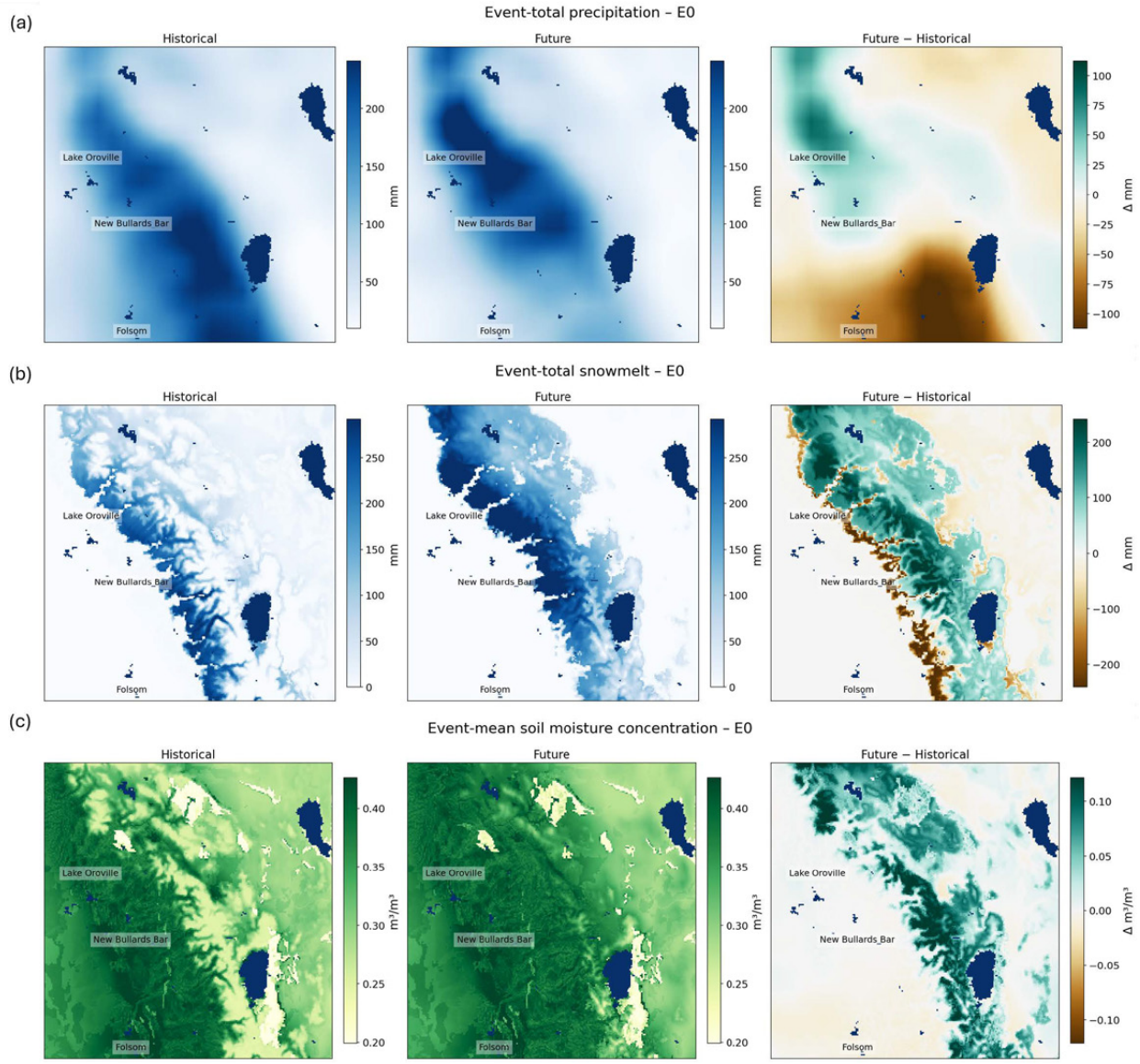
Inflows, Outflows, and Storage changes for December 24, 2022 through January 25, 2023 for Oroville, New Bullards Bar, and Folsom reservoirs for the historical and future median (E0) WRF-Hydro simulation. Each reservoir's total reservoir capacity is provided in parentheses in the first column.

Figure 3.3.2



Future minus historical WRF-Hydro median ensemble member (E0) simulation differences in peak streamflow magnitude (a) and timing (b) for the headwaters of Oroville and New Bullards Bar during December 30, 2022 to January 3, 2023.

Figure 3.3.3



WRF-Hydro simulated event-total for the largest storm of the storyline period (December 30, 2022–January 3, 2023) accumulated precipitation (a), peak SWE during the event (b), event-total snowmelt (c), and event-mean volumetric soil moisture (d) under historical (first column) and future conditions (second column), and inflow differences (future minus historical; third column) from the median (E0) ensemble member of the 2022–2023 storyline.

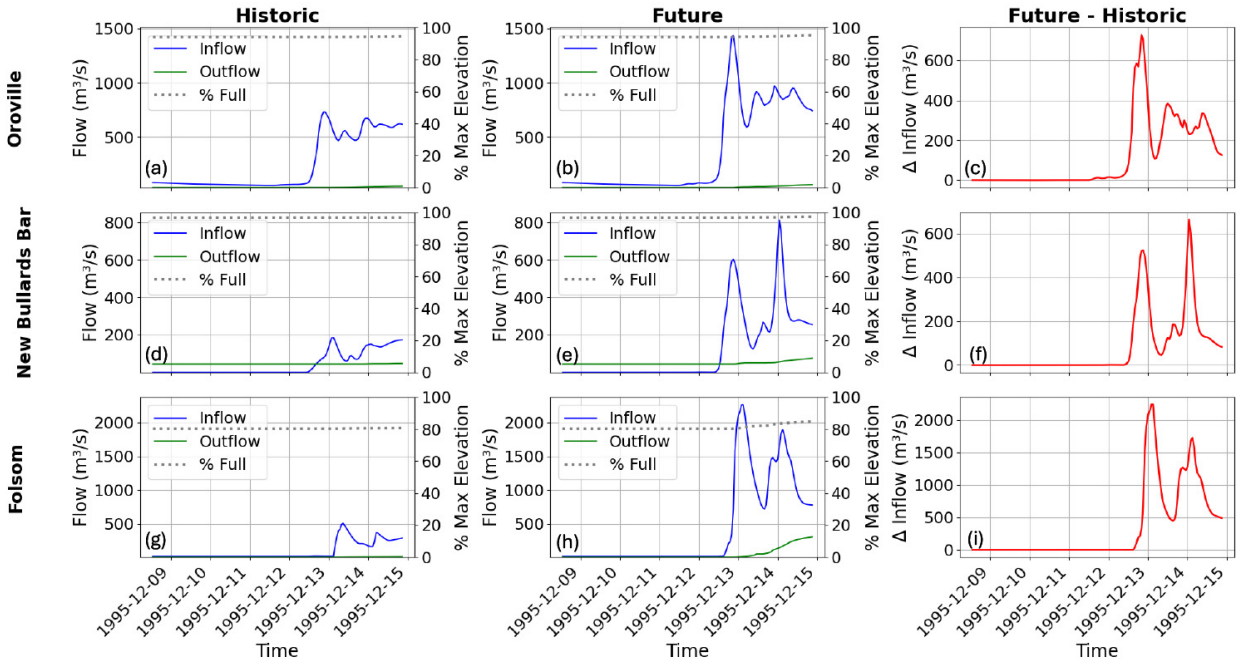
3.3.2.2 1995 Storyline

Similar to the 2022–2023 storyline event, the predicted AR-induced flood potential in 1995 (using the AR Category scale) is substantially increased in a warmer world (Figure A.3.1). This increased flood potential across most of California (save for

portions of Southern California) is spatially consistent across ensemble members. This spatial consistency across ensemble members is because there is less possibility for simulated drift from observed meteorological conditions in the 1995 storyline event (and 1982 storyline event, discussed later) compared with the 2022–2023 storyline event (partly owing to its more spatially constrained inner domain, see Figure 2.3.1). Across ensemble members, a greater area within the state reaches Category 3-4 conditions in the future compared to historically. This is particularly evident over the coastal, mountainous, and valley regions of Northern California. These results suggest a higher potential for flood damages in Northern California in the future.

Figure 3.3.4

Reservoir Time Series for Ensemble E5



Reservoir inflows, outflows, and percent full for Lake Oroville, New Bullards Bar, and Lake Folsom under historical (a, d, g) and future (b, e, h) conditions from the median (E5) 1995 WRF-Hydro ensemble member and differences in future minus historical inflows (c, f, i). The percent full (a, b, d, e, g, h) is the ratio of modeled to maximum reservoir elevations, including the flood pool.

Table 3.3.2

	Total cumulative inflow (MAF)	Total cumulative inflow (MAF)	Total cumulative outflow (MAF)	Total cumulative outflow (MAF)	Net change in storage from event (MAF)	Net change in storage from event (MAF)	% share of total capacity Δ from event	% share of total capacity Δ from event
Reservoir (Storage capacity)	Historical	Future	Historical	Future	Historical	Future	Historical	Future
Oroville (3.43 MAF)	0.07	0.11	0.01	0.01	0.002	0.003	1.7%	2.8%
New Bullards Bar (0.97 MAF)	0.01	0.03	0.02	0.02	0.000	0.001	-0.8%	1.4%
Folsom (0.98 MAF)	0.02	0.12	0.00	0.01	0.001	0.004	2.1%	11.6%

Inflows, Outflows, and Storage Changes for December 10–13, 1995 for Oroville, New Bullards Bar, and Folsom reservoirs for the historical and future median (E5) WRF-Hydro simulation. Each of the reservoir's total reservoir capacity are provided in parentheses in the first column.

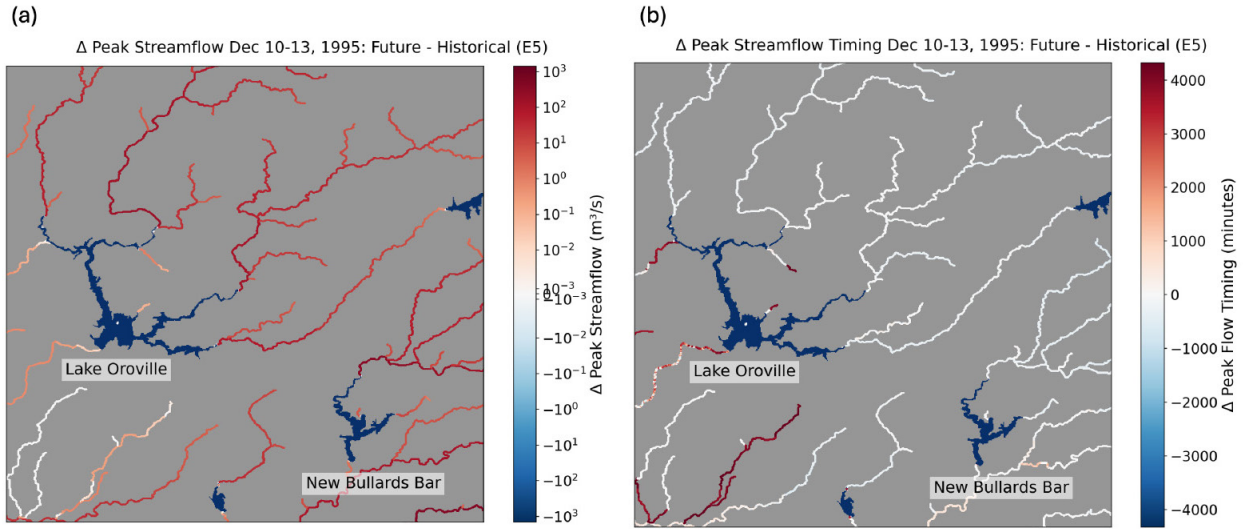
Consistent with the AR Category Scale flood potential predictions, the median (E5) WRF-Hydro simulation indeed sees a dramatic rise in reservoir inflows between December 10–13, 1995 in the future compared to historically (Figure 3.3.4). The peak inflow rates in the future are about two to three times higher than occurred historically for Oroville, New Bullards Bar, and Folsom, and the inflows in the future also exhibit a bi-modal pattern in the hydrograph which differs from historical. The second inflow peak in the future likely occurs because of the enhanced antecedent volumetric soil moisture conditions from the larger event-total rainfall, amplifying the runoff response.

In contrast to the 2022–2023 storyline event, this four-day storm event also fills Folsom more drastically in the future relative to the other reservoirs, filling 11.6% of its total capacity (0.97 MAF), compared to 2.1% of its capacity historically (Table 3.3.2). In comparison, the event contributes 2.8% and 1.4% of Oroville and New Bullards Bar's

capacity in the future, compared to filling 1.7% and releasing 0.8% of its capacity in the past, respectively.

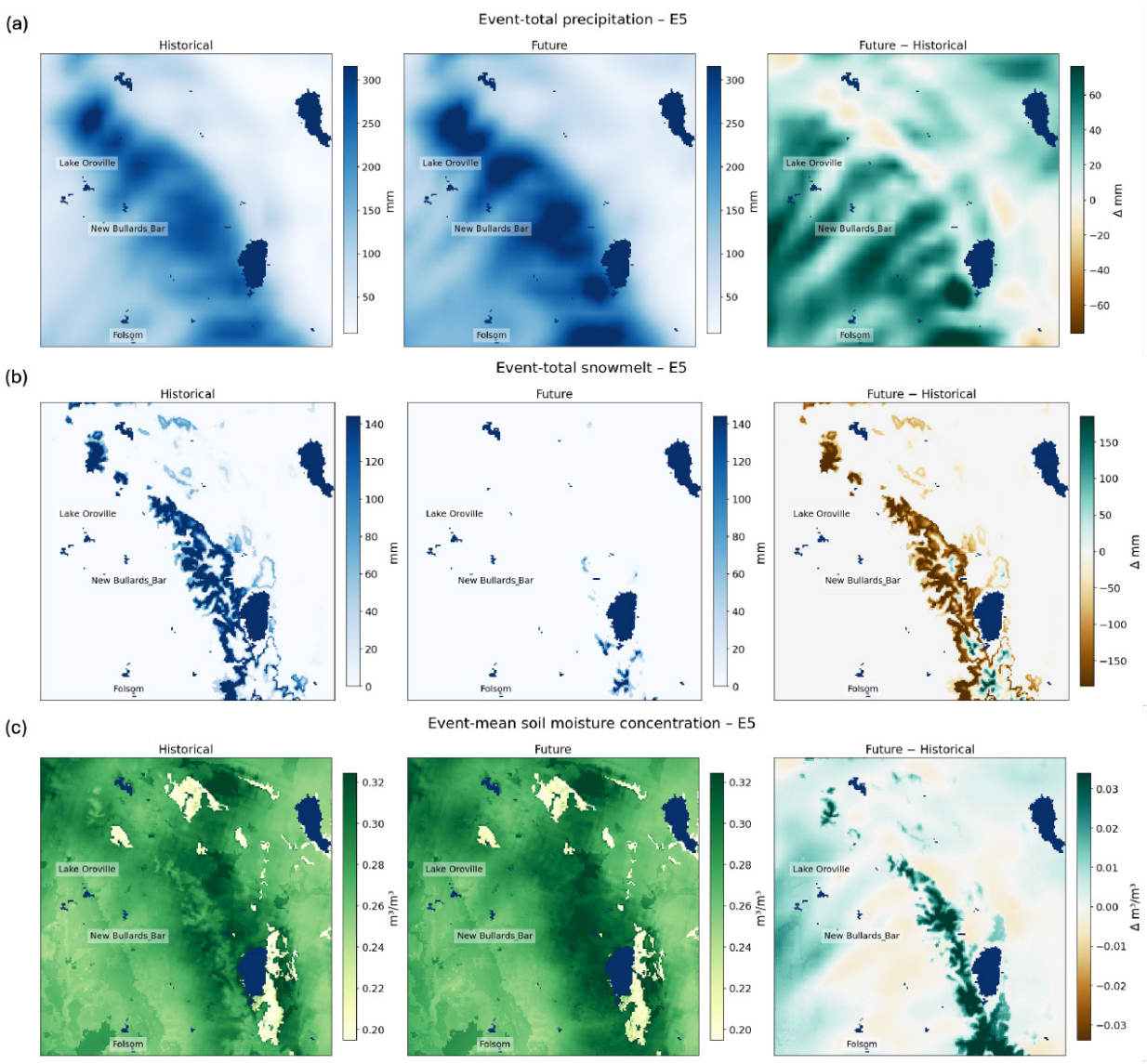
Following the driest volumetric soil moisture conditions across the three storyline events and record low-to-no snow conditions prior to the December 10–13, 1995 AR event (Section 3.3.1), the fill "benefit" for Folsom in the future appears to come from an increased amount of localized precipitation upstream of the reservoir (Figure 3.3.6). In addition to increases in precipitation, there is also an increase in volumetric soil moisture in the regions upstream of Oroville and New Bullards Bar. Notably, the peak SWE amounts and meltwater contributed from the headwaters of the three reservoirs was markedly decreased, possibly attenuating the inflows in the future. Indeed, while the streamflow peaks increase in the future for New Bullards Bar and Oroville (Figure 3.3.5), the peak does not occur earlier as it does in the 2022–2023 storyline. Peak outflows from the reservoirs occur later in the future, possibly due to the changing bi-modal streamflow patterns that differ from historical conditions. Overall, we find that under future warming, due to a larger and more spatially concentrated increase in precipitation, the 1995 storm produces a nearly three-fold increase in reservoir inflow rates that benefits the Folsom reservoir, given the dry and low-to-no snow antecedent conditions.

Figure 3.3.5



Future minus historical WRF-Hydro median ensemble member (E5) simulation differences in peak streamflow magnitude (a) and timing (b) for the headwaters of Oroville and New Bullards Bar during December 10–13, 1995.

Figure 3.3.6



WRF-Hydro simulated event-total (December 10–13, 1995) accumulated precipitation (a), peak SWE during the event (b), event-total snowmelt (c), and event-mean volumetric soil moisture (d) under historical (first column) and future conditions (second column), and inflow differences (future minus historical; third column) from the median (E5) ensemble member of the 1995 storyline.

3.3.2.3 1982 Storyline

Similar to the 2022–2023 and 1995 storylines, the AR-induced flood potential during the 1982 event is increased in a future warmer world, with a large share of the state increasing to Category 3 conditions compared to Category 2 conditions historically (Figure A.4.1). However, the flood potential does not reach Category 4–5, even in

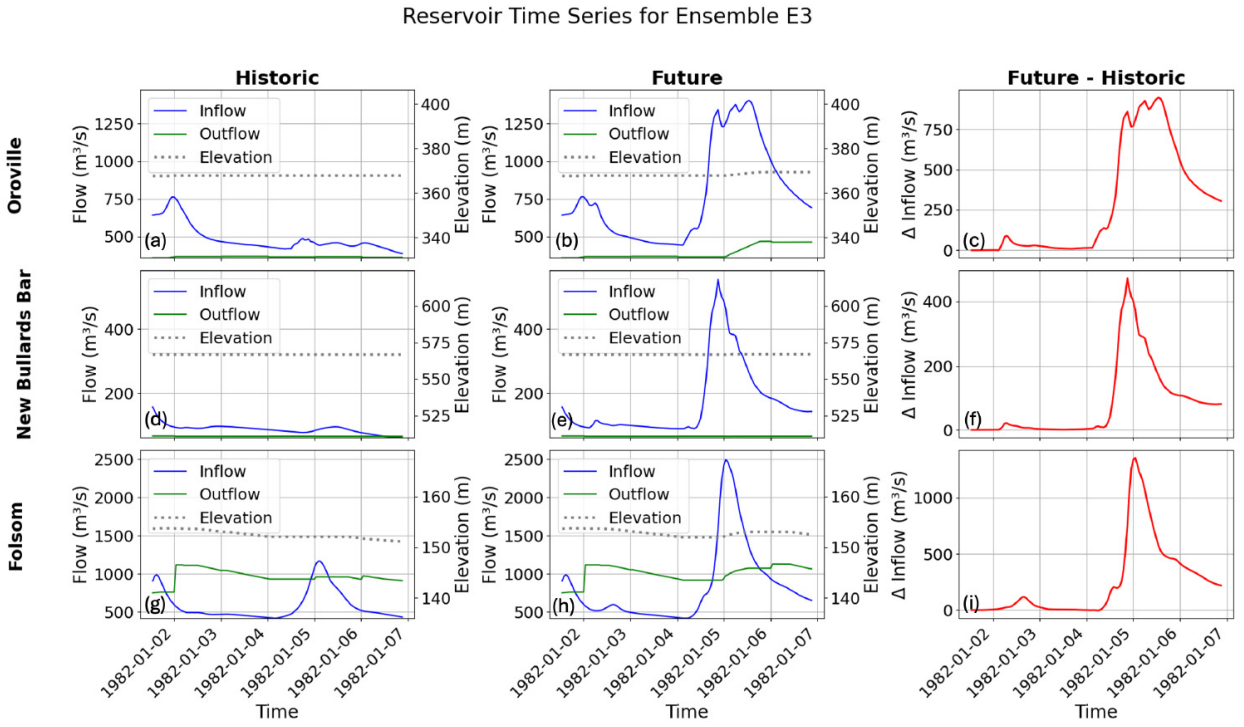
the future, suggesting that this AR event should have the least flood potential for Northern California reservoirs compared to the other storyline events analyzed.

Despite minimal flood potential projected for the 1982 AR event under future warming, the WRF-Hydro simulations show peak inflows to Northern California reservoirs doubling (e.g., Folsom and Oroville) to quintupling (e.g., New Bullards Bar) compared to historical levels (Figure 3.3.7). This highlights the critical role that land surface conditions play prior-to and amidst the storm events in shaping their flood potentials. For Oroville and New Bullards Bar, the dramatic increase in inflows fills 4% of reservoir capacity, compared to 1% historically (Table 3.3.3). For Folsom, the high inflows necessitate releases, but allow for storage to decrease by only 4% in the future compared with 12% historically.

The inflow increases appear to be caused by enhanced accumulated precipitation directly upstream from the reservoirs, significant increases in melt water from the snow bottom, and elevated volumetric soil moisture in the regions surrounding the reservoirs (Figure 3.3.9). These future atmospheric and land surface changes during the storyline event are compounded by record high snow and volumetric soil moisture antecedent conditions (Section 3.3.1). Similar to the 2022–2023 and 1995 storylines, the warming signal increases the magnitude of the peak streamflow for the rivers draining into Oroville and New Bullards Bar, but it also shifts the inflows later by more than a day (~33 hours). Despite these dramatic increases in peak inflows (two to five-fold increases) and earlier timing that could occur in a warmer future, the 1982 storyline event results concur with our prior conclusions that the reservoir infrastructure is resilient and responsive to future hydrometeorological changes.

With the three major reservoirs in our study area projected to face higher cumulative and peak inflows in future AR events, the results suggest potential directions for water management in the region, such as updating intensity, duration, frequency (IDF) curves, modernizing reservoir rule curves, explicit risk planning for rain-on-snow events, and relying on multi-model ensembles for planning. We also recognize several limitations and areas for future refinement of this research. Our WRF-Hydro analysis was limited to three ensemble members per storyline event, which may not capture the full range of storm track variability and/or storm dynamical and thermodynamical responses to warming that could alter flood drivers. Further, we acknowledge that there are biases in the gridded precipitation data from the AORC data set used to establish the antecedent conditions before the storyline events, which contribute to small offsets in the timing and magnitude of peak flows, for example, in the 1995 event, compared to gauge data from the California Data Exchange Center (CDEC). See the Appendix for more information on these biases.

Figure 3.3.7



Reservoir inflows, outflows, and percent full for Lake Oroville, New Bullards Bar, and Lake Folsom under historical (a, d, g) and future (b, e, h) conditions from the median (E3) WRF-Hydro ensemble member for the 1982 storyline simulation. Differences in future minus historical inflows (c, f, i) are also shown. The percent full in the first two columns is the ratio of modeled reservoir elevations to maximum elevations, including flood pool levels.

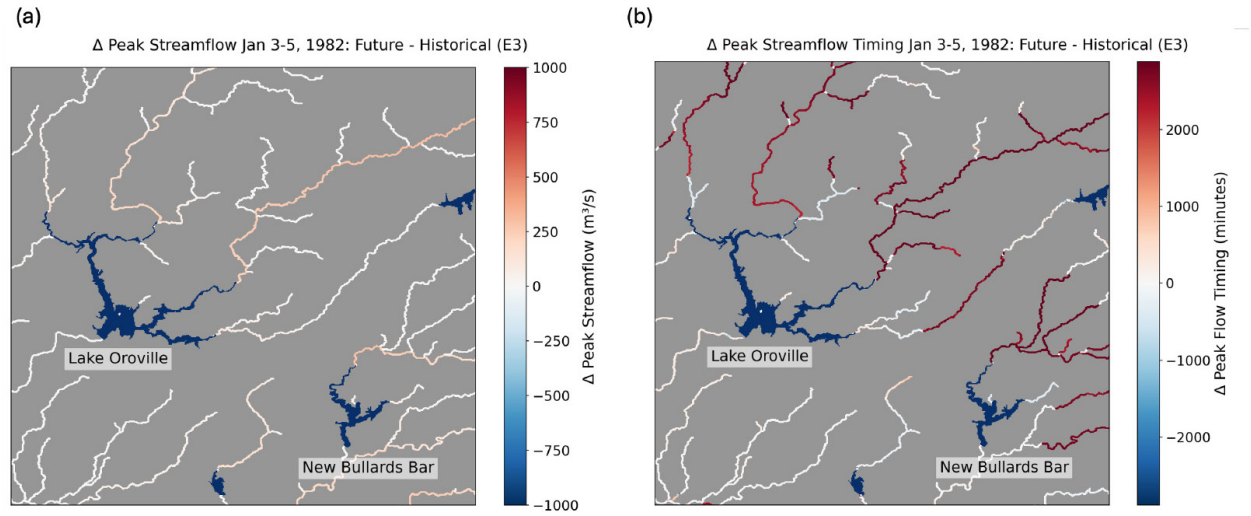
Table 3.3.3

	Total cumulative inflow (MAF)	Total cumulative inflow (MAF)	Total cumulative outflow (MAF)	Total cumulative outflow (MAF)	Net change in storage from event (MAF)	Net change in storage from event (MAF)	% share of total capacity Δ from event	% share of total capacity Δ from event
Reservoir (Storage capacity)	Historical	Future	Historical	Future	Historical	Future	Historical	Future

	Total cumulative inflow (MAF)	Total cumulative inflow (MAF)	Total cumulative outflow (MAF)	Total cumulative outflow (MAF)	Net change in storage from event (MAF)	Net change in storage from event (MAF)	% share of total capacity Δ from event	% share of total capacity Δ from event
Oroville (3.43 MAF)	0.16	0.24	0.11	0.12	0.000	0.002	1%	4%
New Bullards Bar (0.97 MAF)	0.03	0.05	0.02	0.02	0.000	0.000	1%	4%
Folsom (0.98 MAF)	0.19	0.27	0.30	0.31	-0.001	0.000	-12%	-4%

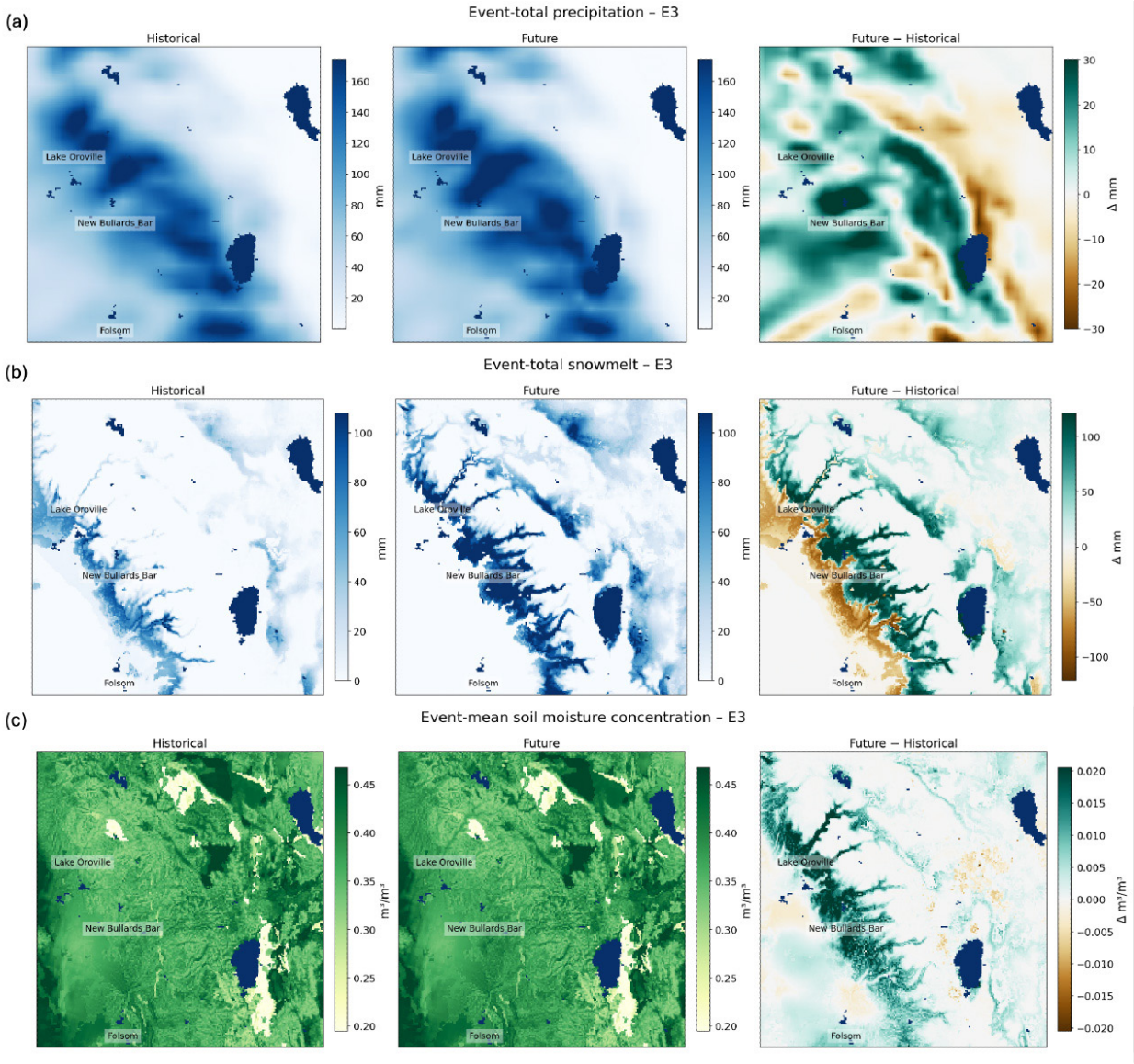
Inflows, Outflows, and Storage Changes between January 3–5, 1982 for Oroville, New Bullards Bar, and Folsom reservoirs for the historical and future median (E3) WRF-Hydro simulation. Each of the reservoir's total reservoir capacity are provided in parentheses in the first column.

Figure 3.3.8



Future minus historical WRF-Hydro median ensemble member (E3) simulation differences in peak streamflow magnitude (a) and timing (b) for the headwaters of Oroville and New Bullards Bar during January 3–5, 1982.

Figure 3.3.9



WRF-Hydro simulated event-total (January 3–5, 1982) accumulated precipitation (a), event-total snowmelt (b), and event-mean volumetric soil moisture (c) under historical (first column) and future conditions (second column), and inflow differences (future minus historical; third column) from the median (E3) ensemble member of the 1982 storyline.

4: Conclusions and Future Directions

In this report, we investigated how the hydrometeorological characteristics of the two main storm types that drive California's annual water cycle, ARs and ETCs, could respond to future warming. In particular, we explored how their hydrometeorological characteristics respond similarly or differently when an AR event occurs in isolation (AR-only) or co-occurs with an ETC event (AR-ETC). To do this, we utilized several Fifth Assessment datasets (e.g., LOCA2 and LOCA2-Hybrid) along with novel, storyline-based model experiments (e.g., WRF and WRF-Hydro). These storyline simulations were used to decipher the physical feedbacks that led to differential AR-only and AR-ETC driven hydrometeorological changes with warming and identify how the natural and managed hydrologic systems of Northern California might respond.

This work led to eight major takeaways about the role that AR-only and AR-ETC events could play in California's future:

- Future water year total precipitation both increases and decreases across regions of California. The sign and magnitude of change is dependent on the model used, region assessed, and if mid-century or end-century changes are evaluated.
- Future precipitation will come from more temporally clustered AR events in the midwinter that produce more rain and less snow.
- Generally, AR-ETC precipitation rates strengthen faster with warming than AR-only events, however, the rate at which that precipitation strengthens differs across Fifth Assessment datasets.
- Precipitation enhancement with warming is muted over the windward portions of mountainous regions.
- AR-ETC events have the potential to produce higher extreme precipitation rates, with more snowfall, and have less rain-on-snow potential than AR-only events.
- A southward shift in rain-on-snow risk in the Sierra Nevada is projected, particularly during AR-only events.
- In Northern California, future warming is expected to produce higher peak reservoir inflows at an earlier time within storm events, with antecedent snowpack and volumetric soil moisture conditions critically shaping inflow dynamics.
- Despite markedly increased and earlier peak inflows in a warmer future, Northern California reservoirs (e.g., Oroville, Folsom, and New Bullards Bar) are resilient and responsive to future hydrometeorological changes in the storyline events tested. Notably, these storyline events are not representative of all possible future AR-ETC flood events.

We note that the magnitudes of AR-only and AR-ETC precipitation changes with warming in Fifth Assessment datasets are sensitive to methodological choices (i.e., dynamical versus statistical downscaling). Other recent CMIP6-based AR studies that used different detection methods and larger sets of global models generally find substantial increases in AR-related extreme precipitation, and in some regions, a much larger fraction of extreme precipitation is attributed to ARs than in the historical climatology (Zhang et al., 2024; Tian et al., 2023; Payne et al., 2020). These studies highlight similar qualitative signals in how ARs could respond to warming, which include more frequent and longer-lasting ARs, stronger AR-related extremes, and the enhancing role of ARs in shaping California extreme precipitation, although the exact percentage changes differ across regions, metrics, and model ensemble members evaluated. While the LOCA2 and LOCA2-Hybrid datasets considered in this report project scaling of extreme precipitation at less than the expected C-C scaling (~6-7%/oC warming), there is observational and reanalysis-based evidence (Najibi & Steinschneider, 2023; Ombadi et al., 2023), global climate model simulation evidence (Ombadi et al., 2023; Zhang, Villarini, & Wehner, 2019), and storyline regional climate simulation evidence (Patricola et al., 2022; Rhoades et al., 2024) that extreme AR events could produce precipitation that exceeds C-C scaling in California. While we do not know the exact cause of the mismatch in precipitation scaling in the LOCA2 datasets versus others in the literature, Siler et al. (2026) posits that it could be due to the LOCA2 algorithms use of equidistant quantile mapping that limits precipitation changes in both LOCA2 and LOCA2-Hybrid. For example, quantile mapping conservatively limits precipitation changes in regions of complex terrain.

Another notable source of uncertainty in the Fifth Assessment precipitation projections arises from California's naturally variable weather and climate (Dettinger et al., 2011). Large interannual variations in the number of landfalling AR-only and AR-ETC events over California can shape precipitation trends and make it difficult to isolate the climate change signal in those trends, particularly when a model simulation provides a limited number of ensemble members (Maher et al., 2021). This is because any single ensemble member can vary greatly in the number of AR events and their extreme precipitation contributions, even at the multi-decadal scale. With that said, any apparent discrepancy between modeled and observed storm counts over a common historical period is not necessarily incorrect, as the observed count of events represents one climatological realization of what could have been possible for a particular climate system state (i.e., the atmosphere is a highly chaotic system). The two aforementioned sources of uncertainty that shape precipitation characteristics in the Fifth Assessment datasets are notable and have practical implications for reservoir operations (e.g., necessary flood pool spaces) and engineering design standards (e.g., intensity-duration-frequency curves).

5: References

Allen, M. R., & Ingram, W. J. (2002). Constraints on future changes in climate and the hydrologic cycle. Nature, 419(6903), 224–232. https://doi.org/10.1038/nature01092

Bales, R. C., Molotch, N. P., Painter, T. H., Dettinger, M. D., Rice, R., & Dozier, J. (2006). Mountain hydrology of the western United States. Water Resources Research, 42(8). https://doi.org/10.1029/2005WR004387

Bao, J.-W., Michelson, S. A., Neiman, P. J., Ralph, F. M., & Wilczak, J. M. (2006). Interpretation of Enhanced Integrated Water Vapor Bands Associated with Extratropical Cyclones: Their Formation and Connection to Tropical Moisture. Monthly Weather Review, 134(4), 1063–1080. https://doi.org/10.1175/MWR3123.1

Brandt, W. T., Haleakala, K., Hatchett, B. J., & Pan, M. (2022). A review of the hydrologic response mechanisms during mountain rain-on-snow. Frontiers in Earth Science, 10, 791760. https://doi.org/10.3389/feart.2022.791760

Choi, J., Ullrich, P. A., Lee, J., Gleckler, P. J., Goodnight, S., & Son, S. W. (2025). Uncertainty in California winter precipitation linked to future projections of North Pacific large-scale atmospheric circulation. Authorea Preprints. https://essopenarchive.org/doi/full/10.22541/essoar.176005819.91719885

Corringham, T. W., Ralph, F. M., Gershunov, A., Cayan, D. R., & Talbot, C. A. (2019). Atmospheric rivers drive flood damages in the western United States. Science advances, 5(12), https://doi.org/10.1126/sciadv.aax4631

Dacre, H.F., Clark, P.A. (2025). A kinematic analysis of extratropical cyclones, warm conveyor belts and atmospheric rivers. npj Clim Atmos Sci 8, 97. https://doi.org/10.1038/s41612-025-00942-z

Dacre, H. F., Martinez-Alvarado, O., & Hodges, K. I. (2023). Precipitation efficiencies in a climatology of Southern Ocean extratropical cyclones. Journal of Geophysical Research: Atmospheres, 128, e2023JD039239. https://doi.org/10.1029/2023JD039239

DeFlorio, M. J., Sengupta, A., Castellano, C. M., Wang, J., Zhang, Z., Gershunov, A., ... & Anderson, M. L. (2024). From California's extreme drought to major flooding: evaluating and synthesizing experimental seasonal and subseasonal forecasts of landfalling atmospheric rivers and extreme precipitation during winter 2022/23. Bulletin of the American Meteorological Society, 105(1), E84-E104. https://doi.org/10.1175/BAMS-D-22-0208.1

Dettinger, M. D., Ralph, F. M., Das, T., Neiman, P. J., & Cayan, D. R. (2011). Atmospheric Rivers, Floods and the Water Resources of California. Water, 3(2), 445–478. https://doi.org/10.3390/w3020445

Easterling, D.R., Arnold, J.R., Knutson, T., Kunkel, K.E., LeGrande, A.N., Leung, L.R., Vose, R.S., Waliser, D.E., Wehner, M.F. (2017). Ch. 7: Precipitation Change in the United States. Climate Science Special Report: Fourth National Climate Assessment, Volume I, Climate Science Special Report: Fourth National Climate Assessment, Volume I. U.S. Global Change Research Program, Washington, DC, DC, USA. https://doi.org/10.7930/J0H993CC

Eidhammer, T., Grubišić, V., Rasmussen, R., et al. (2018). Winter precipitation efficiency of mountain ranges in the Colorado Rockies under climate change. J Geophys Res Atmos 123(5):2573–2590. https://doi.org/10.1002/2017JD027995

Eyring, V., Bony, S., Meehl, G. A., Senior, C. A., Stevens, B., Stouffer, R. J., & Taylor, K. E. (2016). Overview of the Coupled Model Intercomparison Project Phase 6 (CMIP6) experimental design and organization. Geoscientific Model Development, 9(5), 1937–1958. https://doi.org/10.5194/gmd-9-1937-2016

Fall, G., Kitzmiller, D., Pavlovic, S., Zhang, Z., Patrick, N., St. Laurent, M., ... & Miller, D. (2023). The Office of Water Prediction's Analysis of Record for Calibration, version 1.1: Dataset description and precipitation evaluation. JAWRA Journal of the American Water Resources Association, 59(6), 1246–1272. https://doi.org/10.1111/1752-1688.13143

Gershunov, A., Hatchett, B., Weyant, A., Dettinger, M., Su, L., Rhoades, A., ... & Ralph, F. M. (2025). Atmospheric Rivers and Floods in California's Changing Hydroclimate. San Francisco Estuary and Watershed Science, 23(3). https://doi.org/10.15447/sfews.2025v23iss3art3

Gochis, D. J., Barlage, M., Dugger, A., FitzGerald, K., Karsten, L., McAllister, M., ... & Yu, W. (2018). The WRF-Hydro modeling system technical description,(Version 5.0). NCAR Technical Note, 107. https://ral.ucar.edu/sites/default/files/public/WRF-HydroV5TechnicalDescription.pdf

Gonzales, K. R., Swain, D. L., Roop, H. A., & Diffenbaugh, N. S. (2022). Quantifying the relationship between atmospheric river origin conditions and landfall temperature. Journal of Geophysical Research: Atmospheres, 127(20), e2022JD037284. https://doi.org/10.1029/2022JD037284

Hausfather, Z. (2025). An assessment of current policy scenarios over the 21st century and the reduced plausibility of high-emissions pathways. Dialogues on Climate Change, 2(1), 26–32. https://doi.org/10.1177/29768659241304854

Henn, B., Musselman, K. N., Lestak, L., Ralph, F. M., & Molotch, N. P. (2020). Extreme runoff generation from atmospheric river driven snowmelt during the 2017 Oroville dam spillways incident. Geophysical Research Letters, 47, e2020GL088189. https://doi.org/10.1029/2020GL088189

Krantz, W., Pierce, D., Goldenson, N., and Cayan, D. (2021). Memorandum on Evaluating Global Climate Models for Studying Regional Climate Change in California. Interim Deliverable for EPC-20-006. chrome-extension://efaidnbmnnnibpcajpcglclefindmkaj/https://www.energy.ca.gov/sites/default/files/2022-09/20220907_CDAWG_MemoEvaluating_GCMs_EPC-20-006_Nov2021-ADA.pdf

Lafferty, D. C., & Sriver, R. L. (2023). Downscaling and bias-correction contribute considerable uncertainty to local climate projections in CMIP6. npj Climate and Atmospheric Science, 6(1), 158. https://doi.org/10.1038/s41612-023-00486-0

Lamjiri, M. A., Dettinger, M. D., Ralph, F. M., Oakley, N. S., & Rutz, J. J. (2018). Hourly Analyses of the Large Storms and Atmospheric Rivers that Provide Most of California's Precipitation in Only 10 to 100 Hours per Year. San Francisco Estuary and Watershed Science, 16(4). Retrieved from https://escholarship.org/uc/item/3jr7z162

Lee, S. S., Sharma, S., Rosenbloom, N., Rodgers, K. B., Kim, J. E., Kwon, E. Y., ... & Stein, K. (2024). Multi-centennial climate change in a warming world beyond 2100. EGUsphere, 2024, 1–25. https://doi.org/10.5194/egusphere-2024-3377

Li, C., Zwiers, F., Zhang, X., Li, G., Sun, Y., Wehner, M. (2021). Changes in Annual Extremes of Daily Temperature and Precipitation in CMIP6 Models. J Clim 34, 3441–3460. https://doi.org/10.1175/JCLI-D-19-1013.1

Lopez-Marti, F., Ginesta, M., Faranda, D., Rutgersson, A., Yiou, P., Wu, L., & Messori, G. (2025). Future changes in compound explosive cyclones and atmospheric rivers in the North Atlantic. Earth System Dynamics, 16(1), 169–187. https://doi.org/10.5194/esd-16-169-2025

Lynn, E., Cuthbertson, A., He, M., Vasquez, J. P., Anderson, M. L., Coombe, P., ... & Hatchett, B. J. (2020). Precipitation-phase partitioning at landscape scales to regional scales. Hydrology and Earth System Sciences, 24(11), 5317–5328. https://doi.org/10.5194/hess-24-5317-2020

Maher, N., Milinski, S., & Ludwig, R. (2021). Large ensemble climate model simulations: introduction, overview, and future prospects for utilising multiple types of large ensemble. Earth System Dynamics, 12(2), 401–418. https://doi.org/10.5194/esd-12-401-2021

Musselman, K. N., Lehner, F., Ikeda, K., Clark, M. P., Prein, A. F., Liu, C., ... & Rasmussen, R. (2018). Projected increases and shifts in rain-on-snow flood risk over western North America. Nature Climate Change, 8(9), 808–812. https://doi.org/10.1038/s41558-018-0236-4

Patricola, C. M., & Cook, K. H. (2010). Northern African climate at the end of the twenty-first century: an integrated application of regional and global climate models. Climate Dynamics, 35(1), 193–212. https://doi.org/10.1007/s00382-009-0623-7

Patricola, C. M., & Cook, K. H. (2013). Mid-twenty-first century warm season climate change in the Central United States. Part I: regional and global model predictions. Climate dynamics, 40(3), 551–568. https://doi.org/10.1007/s00382-012-1605-8

Patricola, C. M., Wehner, M. F., Bercos-Hickey, E., Maciel, F. V., May, C., Mak, M., ... & Leal, S. (2022). Future changes in extreme precipitation over the San Francisco Bay Area: Dependence on atmospheric river and extratropical cyclone events. Weather and Climate Extremes, 36, 100440. https://doi.org/https://doi.org/10.1016/j.wace.2022.100440

Peng, Y.-M., Fu, G., Li, P.-Y., & Ni, J. (2025). Characteristics of super atmospheric rivers associated with explosive extratropical cyclones over the Northern Pacific Ocean. Geophysical Research Letters, 52, e2025GL114654. https://doi.org/10.1029/2025GL114654

Ombadi, M., Risser, M. D., Rhoades, A. M., & Varadharajan, C. (2023). A warming-induced reduction in snow fraction amplifies rainfall extremes. Nature, 619(7969), 305–310. https://doi.org/10.1038/s41586-023-06092-7

O'Neill, B. C., Tebaldi, C., Van Vuuren, D. P., Eyring, V., Friedlingstein, P., Hurtt, G., ... & Sanderson, B. M. (2016). The scenario model intercomparison project (ScenarioMIP) for CMIP6. Geoscientific Model Development, 9(9), 3461–3482. https://doi.org/10.5194/gmd-9-3461-2016

Payne, A. E., Demory, M. E., Leung, L. R., Ramos, A. M., Shields, C. A., Rutz, J. J., ... & Ralph, F. M. (2020). Responses and impacts of atmospheric rivers to climate change. Nature Reviews Earth & Environment, 1(3), 143–157. https://doi.org/10.1038/s43017-020-0030-5

Pierce, D. W., Cayan, D. R., Feldman, D. R., & Risser, M. D. (2023). Future increases in North American extreme precipitation in CMIP6 downscaled with LOCA. Journal of Hydrometeorology, 24(5), 951–975. https://doi.org/10.1175/JHM-D-22-0194.1

Ralph, F. M., Rutz, J. J., Cordeira, J. M., Dettinger, M., Anderson, M., Reynolds, D., et al. (2019). A Scale to Characterize the Strength and Impacts of Atmospheric Rivers. Bulletin of the American Meteorological Society, 100(2), 269–289. https://doi.org/10.1175/BAMS-D-18-0023.1

Rhoades, A. M., Jones, A. D., Srivastava, A., Huang, H., O'Brien, T. A., Patricola, C. M., ... & Zhou, Y. (2020). The shifting scales of western US landfalling atmospheric rivers under climate change. Geophysical Research Letters, 47(17), e2020GL089096. https://doi.org/10.1029/2020GL089096

Rhoades, A. M., Risser, M. D., Stone, D. A., Wehner, M. F., & Jones, A. D. (2021). Implications of warming on western United States landfalling atmospheric rivers and their flood damages. Weather and Climate Extremes, 32, 100326. https://doi.org/10.1016/j.wace.2021.100326

Rhoades, A. M., Zarzycki, C. M., Hatchett, B. J., Inda-Diaz, H., Rudisill, W., Bass, B., ... & Jones, A. D. (2024). Anticipating how rain-on-snow events will change through the 21st century: lessons from the 1997 new year's flood event. Climate Dynamics, 62(9), 8615-8637. https://doi.org/10.1007/s00382-024-07351-7

Schär, C., Frei, C., Lüthi, D., & Davies, H. C. (1996). Surrogate climate -change scenarios for regional climate models. Geophysical Research Letters, 23(6), 669–672. https://doi.org/10.1029/96gl00265

Shepherd, T. G. (2019). Storyline approach to the construction of regional climate change information. Proceedings of the Royal Society A, 475(2225), 20190013. https://doi.org/10.1098/rspa.2019.0013

Shields, C. A., Payne, A. E., Shearer, E. J., Wehner, M. F., O'Brien, T. A., Rutz, J. J., et al. (2023). Future atmospheric rivers and impacts on precipitation: Overview of the ARTMIP Tier 2 high-resolution global warming experiment. Geophysical Research Letters, 50, e2022GL102091. https://doi.org/10.1029/2022GL102091

Skamarock, W.C., Klemp, J.B. (2008). A time-split nonhydrostatic atmospheric model for weather research and forecasting applications. J. Comput. Phys. 227, 3465–3485. https://doi.org/10.1016/j.jcp.2007.01.037

Siirila-Woodburn, E. R., Rhoades, A. M., Hatchett, B. J., Huning, L. S., Szinai, J., Tague, C., et al. (2021). A low-to-no snow future and its impacts on water resources in the western United States. Nature Reviews Earth & Environment, 2(11), 800–819. https://doi.org/10.1038/s43017-021-00219-y

Siler, N., & Roe, G. (2014). How will orographic precipitation respond to surface warming? An idealized thermodynamic perspective. Geophysical Research Letters, 41(7), 2606–2613. https://doi.org/10.1002/2013GL059095

Siler, N., Koszuta, M., Rahimi, S., Norris, J., Hall, A., & Ullrich, P. (2026). Examining the robustness of weakened orographic influence on precipitation in downscaled climate projections over the western US. Geophysical Research Letters, 53(1), e2025GL119251. https://doi.org/10.1029/2025GL119251

Tian, Y., Zhao, Y., Son, S. W., Luo, J. J., Oh, S. G., & Wang, Y. (2023). A deep -learning ensemble method to detect atmospheric rivers and its application to projected changes in precipitation regime. Journal of Geophysical Research: Atmospheres, 128(12), e2022JD037041. https://doi.org/10.1029/2022JD037041

Ullrich, P. A., Zarzycki, C. M., McClenny, E. E., Pinheiro, M. C., Stansfield, A. M., & Reed, K. A. (2021). TempestExtremes v2. 1: A community framework for feature detection, tracking, and analysis in large datasets. Geoscientific Model Development, 14(8), 5023–5048. https://doi.org/10.5194/gmd-14-5023-2021

Zhang, Z., Ralph, F. M., & Zheng, M. (2019). The Relationship Between Extratropical Cyclone Strength and Atmospheric River Intensity and Position. Geophysical Research Letters, 46(3), 1814–1823. https://doi.org/10.1029/2018GL079071

Zhang, L., Zhao, Y., Cheng, T. F., & Lu, M. (2024). Future changes in global atmospheric rivers projected by CMIP6 models. Journal of Geophysical Research: Atmospheres, 129(3), e2023JD039359. https://doi.org/10.1029/2023JD039359

Zhang, W., Villarini, G., & Wehner, M. (2019). Contrasting the responses of extreme precipitation to changes in surface air and dew point temperatures. Climatic change, 154(1), 257–271. https://doi.org/10.1007/s10584-019-02415-8

Zhang, Z., & Ralph, F. M. (2021). The Influence of Antecedent Atmospheric River Conditions on Extratropical Cyclogenesis. Monthly Weather Review, 149(5), 1337–1357. https://doi.org/10.1175/MWR-D-20-0212.1

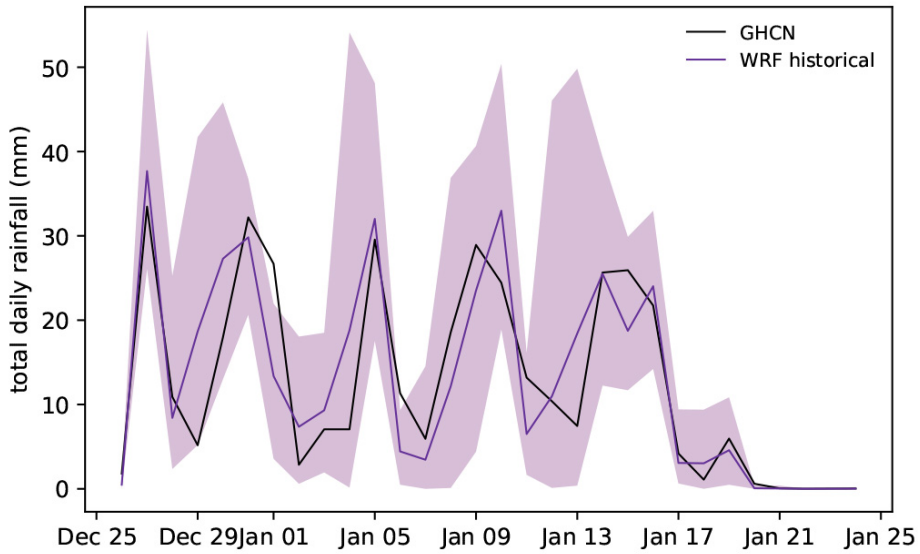
Zhou, Y., North, J. S., Rhoades, A. M., Tao, J., Rudisill, W., Risser, M. D., & Collins, W. D. (2025). Atmospheric river frequency -category characteristics shape US West Coast runoff. Journal of Geophysical Research: Atmospheres, 130(2), e2024JD041805. https://doi.org/10.1029/2024JD041805

Zhou, Y., Wehner, M. M., Rhoades, A. M., & Jones, A. D. (2025). The role of wind -moisture characteristics in shaping atmospheric river flood hazards. Geophysical Research Letters, 52(20), e2025GL117548. https://doi.org/10.1029/2025GL117548

Appendix A: Additional WRF and WRF-Hydro Storyline Event Results

For each storyline event, we evaluated its potential to produce flooding across the state using the Ralph et al. (2019) AR Category scale for the three WRF storyline ensemble members that provided meteorological forcing to WRF-Hydro. These ensemble members were selected based on their California-wide event-total accumulated rainfall amounts (as shown for the 2022–2023 storyline in Figure A.0.1), representing the maximum, median, and minimum.

Figure A.0.1



Time series of California-wide mean total daily rainfall (mm) from the ensemble-averaged WRF historical simulations (solid purple line) and the Global Historical Climate Network (GHCN) daily observational data (solid black line). Purple shading indicates the spread between the WRF ensemble minimum and maximum California-wide mean total daily rainfall.

Notably, AR Category estimates indicate the potential for flooding based on atmospheric conditions, however they do not account for the antecedent and within-storm land surface conditions and the role of infrastructure in attenuating AR flood potential. Therefore, we also evaluate the observed SWE conditions prior to each storyline event and the antecedent volumetric soil moisture. Further, we investigated how the freezing levels during the storyline events shift with warming. These analyses were conducted to elucidate how land surface conditions play a key role in Northern California streamflow responses.

TempestExtremes version 2 (TEv2) is used to track AR-only, ETC-only, and AR-ETC events (Ullrich et al., 2021). To track AR events, we leverage sub-daily fields (e.g., 3-hourly and 6-hourly, based on availability in a given dataset) of meridional and zonal winds, specific humidity, and mean sea level pressure to compute integrated vapor transport (IVT) in both the GCMs used to inform LOCA2 downscaling (i.e., CMIP6 models) and the storyline-based WRF simulations. More specifically, using the WRF-based tracking results as an example, we feed the IVT fields into the TEv2 function DetectBlobs using the following settings:

```
--thresholdcmd "_LAPLACIAN{8,10.0}(_VECMAG(QU,QV)),<=,-30000,0"
--minabslat 20 --geofiltercmd "area,>,850000km2"
--timefilter "6hr"
--tagvar "AR_binary_tag"
```

The AR binary masks are then assigned individual storm identifiers (i.e., AR#1, AR#2, … AR#X) based on temporal overlap of the AR binary masks (in this case, spatiotemporal overlaps for, at least, six hours).
To track ETC events, we also leverage sub-daily fields of sea level pressure (SLP) utilizing the following command line options for the TEv2 functions DetectNodes with the following settings:

```
--closedcontourcmd "SLP,200.0,5.5,0"
--mergedist 6.0
--searchbymin "SLP"
--outputcmd "SLP,min,0"
```

This generates estimates of the SLP low-pressure epicenter latitude and longitude location of the ETC events at each timestep. These epicenters are then fed into the TEv2 StitchNodes function with the following settings:

```
--in_fmt "lon,lat,SLP"
--range "6.0"
--mintime "24h"
--maxgap "1"
--min_endpoint_dist "12.0"
```

Thisgenerates ETC binary masks based on the SLP low-pressure epicenters of the ETC event and an assumption of a close contoured circle about that epicenter. Individual ETC events are identified using spatiotemporal overlaps (i.e., 24 hours).

To estimate when an AR and ETC event overlap (i.e., an AR-ETC event) we assumed that they only need to overlap for, at least, one timestep during AR landfall. We then use a series of Climate Data Operators and netCDF Operators to identify when the AR-only, ETC-only, and AR-ETC events make landfall within California and identify the start and end timesteps (i.e., the first and last timestep when a storm mask exists within California). For each year, we generate a CSV file that includes timestamps, landfall flags for AR-only, ETC-only, and AR-ETC, and landfall latitudes (Figure A.0.2). A landfalling event is determined when its binary mask overlaps with the region of interest. In this project, we created two sets of landfall flags based on different regions: one for events that landfall in the Fifth Assessment regions and the other for events affecting the entire U.S. West Coast. In this report, we mainly use landfall flags over the Fifth Assessment regions. The landfall flags are marked with: 0 for no landfall activity, 1 for AR-only or ETC-only events, and 2 for AR-ETC co-occurring events. The AR-ETC flags are determined when, during the landfall period of an AR, there is at least one ETC landfall timestamp. The storm catalogs are made available here: https://portal.nersc.gov/archive/home/y/yangzhou/www/CMIP6/landfall_flags Besides CSV files of the storm catalogs, the netCDF binary mask files for AR and ETC events extracted from CMIP6 can be retrieved from: https://portal.nersc.gov/archive/home/y/yangzhou/www/CMIP6/

Figure A.0.2

EC-Earth3.historical.2010.CCCA5_landfall_flag

Date	AR_landfall_flag	ETC_landfall_flag	AR_ETC_landfall_flag	Landfall latitude
2010-01-01 00:00:00	0.0	0.0	0.0	
2010-01-01 06:00:00	0.0	0.0	0.0	
2010-01-01 12:00:00	0.0	0.0	0.0	
2010-01-01 18:00:00	0.0	0.0	0.0	
2010-01-02 00:00:00	0.0	0.0	0.0	
2010-01-02 06:00:00	1.0	0.0	2.0	42.45604075651
2010-01-02 12:00:00	1.0	0.0	2.0	42.45604075651
2010-01-02 18:00:00	1.0	0.0	2.0	42.45604075651
2010-01-03 00:00:00	1.0	0.0	2.0	42.45604075651
2010-01-03 06:00:00	1.0	0.0	2.0	38.9472804370071
2010-01-03 12:00:00	1.0	1.0	2.0	38.9472804370071
2010-01-03 18:00:00	1.0	1.0	2.0	38.2455282337738
2010-01-04 00:00:00	1.0	0.0	2.0	38.2455282337738
2010-01-04 06:00:00	1.0	0.0	2.0	38.2455282337738
2010-01-04 12:00:00	1.0	0.0	2.0	38.9472804370071
2010-01-04 18:00:00	0.0	0.0	0.0	
2010-01-05 00:00:00	0.0	0.0	0.0	
2010-01-05 06:00:00	0.0	0.0	0.0	
2010-01-05 12:00:00	0.0	0.0	0.0	
2010-01-05 18:00:00	0.0	0.0	0.0	

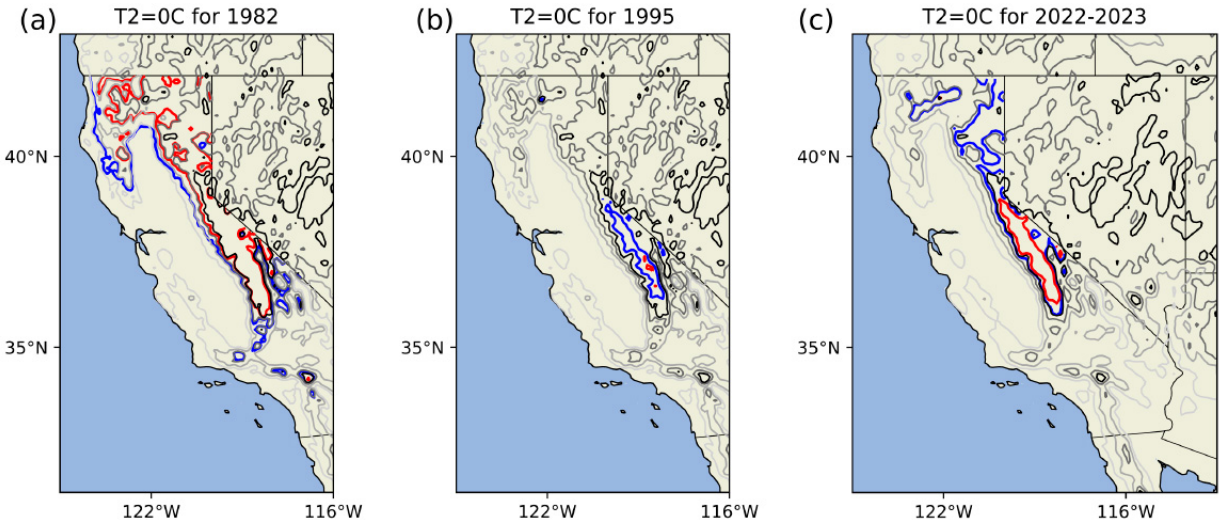
Snapshot of the CSV file for AR and ETC events tracked using TEv2 for an example CMIP6-model (EC-Earth3) that was downscaled with LOCA2.

For AR-related precipitation over California, we analyze six of the CMIP6 GCMs that were used to produce LOCA2 precipitation, including ACCESS-CM2, CNRM-CM6-1, EC-Earth3, EC-Earth3-Veg, HadGEM3-GC31-LL, and HadGEM3-GC31-MM. We selected these six models because they provide the six-hourly fields needed for AR detection (as daily fields can miss short-lived AR events), and align with California model-evaluation guidance that recommends the use of a vetted subset of CMIP6 GCMs for downscaling and assessment applications (Krantz et al., 2021). We then use the GCM-based AR landfall flags to isolate AR-related precipitation in LOCA2. Future AR-precipitation projections are limited to SSP585. This is because six-hourly output is not broadly available in SSP370 simulations. With that said, mid-century warming is expected to be more similar in SSP370 and SSP585 scenarios (Hausfather, 2025). Therefore, mid-century precipitation projections shown in this report should be consistent with SSP370, while end-century precipitation projections could be more pessimistic. Notably, the level of warming at end-century that occurs in SSP585 could still be reached under SSP370 in the 2200s (Lee et al., 2024).

A.1 Storyline Event Land Surface Conditions

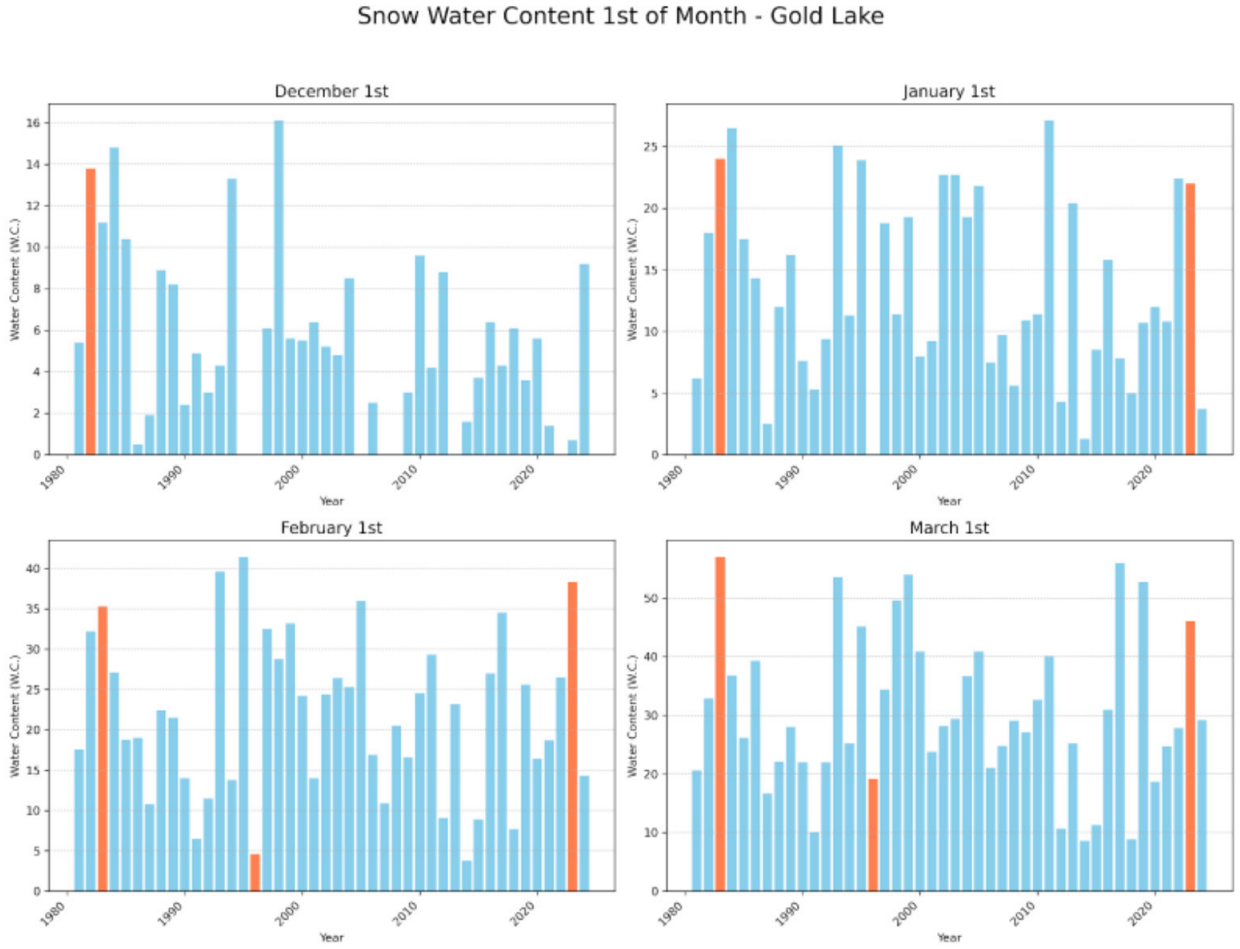
Figure A.1.1 shows the freezing level elevation during each of the storyline events. Figure A.1.2 shows observed SWE depths at the start of each month across the three storyline events. These SWE depths are derived from the Gold Lake (G) measurement site (California Data Exchange Center, CDEC https://cdec.water.ca.gov/snow.html) in the Feather River for the entirety of its record (1980–2024), providing climatological context of the antecedent land surface conditions. Figure A.1.3 shows the location of the G measurement site overlaid on the WRF-Hydro estimates of antecedent land surface conditions (i.e., SWE and volumetric soil moisture).

Figure A.1.1



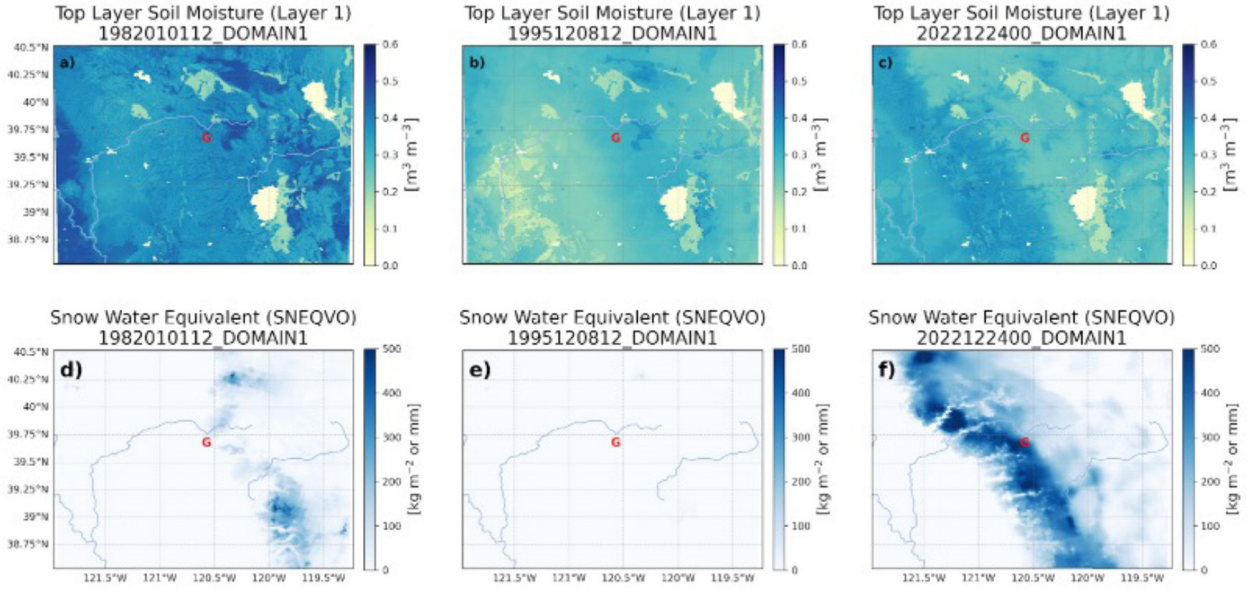
Freezing level elevations (two-meter air temperature, T2, at 0°C) under historical (blue) and future (red) conditions overlaid on topographic elevations at 500 m elevation intervals between 500 m (light gray) and 2000 m (black).

Figure A.1.2



Snow water equivalent (SWE or water content, W.C.) conditions at the Gold Lake measurement site within the Feather watershed on the first day of December, January, February, and March from 1980 to 2024. The storyline years (1982, 1995, and 2023) are highlighted in red.

Figure A.1.3

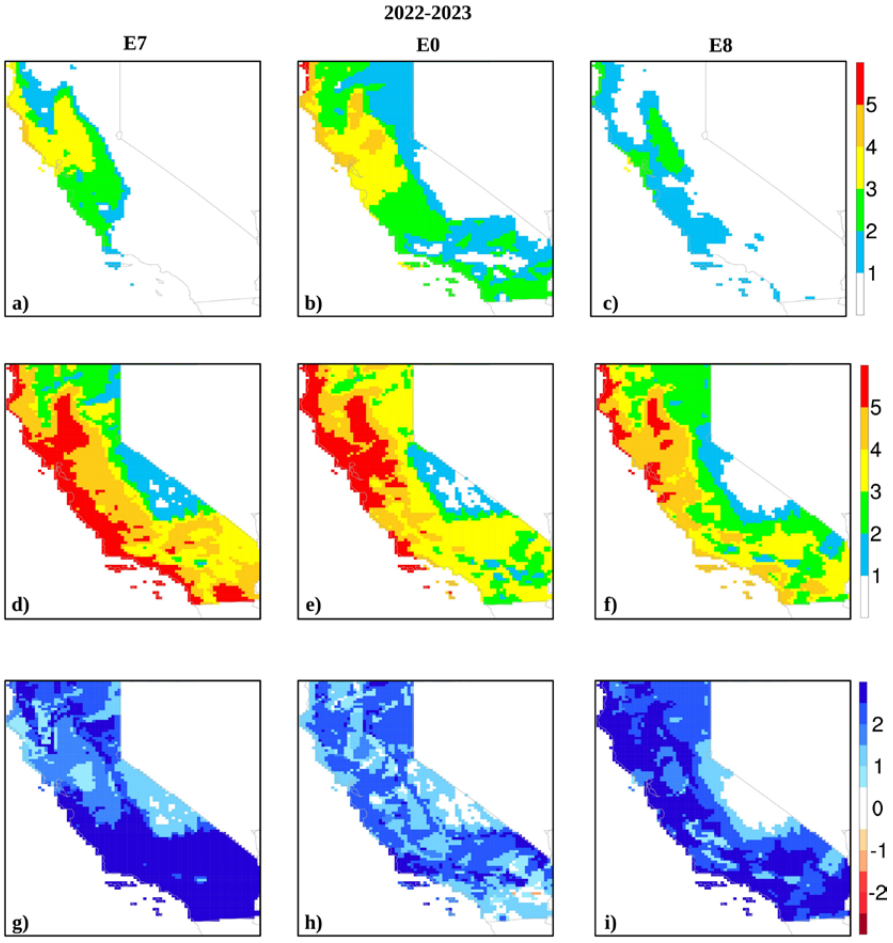


Antecedent snow water equivalent (SWE; top row) and volumetric soil moisture (bottom row) conditions from the AORC-forced WRF-Hydro simulations for 1982 (a, d), 1995 (b, e), and 2022–2023 (c, f). 'G' is the location of the Gold Lake site in Figure A.1.2.

A.2 2022-2023 Storyline

Figure A.2.1 shows the highest Ralph et al. (2019) AR Category Scale reaching ARs (December 30, 2022, to January 3, 2023) within the 2022–2023 storyline simulation. Table A.2.1 and Figure A.2.2 show the reservoir inflows, outflows, elevations, and change in storage during the 2022–2023 storyline event for the complete set of ensemble members (E7 - maximum, E0 - median, and E8 - minimum), in the historical and future WRF-Hydro simulation.

Figure A.2.1



The highest Ralph et al. (2019) AR Category Scale reaching ARs (December 30, 2022, to January 3, 2023) within the 2022–2023 storyline simulation. Each gridcell represents the maximum AR Category reached over the duration of the AR landfall for each of the three ensemble members downscaled using WRF-Hydro for the historical (a–c) and future (d–f) periods. The differences (future - historical) are shown (g–i).

Table A.2.1

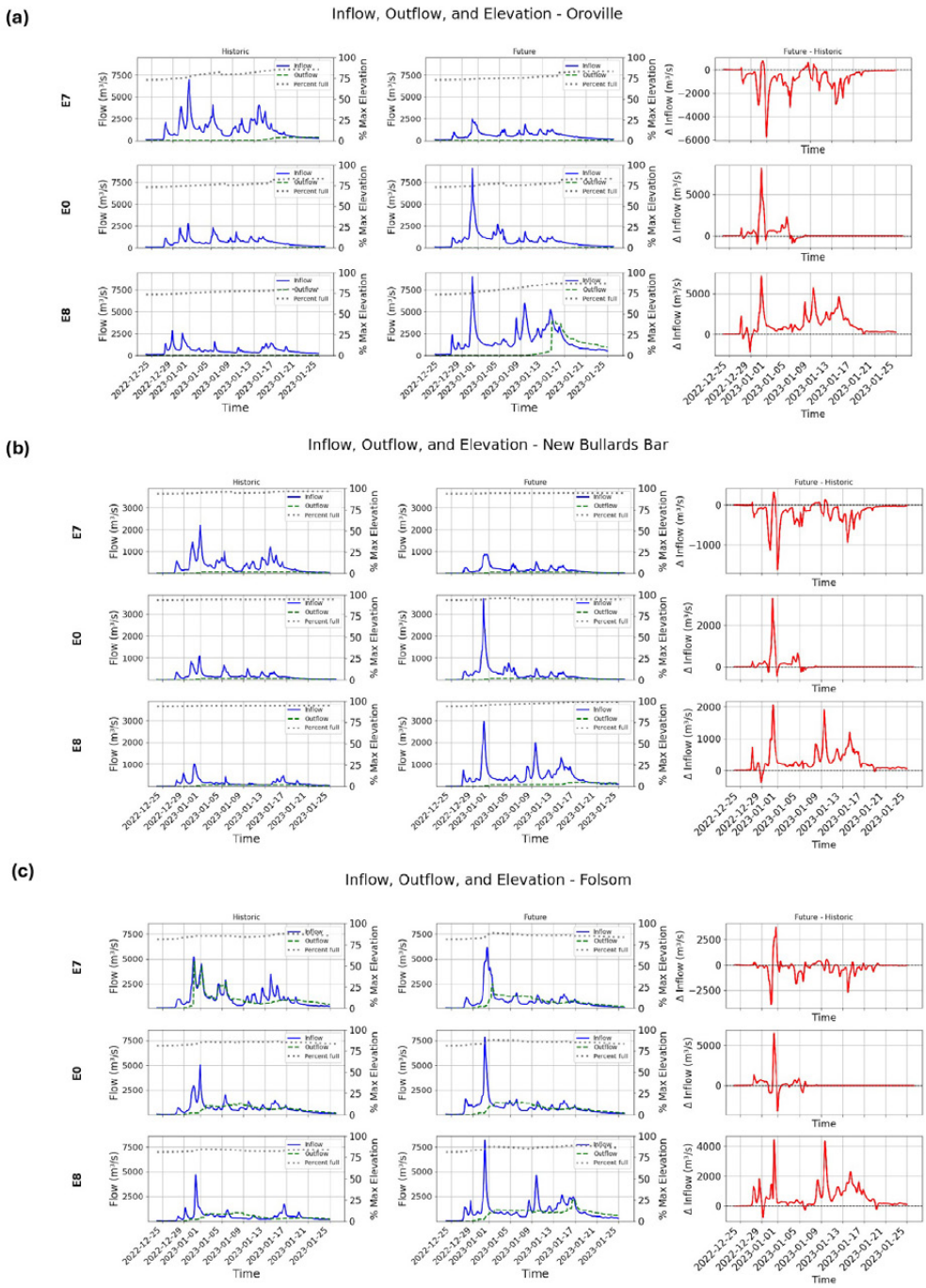
Reservoir (Storage Capacity)	Ensemble Member	Period	Total Inflow (MAF)	Total Outflow (MAF)	Net Change in Storage (MAF)	Net Change % of Total capacity
Oroville (3.43 MAF)	E7	Historical	2.84	0.25	2.59	75.5%

Reservoir (Storage Capacity)	Ensemble Member	Period	Total Inflow (MAF)	Total Outflow (MAF)	Net Change in Storage (MAF)	Net Change % of Total capacity
Oroville (3.43 MAF)	E7	Future	1.38	0.03	1.34	39.2%
Oroville (3.43 MAF)	E0	Historical	1.51	0.04	1.47	43.0%
Oroville (3.43 MAF)	E0	Future	2.05	0.04	2.027	58.9%
Oroville (3.43 MAF)	E8	Historical	1.28	0.01	1.27	37.0%
Oroville (3.43 MAF)	E8	Future	3.81	1.49	2.32	67.7%
New Bullards Bar (0.97 MAF)	E0	Historical	0.39	0.11	0.29	29.5%
New Bullards Bar (0.97 MAF)	E0	Future	0.57	0.11	0.46	48.0%
New Bullards Bar (0.97 MAF)	E7	Historical	0.75	0.11	0.64	65.9%
New Bullards Bar (0.97 MAF)	E7	Future	0.37	0.11	0.26	27.1%
New Bullards Bar (0.97 MAF)	E8	Historical	0.32	0.11	0.21	21.7%
New Bullards Bar (0.97 MAF)	E8	Future	0.95	0.18	0.77	79.2%
Folsom (0.98 MAF)	E0	Historical	1.53	1.21	0.32	33.5%
Folsom (0.987 MAF)	E0	Future	1.76	1.39	0.38	38.9%
Folsom (0.987 MAF)	E7	Historical	2.20	1.90	0.30	31.4%

Reservoir (Storage Capacity)	Ensemble Member	Period	Total Inflow (MAF)	Total Outflow (MAF)	Net Change in Storage (MAF)	Net Change % of Total capacity
Folsom (0.987 MAF)	E7	Future	1.75	1.45	0.30	30.7%
Folsom (0.987 MAF)	E8	Historical	1.09	0.86	0.23	23.8%
Folsom (0.987 MAF)	E8	Future	2.37	1.77	0.59	61.3%

Inflows, Outflows, and Storage Changes between December 24, 2022, through January 25, 2023, for Oroville, New Bullards Bar, and Folsom reservoirs for historical and future time periods, for the maximum (E7), median (E0), and minimum (E8) WRF storyline simulation ensemble members. Each reservoir's total reservoir capacity is provided in parenthesis in the first column.

Figure A.2.2

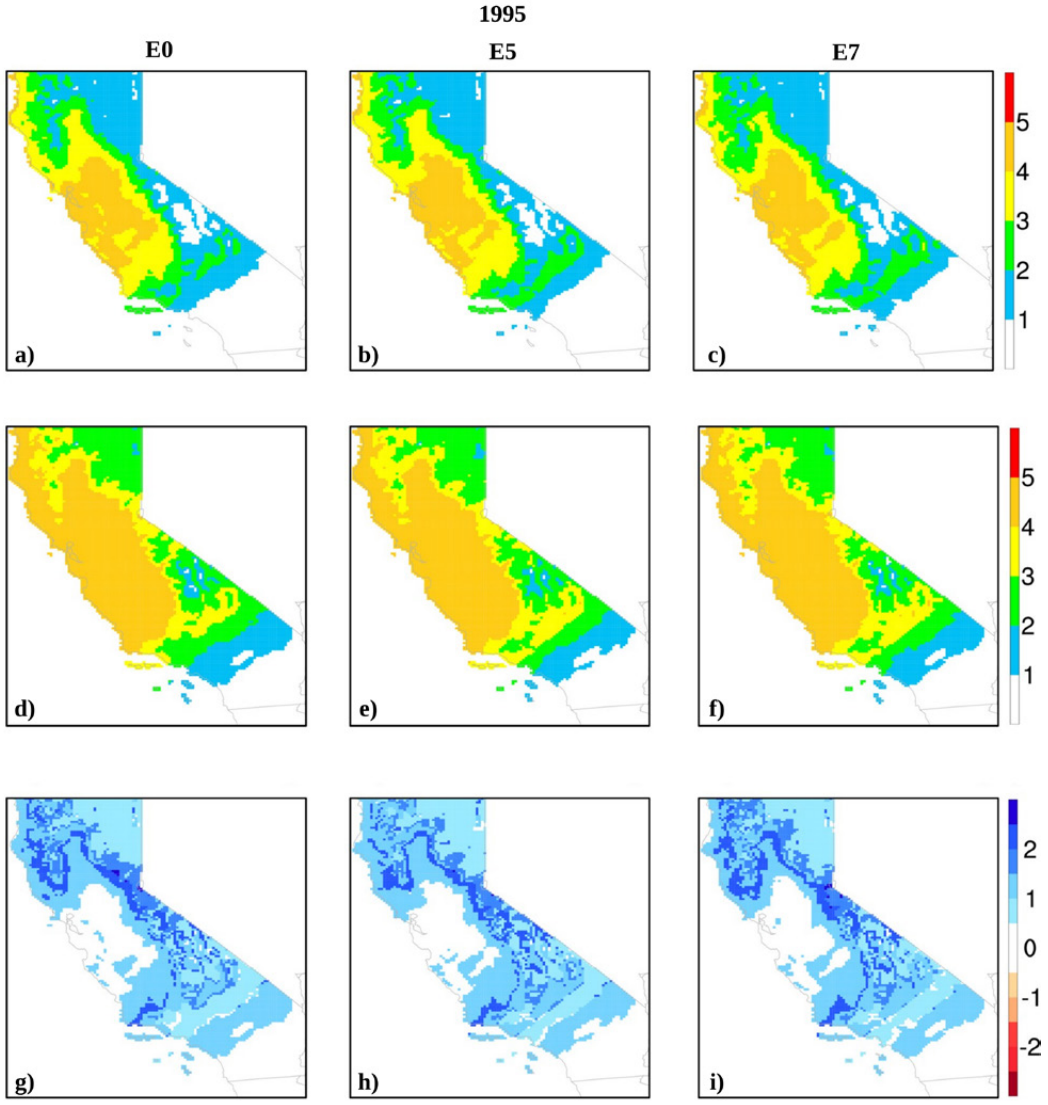


Reservoir inflows, outflows, and percent full for Lake Oroville (a), New Bullards Bar (b), and Lake Folsom (c) under historical conditions (first column), future warming (second column), and the difference in future and historical inflows (third column) from all three WRF-Hydro ensemble member simulations of the 2022–2023 storyline. The percent full in the first two columns is the ratio of modeled reservoir elevations to maximum elevations, including the flood pool.

A.3 1995 Storyline

Figure A.3.1 shows the highest Ralph et al. (2019) AR Category Scale reaching ARs (December 10-13, 1995) within the 1995 storyline simulation. Table A.3.1 and Figure A.3.2 show the reservoir inflows, outflows, elevations, and change in storage during the 1995 storyline event for the complete set of ensemble members (E0 - maximum, E5 - median, and E7 - minimum), in the historical and future WRF-Hydro simulation.

Figure A.3.1



The highest Ralph et al. (2019) AR Category Scale reaching ARs within the 1995 storyline simulation. Each gridcell represents the maximum AR Category reached over the duration of the AR landfall for each of the three ensemble members downscaled using WRF-Hydro for the historical (a-c) and future (d-f) periods. The differences (future - historical) are shown (g-i).

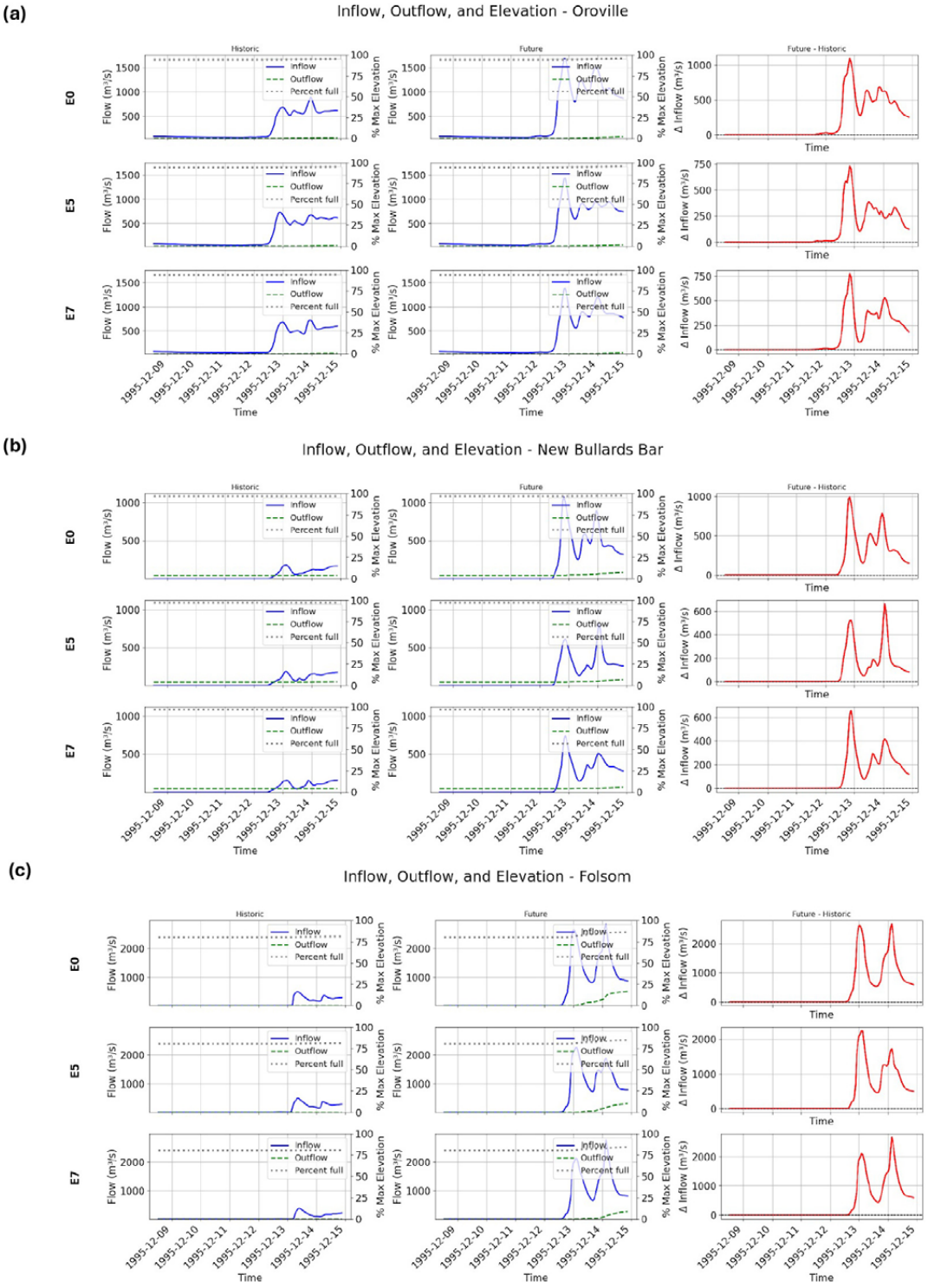
Table A.3.1

Reservoir (Storage Capacity)	Ensemble Member	Period	Total Inflow (MAF)	Total Outflow (MAF)	Net Change in Storage (MAF)	Net Change % of Total capacity
Oroville (3.43 MAF)	E7	Historical	0.08	0.01	0.002	1.8%
Oroville (3.43 MAF)	E7	Future	0.08	0.00	0.003	2.1%
Oroville (3.43 MAF)	E0	Historical	0.07	0.01	0.002	1.7%
Oroville (3.43 MAF)	E0	Future	0.11	0.01	0.003	2.8%
Oroville (3.43 MAF)	E8	Historical	0.07	0.01	0.002	1.6%
Oroville (3.43 MAF)	E8	Future	0.11	0.01	0.003	2.7%
New Bullards Bar (0.97 MAF)	E0	Historical	0.01	0.02	0.000	-0.8%
New Bullards Bar (0.97 MAF)	E0	Future	0.03	0.01	0.001	2.2%
New Bullards Bar (0.97 MAF)	E7	Historical	0.01	0.02	0.000	-0.8%
New Bullards Bar (0.97 MAF)	E7	Future	0.03	0.02	0.001	1.4%
New Bullards Bar (0.97 MAF)	E8	Historical	0.01	0.02	0.000	-0.9%
New Bullards Bar (0.97 MAF)	E8	Future	0.03	0.02	0.001	1.8%
Folsom (0.98 MAF)	E0	Historical	0.02	0.00	0.001	2.1%

Reservoir (Storage Capacity)	Ensemble Member	Period	Total Inflow (MAF)	Total Outflow (MAF)	Net Change in Storage (MAF)	Net Change % of Total capacity
Folsom (0.987 MAF)	E0	Future	0.10	0.00	0.004	10.6%
Folsom (0.987 MAF)	E7	Historical	0.02	0.00	0.001	2.1%
Folsom (0.987 MAF)	E7	Future	0.12	0.01	0.004	11.6%
Folsom (0.987 MAF)	E8	Historical	0.02	0.00	0.000	1.5%
Folsom (0.987 MAF)	E8	Future	0.11	0.01	0.004	10.7%

Inflows, Outflows, and Storage Changes from December 10–13, 1995 for Oroville, New Bullards Bar, and Folsom reservoirs for historical and future time periods, for the maximum (E0), median (E5), and minimum (E7) WRF storyline simulation ensemble members. Each of the reservoir's total reservoir capacity are provided in parentheses in the first column.

Figure A.3.2



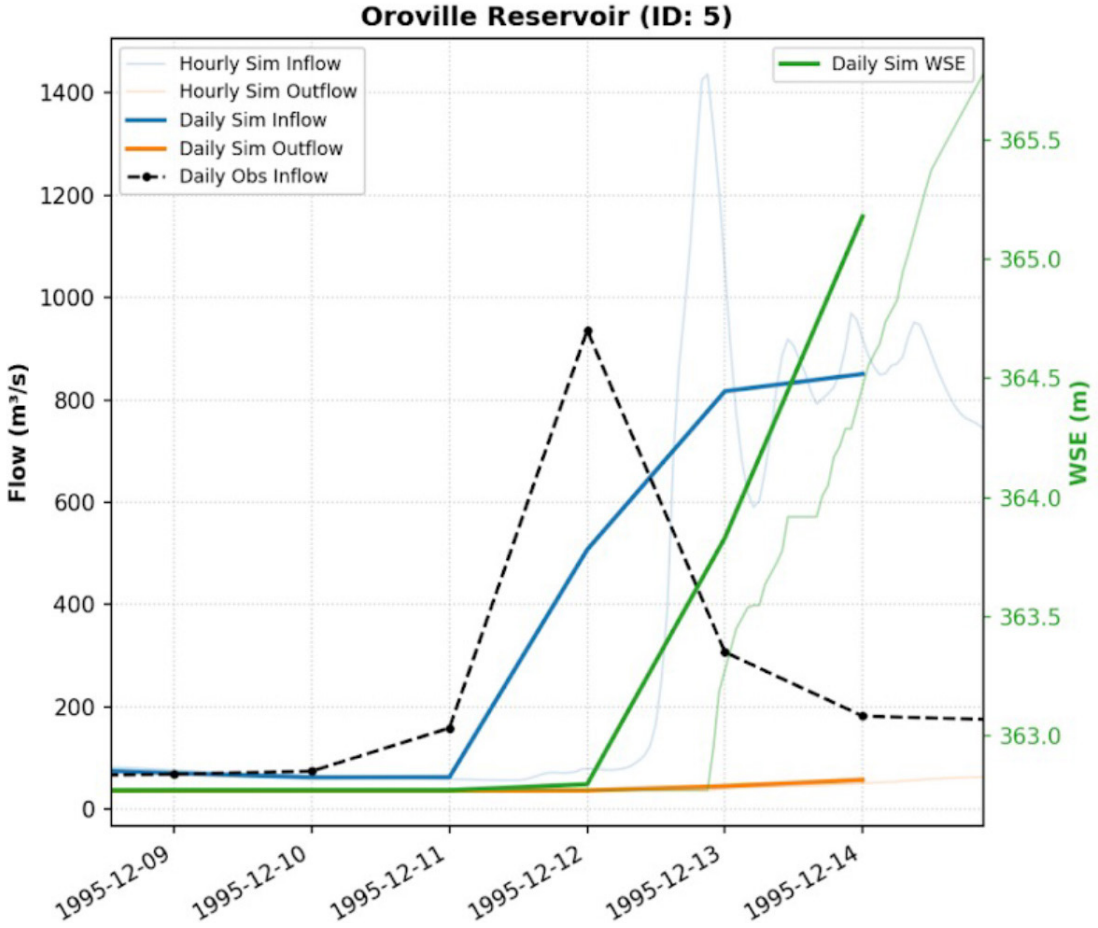
Reservoir inflows, outflows, and percent full for Lake Oroville (a), New Bullards Bar (b), and Lake Folsom (c) under historical conditions (first column), future warming

(second column), and difference in future minus historical inflows (third column) from all three WRF-Hydro ensemble member simulations of the 1995 storyline. The percent full in the first two columns is the ratio of modeled reservoir elevations to maximum elevations, including the flood pool.

We also conducted additional analysis of the WRF-Hydro-based inflow results of our 1995 storyline event simulations, by comparing gauge data from the California Data Exchange Center (CDEC), to validate our simulation and examine any biases in our results. We focus here on the 1995 storyline event, because it has the driest antecedent conditions of the three events we modeled in this study.

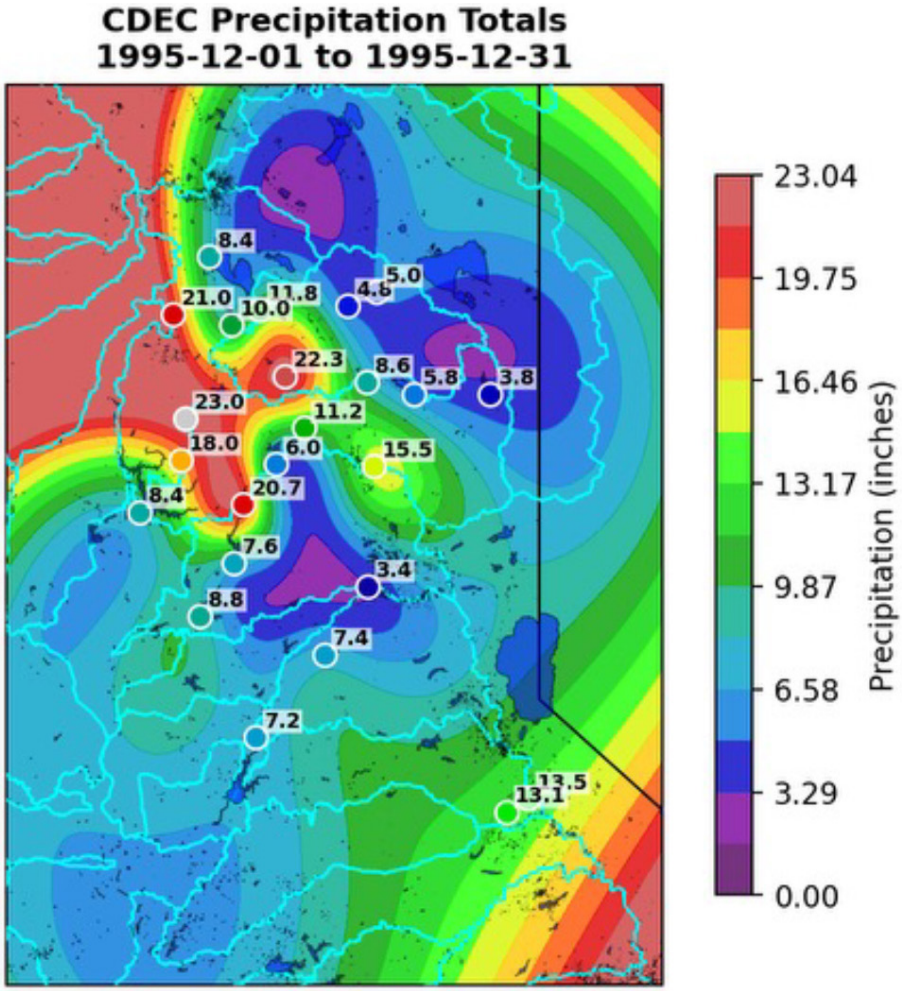
Comparing modeled 1995 reservoir inflow results for the median ensemble member (E5) to the CDEC reservoir inflow gauge data, we find WRF-Hydro shows relatively good skill, but the simulation shows slightly lower magnitude and lagged timing of peak inflows. For example, WRF-Hydro has peak flows around 800 cms for Oroville, compared to 955 cms from CDEC for December 12, 1995 (Figure A.3.3). There is also a one-day lag in peak flow timing, which is partly due to the fact that the CDEC reports at daily frequency whereas WRF-Hydro provides hourly output (i.e., the WRF-Hydro inflow peak is at the dawn/midnight following the CDEC reported peak). To understand the underestimate of WRF-Hydro compared to CDEC we compare storm total precipitation data across the CDEC stations (Figure A.3.4), the AORC gridded storm total precipitation data used in the days prior to the storyline event (Figure A.3.5), and the WRF storm total precipitation estimates used for the event days (Figure A.3.5). The lower peak magnitude and slight lag in timing in WRF-Hydro (Figure A.3.3) appears to be driven by spatial biases in the gridded AORC storm total precipitation amounts (Figure A.3.5) used to generate the WRF-Hydro antecedent conditions in the spinup process. This is particularly evident when compared to observed CDEC storm total precipitation amounts (Figure A.3.4).

Figure A.3.3



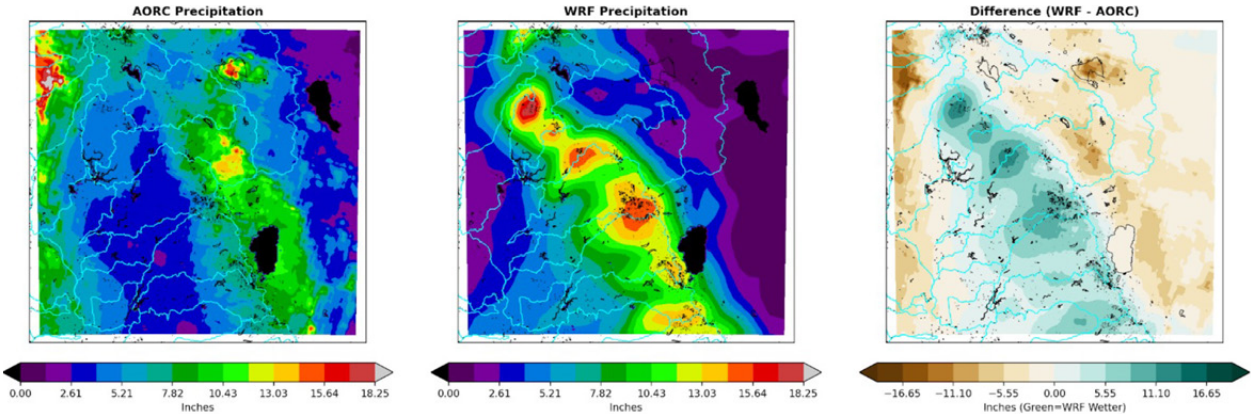
Hourly and daily historical simulated reservoir inflows, outflows, and water surface elevations (WSE) from WRF-Hydro ensemble member E5 compared to daily observed reservoir inflows from CDEC for Oroville reservoir. Simulated time series are in solid lines, with dark lines aggregated to daily and light lines showing hourly simulation results. The black dotted line shows the daily observed inflows.

Figure A.3.4



CDEC storm total precipitation amounts (colored contours) and gauge locations (dots) for December 1995.

Figure A.3.5

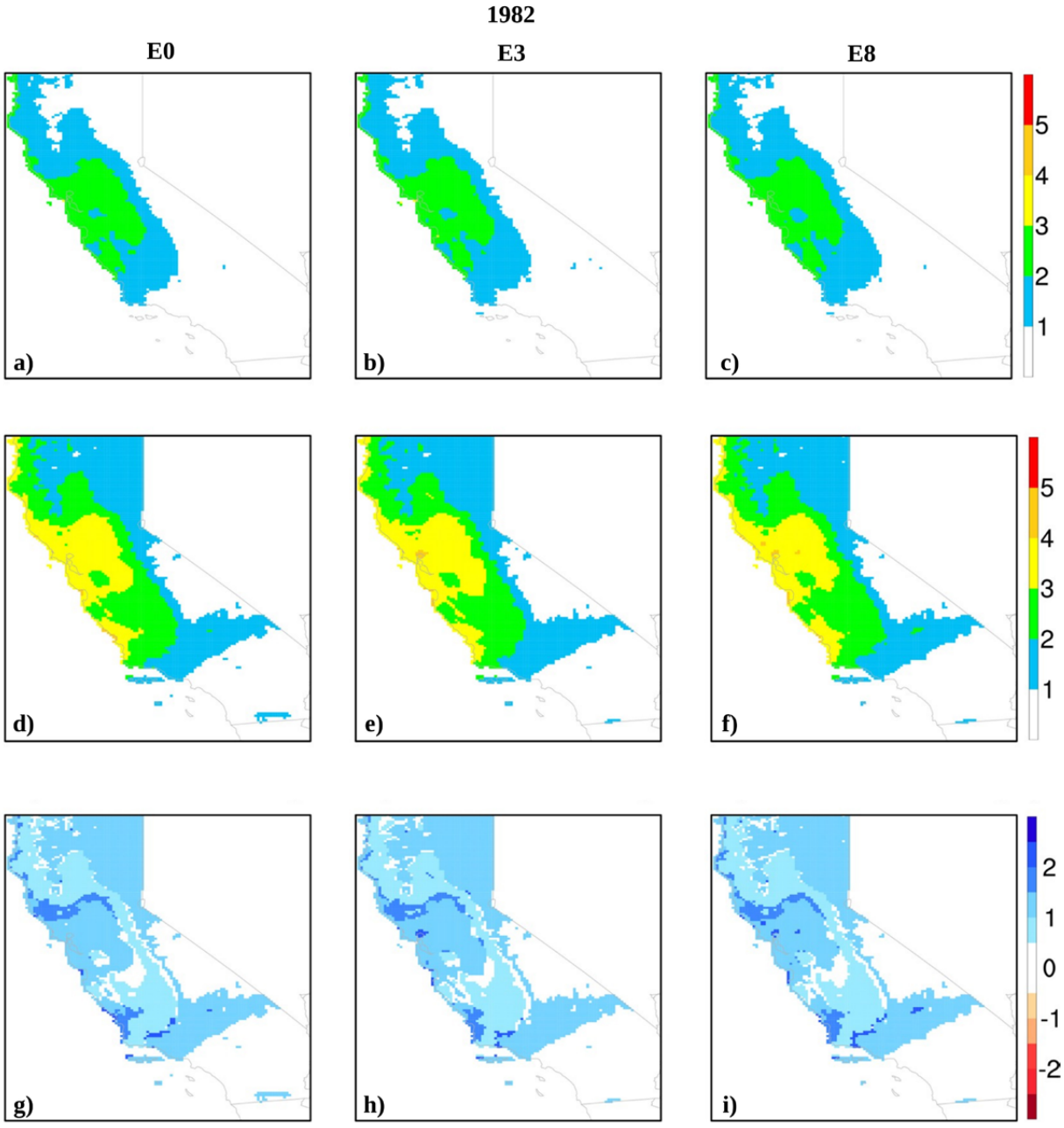


AORC and WRF storm total precipitation amounts and differences (WRF minus AORC) for December 1995.

A.4 1982 Storyline

Figure A.4.1 shows the highest Ralph et al. (2019) AR Category Scale reaching ARs (January 3–January 5, 1982) within the 1982 storyline simulation. Table A.4.1 and Figure A.4.2 show the reservoir inflows, outflows, elevations, and change in storage during the 1982 storyline event for the complete set of ensemble members (E0 - maximum, E3 - median, and E8 - minimum), in the historical and future WRF-Hydro simulation.

Figure A.4.1



The highest Ralph et al. (2019) AR Category Scale reaching ARs within the 1982 storyline simulation. Each gridcell represents the maximum AR Category reached over the duration of the AR landfall for each of the three ensemble members downscaled using WRF-Hydro for the historical (a-c) and future (d-f) periods. The differences (future - historical) are shown (g-i).

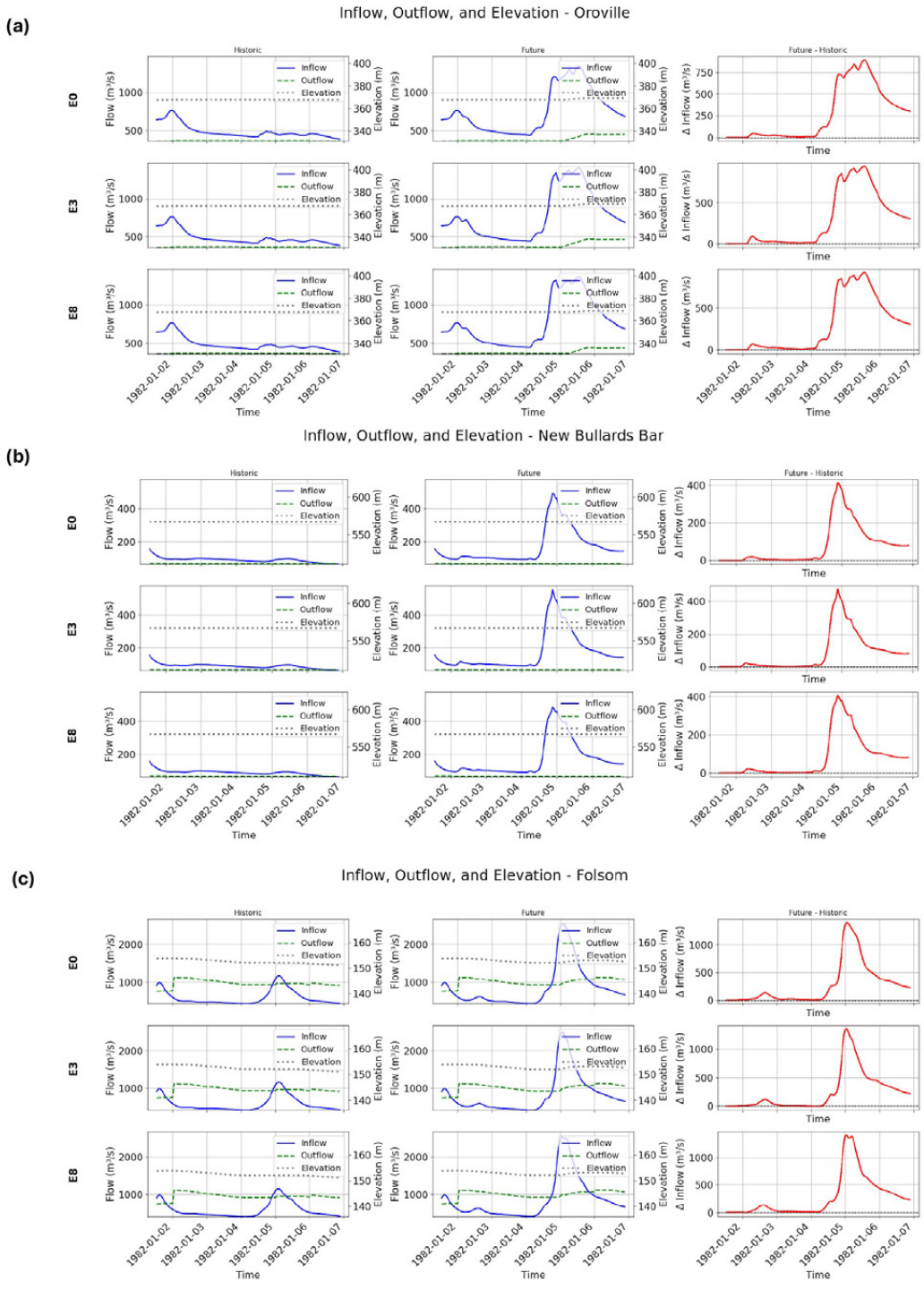
Table A.4.1

Reservoir (Storage Capacity)	Ensemble Member	Period	Total Inflow (MAF)	Total Outflow (MAF)	Net Change in Storage (MAF)	Net Change % of Total capacity
Oroville (3.43 MAF)	E7	Historical	0.16	0.11	0.000	1%
Oroville (3.43 MAF)	E7	Future	0.23	0.12	0.002	3%
Oroville (3.43 MAF)	E0	Historical	0.16	0.11	0.000	1%
Oroville (3.43 MAF)	E0	Future	0.24	0.12	0.002	4%
Oroville (3.43 MAF)	E8	Historical	0.16	0.11	0.000	1%
Oroville (3.43 MAF)	E8	Future	0.24	0.12	0.002	4%
New Bullards Bar (0.97 MAF)	E0	Historical	0.03	0.02	0.000	1%
New Bullards Bar (0.97 MAF)	E0	Future	0.05	0.02	0.000	3%
New Bullards Bar (0.97 MAF)	E7	Historical	0.03	0.02	0.000	1%
New Bullards Bar (0.97 MAF)	E7	Future	0.05	0.02	0.000	4%
New Bullards Bar (0.97 MAF)	E8	Historical	0.03	0.02	0.000	1%
New Bullards Bar (0.97 MAF)	E8	Future	0.05	0.02	0.000	3%
Folsom (0.98 MAF)	E0	Historical	0.19	0.30	-0.001	-12%

Reservoir (Storage Capacity)	Ensemble Member	Period	Total Inflow (MAF)	Total Outflow (MAF)	Net Change in Storage (MAF)	Net Change % of Total capacity
Folsom (0.987 MAF)	E0	Future	0.27	0.31	0.000	-3%
Folsom (0.987 MAF)	E7	Historical	0.19	0.30	-0.001	-12%
Folsom (0.987 MAF)	E7	Future	0.27	0.31	0.000	-4%
Folsom (0.987 MAF)	E8	Historical	0.19	0.30	-0.001	-11%
Folsom (0.987 MAF)	E8	Future	0.28	0.31	0.000	-3%

Inflows, Outflows, and Storage Changes between January 3–5, 1982 for Oroville, New Bullards Bar, and Folsom reservoirs for historical and future time periods, for the maximum (E0), median (E3), and minimum (E8) WRF storyline simulation ensemble members. Each reservoir's total reservoir capacity is provided in parentheses in the first column.

Figure A.4.2



Reservoir inflows, outflows, and percent full for Lake Oroville (a), New Bullards Bar (b), and Lake Folsom (c) under historical conditions (first column), future warming (second column), and difference in future minus historical inflows (third column) across all three WRF-Hydro ensemble simulations of the 1982 storyline.